Technische Universität München
TUM School of Medicine and Health

Tumor cell-intrinsic RIG-I signaling regulates anti-tumor T-cell immunity through programmed cell death and extracellular vesicle biogenesis

Florian Jonas Max Stritzke

Vollständiger Abdruck der von der TUM School of Medicine and Health der Technischen Universität München zur Erlangung eines

Doktors der Medizinischen Wissenschaften (Dr. med. sci.)

genehmigten Dissertation.

Vorsitz: apl. Prof. Dr. Klaus-Peter Janssen

Prüfer*innen der Dissertation:

1. Prof. Dr. Hendrik Poeck
2. Priv-Doz. Dr. Veit Buchholz
3. Prof. Dr. Percy A. Knolle

Die Dissertation wurde am 17.04.2023 bei der Technischen Universität München eingereicht und durch die TUM School of Medicine and Health am 20.12.2023 angenommen.

Table of contents

Table of contents I

1. Abstract ..... - 1 -

2. Zusammenfassung ..... - 3 -

3. Introduction ..... - 5 -

3.1. Immunity shapes cancer development and control ..... - 5 -

3.2. Innate immunity governs cancer immunosurveillance ..... - 7 -

3.3. Dying tumor cells can stimulate potent immune responses ..... - 11 -

3.4. Tumor-derived extracellular vesicles modulate cancer immunity ..... - 13 -

3.5. Harnessing innate immune signaling to improve immunotherapies ..... - 17 -

4. Objectives ..... - 19 -

5. Methods ..... - 20 -

6. Summary of selected original publications ..... - 23 -

6.1. "Targeting intrinsic RIG-I signaling turns melanoma cells into type I interferon-releasing cellular antitumor vaccines" ..... - 23 -

6.2. "Harnessing nucleic acid sensors in tumor cells to reprogram biogenesis and RNA cargo of extracellular vesicles for T-cell-mediated cancer immunotherapy" .. - 25 -

6.3. "In Vivo Immunogenicity Screening of Tumor-Derived Extracellular Vesicles by Flow Cytometry of Splenic T Cells" ..... - 27 -

7. Discussion ..... - 28 -

8. List of abbreviations ..... - 35 -

9. References ..... - 37 -

10. Attachments ..... **- 49 -**

10.1. Publication list ..... **- 49 -**

10.2. Included publications ..... **- 50 -**

11. Acknowledgement ..... **- 118 -**

1. Abstract

By enhancing T cell responses targeted against tumor cells, immune checkpoint blockade (ICB) with anti-CTLA4 or anti-PD1 can provide durable remissions for cancer patients. Still, substantial variation between patients in the therapy response, and the limited understanding of underlying mechanisms remain a major clinical challenge. Our group and others have recently shown that innate immune receptors that detect aberrant nucleic acids do play an important role in the initiation of anti-neoplastic T cell responses. Our previous data demonstrated that anti-CTLA-4 and its combination with anti-PD-1 rely on tumor cell-intrinsic activation of the cytosolic RNA receptor RIG-I, but not the cGAS/STING DNA receptor system. However, the means of communication between RIG-I-activated tumor cells and host immune cells remained largely unknown. In the work underlying this cumulative thesis, we now show that RIG-I activation (i) triggers immunogenic cancer cell death with substantial IFN-I release and (ii) governs cancer cell-derived extracellular vesicles' biogenesis including its RNA cargo, thereby modulating antineoplastic T cell immunity and ICB response.

We found that targeting tumor-intrinsic RIG-I signaling triggered tumor and host IFN-I production that stimulated $CD103^+$ dendritic cells to cross-prime antineoplastic T cells. Given their inherit capacity to transfer functional molecules, thereby reflecting the status of their originating cells, we investigated the role of extracellular vesicles (EVs) in RIG-I-induced tumor-host communication. Though cancer-derived EVs are commonly regarded as immunosuppressive, RIG-I-induced EVs were found to be loaded with endogenous immunostimulatory nucleic acids, including small nuclear (sn) and small nucleolar (sno)RNAs, as well as exogenously transfected triphosphate RNA, prompting IFN-I production by the host. Mechanistically, RIG-I, autocrine IFN-I-signaling, and Rab27a were required in the tumor to produce immunostimulatory EVs, which were ingested into dendritic cells by macropinocytosis. In a murine melanoma model, RIG-I-mediated tumor cell death and therapeutic application of RIG-I-induced EVs resulted in the accumulation of activated T cells in the tumor microenvironment and, thus, synergized with anti-CTLA4 plus anti-PD1. Consistently, retrospective clinical data linked simultaneously high transcriptional activity of *DDX58* (encoding RIG-I) and EV pathway genes to beneficial ICB response in melanoma patients.

In summary, our work shows that intratumoral RIG-I signaling can reprogram EV biogenesis and their RNA cargo. Such RIG-I-induced EVs stimulate host and tumor-intrinsic IFN-I

production, cross-priming of antineoplastic T cells, thereby improving therapy response to ICB. Hence, we propose RIG-I-induced EVs from autologous tumor tissue as a personalized cancer treatment with the potential to overcome cancer resistance to established immunotherapies.

(Please see Fig. 1 at p. 34 for a schematic overview of findings.)

2. Zusammenfassung

Die Immun-Checkpoint-Blockade (ICB) mit anti-CTLA4 oder anti-PD1 kann bei Krebspatient:innen zu dauerhaften Remissionen führen, indem sie die gegen Tumorzellen gerichteten T-Zell-Reaktionen verstärkt. Dennoch stellen die Variabilität im Therapieansprechen und das begrenzte Verständnis zugrunde liegender Mechanismen nach wie vor eine große klinische Herausforderung dar. Unsere Arbeitsgruppe und andere haben vor kurzem gezeigt, dass Rezeptoren des angeborenen Immunsystems zur Erkennung aberranter Nukleinsäuren eine wichtige Rolle bei der Auslösung antineoplastischer T-Zell-Reaktionen spielen. Unsere Daten haben demonstriert, dass anti-CTLA-4 und seine Kombination mit anti-PD-1 auf die tumorzelleigene Aktivierung des zytosolischen RNA-Rezeptors RIG-I, nicht aber des cGAS/STING-DNA-Rezeptorsystems angewiesen sind. Die Mechanismen der Kommunikation zwischen RIG-I-aktivierten Tumorzellen und Immunzellen des Wirtes waren jedoch bisher weitgehend unbekannt. In der Arbeit, die dieser kumulativen Dissertation zugrunde liegt, zeigen wir nun, dass RIG-I-Aktivierung (i) einen immunogenen Krebszelltod mit substanzieller IFN-I-Freisetzung auslöst und (ii) die Biogenese aus Krebszellen stammender extrazellulärer Vesikel und ihre RNA-Fracht steuert, wodurch die antineoplastische T-Zell-Immunantwort und das Ansprechen auf eine ICB moduliert werden.

Wir entdeckten, dass die gezielte Aktivierung des tumoreigenen RIG-I-Signalweges die IFN-I-Produktion durch Tumor und Wirt auslöste, wodurch CD103+ dendritische Zellen antineoplastische T-Zellen kreuzanregten. Angesichts ihrer inhärenten Fähigkeit, funktionelle Moleküle zu übertragen, die den Status ihrer Ursprungszellen widerspiegeln, haben wir die Rolle extrazellulärer Vesikel (EVs) bei der RIG-I-induzierten Tumor-Wirt-Kommunikation untersucht. Obwohl krebsbedingte EVs gemeinhin als immunsuppressiv angesehen werden, beobachteten wir, dass RIG-I-induzierte EVs mit endogenen immunstimulierenden Nukleinsäuren beladen wurden, darunter kleine nukleäre (sn) und kleine nukleoläre (sno) RNAs sowie exogen transfizierte Triphosphat-RNA, welche die IFN-I-Produktion durch den Wirt anregten. Mechanistisch gesehen waren RIG-I, autokrine Aktivierung des IFN-I-Signalweges und Rab27a im Tumor erforderlich, um immunstimulierende EVs zu produzieren, die durch Makropinozytose in dendritische Zellen aufgenommen wurden. Im murinen Melanommodell führten ein RIG-I-induzierter Zelltod und die therapeutische Anwendung RIG-I-induzierter EVs zu einer Ansammlung aktivierter T-Zellen in der Tumormikroumgebung und hiermit zu einer Synergie mit anti-CTLA4 plus anti-PD1. Eine simultan hohe Transkriptionsaktivität von DDX58 (kodierend für RIG-I) und

EV-Biogenese assoziierten Genen korrelierte in retrospektiven klinischen Daten mit einem verbesserten Therapieansprechen auf eine ICB bei Melanompatient:innen.

Zusammenfassend zeigen unsere Arbeiten, dass intratumorale RIG-I-Signale die EV-Biogenese und ihre RNA-Beladung umprogrammieren können. Solche RIG-I-induzierten EVs stimulieren die wirts- und tumoreigene IFN-I-Produktion sowie die Kreuzaktivierung von antineoplastischen T-Zellen und verbessern so das Ansprechen auf eine ICB. Daher schlagen wir RIG-I-induzierte EVs aus autologem Tumorgewebe als personalisierte Krebstherapie vor, die das Potenzial hat, Resistenzen gegen etablierte Immuntherapien zu überwinden.

3. Introduction

3.1. Immunity shapes cancer development and control

In 2020, cancer was diagnosed 19.3 million times and accounted for 10.0 million deaths worldwide. By 2040, the annual cancer incidence is projected to surpass 30 million (International Agency for Research on Cancer, 2022). Hence, cancer therapies that induce durable remissions are urgently sought-for. Advanced scientific understanding of cancer biology continuously provides the foundation for novel approaches. Considerably, the ability of malignant cells to divide and infiltrate relies not only on intrinsic features, such as sustaining proliferative signaling and evading cell cycle checkpoints, but instead includes the tumor's coercion of neighboring cells to tolerate or support them (Hanahan & Weinberg, 2011). This tumor microenvironment is shaped by immune cells that, if targeted therapeutically, can turn back against the tumor.

Whether the immune system protects individuals from non-pathogen-derived cancers has long been disputed among scientists before becoming a commonly shared concept. Whereas Ehrlich was one of the first to postulate a protective role for the immune system against cancer in 1909 (Ehrlich, 1909), cancer immunology remained a contested concept until the end of the last century. Significantly, Thomas and Burnet proposed new perspectives on the interaction between the immune system and cancer. Presuming that long-lived organisms with complex self-renewing tissues, such as humans, are regularly challenged by neoplastic cell clones, Thomas concluded that evolution would have equipped those organisms with some defense mechanism outside the transformed cell and hypothesized cellular immunity might fulfill that role (Thomas, 1982). Based on observations about immunotolerance, Burnet observed that somatic mutations eventually generate foreign antigens. As lymphocytes targeting such antigens naturally are not subjected to self-tolerogenic inhibition, he concluded that they might exert "immunosurveillance" against cancer (Burnet, 1967).

T cells play a paramount role in the interaction between cancer and immunity, as they can distinguish malignant cells from their physiological counterparts. Infiltration of cytotoxic T cells into the tumor site independently predicts prolonged survival for many cancer patients, including colorectal (Naito et al., 1998) and esophageal (Schumacher, Haensch, Roefzaad, & Schlag, 2001) carcinomas. Circulating cytotoxic T cells from patients with NY-ESO-1 expressing cancers frequently target this specific tumor antigen (Jager et al., 2000), marking

a tumor antigen-specific cellular immune response. When tumor cells express aberrant peptides and present them on MHC-I, they may be recognized and targeted by specific T cells. These tumor antigens can be classified into three main categories (Wang & Wang, 2017) (i) tissue-specific antigens overexpressed in tumor cells (e.g., gp100), (ii) cancer-testis antigens expressed exclusively by tumor cells and testis tissue (e.g., NY-ESO-1), and (iii) tumor-specific neoantigens derived from (individual) non-synonymous somatic mutations.

T cell responses against neoantigens can be so effective that, in some cases, targeted cancer clones perish and are outgrown by clones without this neoantigen, escaping the immune response (Balachandran et al., 2017; Verdegaal et al., 2016). Immunotherapies, like anti-PD-1 or anti-CTLA4, rely strongly on preexisting or recently emerged antitumor T cell responses that arise in the presence of neoantigens (Gubin et al., 2014; Rizvi et al., 2015; Van Allen et al., 2015; Yost et al., 2019). Clinical studies have demonstrated that peptide- and RNA-based vaccines against neoantigens can induce poly-specific T cell responses (Ott et al., 2017; Sahin et al., 2017) with the potential to bolster current immunotherapies.

Importantly, peripheral tolerance constitutes a complementary checkpoint. To activate T cells, besides interaction with tumor antigens, a “second signal” is required (Lafferty & Cunningham, 1975), e.g., in the form of the costimulatory molecules CD80 and CD86, interacting with the CD28 receptor on T cells (F. A. Harding, McArthur, Gross, Raulet, & Allison, 1992; Linsley et al., 1994). Costimulatory molecules on antigen-presenting cells are induced when innate immune receptors recognize microbial patterns (PAMPs) (Janeway, 1992) and patterns of “danger” (DAMPs), including molecules released during cell stress or cell lysis (Matzinger, 1994). Given the reliance of adaptive immunity on a limited set of innate receptors, Janeway concluded that a “successful pathogen would simply avoid these receptors and should thus induce tolerance rather than immunity” (Janeway, 1992). Immunosuppressive tumors also inhibit costimulation by antigen-presenting cells after DAMP-sensing so that T cells become refractory, anergic, or undergo apoptosis (Zappasodi, Merghoub, & Wolchok, 2018).

The immune system eventually protects individuals by detecting and eliminating cancer cells. However, this interaction exerts selective pressure and thereby sculpts the tumor, resulting in various mechanisms of immunosuppression, described as “immunoediting” (Dunn, Old, & Schreiber, 2004). This neoplastic versatility strengthens the case for a multimodal reinvigoration of the immune response to prevail in control over cancer.

3.2. Innate immunity governs cancer immunosurveillance

The following section examines the role of innate immunity in the multistep process from dendritic cells' engulfment of tumor antigens to T cell-mediated tumor cell lysis. Whereas the tumor might deploy checkpoints to undercut this process, these checkpoints may also constitute clinical targets to support cancer immunosurveillance (Mellman, Coukos, & Dranoff, 2011).

Dendritic cell (DC) uptake of tumor antigens is essential to initiate T cell-based anticancer immunity. Tumor-derived antigens are preferentially taken up if enclosed in membranes exhibiting calreticulin, heat shock proteins HSP30 and HSP70 (Galluzzi, Buque, Kepp, Zitvogel, & Kroemer, 2017), phosphatidylserine or tetraspanins CD9 and CD81 (Morelli et al., 2004), which are regularly found on dying tumor cells and tumor-derived extracellular vesicles (EVs). Tumor-derived EVs and dying cells are an especially immunostimulatory source of tumor-antigens (Albert, Sauter, & Bhardwaj, 1998; Wolfers et al., 2001), inducing cross-presentation and T cell priming. Effective cross-presentation, presumably by lymphoid tissue-resident conventional dendritic cell type 1 (cDC1) expressing Batf3 and CD8α, after antigen transfer depends on adequate maturation signals (Gardner & Ruffell, 2016). Stimuli of DC maturation are DAMPs that activate pattern recognition receptors (PRRs), proinflammatory cytokines (like TNF-α and IL-1β), and, especially in antitumor immunity, type-I interferon (IFN-I). Conversely, low levels of IFN-I induce tolerance (Melief, 2008). Thus, IFN-I sensing by CD8α^+ DCs is crucial for effective cross-presentation and T cell-mediated elimination of immunogenic tumors (M. S. Diamond et al., 2011; Fuertes et al., 2011).

Beyond delivering antigens to the lymph node, CD103$^+$ cDC1s can support cytotoxic T cell activity in the tumor by re-stimulatory antigen presentation and cytokines. Intratumoral cDC1s secrete IL-12 in an IFN-γ-dependent manner, potentially creating a positive feedback loop with T cells (Bottcher & Reis e Sousa, 2018). Recent studies identified NK cells to be central for recruiting and retaining (via CCL5 and XCL1), promoting differentiation, and preserving viability (via FLT3L) of this critical DC subset (Barry et al., 2018; Bottcher et al., 2018). In patients, these intratumoral CD103$^+$ cDC1s correlate with longer survival and better response to anti-PD1 immunotherapy (Barry et al., 2018; Bottcher et al., 2018; Broz et al., 2014).

For cancer immunosurveillance, the activation of innate immune receptors plays a central role. Activation of pattern recognition receptors (PRRs) can trigger tumor cell death that

itself potentially results in the release of additional danger signals that can activate immune cells. This feedback loop makes PRRs promising targets for immunotherapeutic interventions against cancer (Amarante-Mendes et al., 2018). Indeed, many established cancer therapies rely on PRR-induced, potentially immunogenic cell death. Some of these therapies alter the cellular localization, composition, abundance, and transfer of nucleic acids within tumor cells, thereby generating potent PRR-activating danger signals capable of initiating adaptive immunity (J. M. Diamond et al., 2018; Ranoa et al., 2016). Given their clinical and translational relevance, the most relevant PRRs in the context of cancer cell death are introduced.

Toll-like receptors (TLRs) bind to typical components of bacteria, like lipopolysaccharide and flagellin, as well as aberrant nucleic acids. Thus, TLRs can detect both infectious pathogens and non-infectious tissue damage. TLR3, TLR7, and TLR9, for instance, are activated by double-stranded RNAs, single-stranded RNAs, and unmethylated 2′-deoxyribocytidine-phosphate guanosine (CpG) DNA motifs, respectively, if localized in endosomal or lysosomal compartments. Importantly, self-nucleic acids mostly do not activate innate immune receptors under physiologic conditions because they are degraded, walled off, or molecularly modified to circumvent detection. Upon activation, the adapter Myd88, employed by all TLRs except for TLR3, signals via NFκb and MAPKs, inducing the expression of inflammatory cytokines. The adapter TRIF, in contrast, solely deployed by TLR3 and TLR4, activates NFκb and IRF3, culminating in the transcription of IFN-I (Kawai & Akira, 2010). Antineoplastic anthracycline treatment of tumor cells generates TLR3-activating RNAs, consequently mediating IFN-I production, which is essential for its therapeutic efficacy in experimental procedures and clinical settings. This “viral mimicry” has been proposed as a hallmark of antineoplastic treatments (Sistigu et al., 2014).

Retinoic acid-inducible gene I (RIG-I)-like receptors (RLRs) in the cytosol constitute essential detectors of viral infection but can also be activated by epigenetic modulator treatment with 5-azacytidine, ionizing radiation, and others (Chiappinelli et al., 2015; Ranoa et al., 2016; Yoneyama et al., 2004). When binding viral or endogenous immunostimulatory RNA, RLRs mediate the transcription of IFN-I and other genes that collectively mount an antiviral-like immune response. The RLR family consists of the eponymous member RIG-I, melanoma differentiation-associated protein 5 (MDA5), and laboratory of genetics and physiology 2 (LGP2) (Rehwinkel & Gack, 2020). Cytosolic RNAs which bind to RIG-I display several characteristics, including a triphosphate or a diphosphate group at its ultimate 5’ nucleotide (Hornung et al., 2006; Pichlmair et al., 2006) and a lack of methylation at its 2′-O position (Schoggins, 2015). In the case of endogenous mRNAs, both characteristics are

eliminated during capping and other posttranslational modifications in the nucleus. Conversely, RNA polymerase III (Pol-3) can convert AT-rich DNA sections into short immunostimulatory dsRNA with a triphosphate moiety (Ablasser et al., 2009; Chiu, Macmillan, & Chen, 2009). In viral infection and under some conditions of cytotoxic stress, endogenous non-coding RNAs, especially retroviral transcripts and snRNAs, usually shielded by specific proteins, cumulate in the cytosol, activating RIG-I (Chiang et al., 2018; Chiappinelli et al., 2015; Nabet et al., 2017; Ranoa et al., 2016).

On the molecular level, when RIG-I binds its ligand, its DExD/H-box-helicase domain wraps around the RNA. This domain cooperates with the carboxy-terminal domain to induce conformational changes, which expose two caspase recruitment and activation domains (CARDs). Those CARDs, then, bind to the mitochondrial antiviral-signaling protein (MAVS). MDA5, like RIG-I, consists of the same highly conserved modules, thus, interacting similarly with ligands and MAVS. LGP2, though, lacks CARDs required for downstream signal transduction and proposedly regulates the activity of RIG-I and MDA5. Complementing each other, RIG-I and MDA5 bind different RNAs since MDA5 prefers long dsRNA, like poly(I:C). However, their downstream pathways converge in MAVS. Upon CARD-CARD interactions, MAVS aggregates in the outer mitochondrial membrane in a self-perpetuating prion-like fashion, amplifying its initial signal. MAVS passes on the signal to TANK-binding kinase 1 (TBK1), and IκB kinase-ε (IKKε) again activates interferon regulatory factor 3 (IRF3), IRF7, and NF-κb. Those, cooperatively, induce the transcription of IFN-I and proinflammatory genes (Rehwinkel & Gack, 2020; Wu & Chen, 2014). Additionally, the IFN-I induction might be regulated by the interaction of RIG-I with the cell death protein RIP1 (Michallet et al., 2008; Rajput et al., 2011), constituting an intersection with RIG-I-induced necroptosis (Schock et al., 2017). Beyond changes in transcription, RLRs may cause cell death through intrinsic apoptosis as aggregated MAVS can trigger the expression of proapoptotic BH3-only proteins, namely Noxa and Puma, permeabilizing the mitochondrial membrane (Besch et al., 2009). Independent of MAVS, RIG-I may bind ASC to trigger a caspase-1-dependent inflammasome with consequent cleavage of IL-1β (Poeck et al., 2010). In conclusion, RIG-I is an upstream regulator of numerous cell death and immune pathways. RIG-I activation within tumor cells has been linked to potent immune responses (Dassler-Plenker et al., 2016; Duewell et al., 2014; Heidegger, Wintges, et al., 2019; Such et al., 2020). However, subliminal RIG-I activation with chronic inflammation has also been implicated in promoting cancer progression (Hu et al., 2013).

The cytosolic DNA sensor cyclic GMP–AMP (cGAMP) synthase (cGAS) and stimulator of interferon genes (STING) pathway is the central cytosolic double-strand DNA sensor. If

activated, cGAS generates cyclic dinucleotide 2´3´cGAMP as a second messenger. Upon binding cGAMP, STING translocates from the endoplasmic reticulum membrane to the Golgi complex, where it recruits TBK1 to become phosphorylated at its carboxy-terminal tail to elicit its downstream effects. Following activation of cGAS/STING, the transcription factors NF-κb and IRF3 mediate the expression of inflammatory genes and IFN-I, respectively (Wu & Chen, 2014). Notably, both DNA and RNA sensing may trigger programmed cell death. STING, much like its RNA-sensing counterpart MAVS, may induce several types of cell death, such as apoptosis via the mitochondrial pathway, necroptosis upon IFN-I and TNF-alpha sensing, lysosomal leakage mediated cell death, and inflammasome-dependent pyroptosis with IL-1β release (Paludan, Reinert, & Hornung, 2019).

In contrast to healthy tissues, cancer is characterized by uncontrolled proliferation, increased cell turnover, and, in many cases, genomic instability. As a result, DNA often accumulates in the cytosol, eventually forming micronuclei, which is enhanced by genotoxic stress (S. M. Harding et al., 2017; Mackenzie et al., 2017). Such cytosolic DNA naturally conveys a potent danger signal. As a mechanism of immune escape, the tumor-intrinsic IFN-I response to cytosolic DNA is often impaired (Xia, Konno, Ahn, & Barber, 2016). Nonetheless, tumor-derived cGAS/STING pathway agonists can be transferred to DCs, macrophages, and also endothelial cells, thereby critically promoting the priming of T cells, their infiltration into the tumor, and reinstatement of immune surveillance (Demaria et al., 2015; Schadt et al., 2019; Woo et al., 2014). It has been proposed that tumor-derived dsDNA, allegedly transported via extracellular vesicles and taken up by dendritic cells, could be responsible for this effect (Kitai et al., 2017; Woo et al., 2014). Recent evidence proposes an alternative explanation that mainly the second messenger cGAMP, derived from tumor-intrinsic cGAS, activates STING within surrounding non-malignant cells and triggers T and NK cell-based antitumor immunity (Marcus et al., 2018; Schadt et al., 2019). Consistently, the downregulation of the cGAS/STING pathway in several human cancers correlates with poor prognosis (Bu, Liu, Jia, & Yu, 2016; Song et al., 2017; Xia et al., 2016). However, in specific cases, DNA sensing-driven inflammation allegedly promotes tumorigenesis and cancer progression (Ahn et al., 2014; Q. Chen et al., 2016).

3.3. Dying tumor cells can stimulate potent immune responses

Dying cells release plenty of antigens and play a critical role in initiating adaptive immunity. Under physiological homeostatic conditions cells continuously perish and are cleared to maintain the equilibrium with stem cell-driven proliferation, reinforcing immunological tolerance or not being detected by the immune system. Conversely, under certain circumstances, just a few dying cancer cells trigger an adaptive immune response and, through immunological memory, can convey lifelong protection (Kroemer, Galluzzi, Kepp, & Zitvogel, 2013). Notably, the immunogenicity of cell death cannot be distinguished by morphological features of the dying cell but relies on the molecular activation of distinct cellular programs (Galluzzi et al., 2017; Yatim, Cullen, & Albert, 2017).

However, the underlying mechanisms and markers of immunogenic cell death (ICD) remain incompletely characterized. The gold standard for detection of ICD consists of *in vivo* vaccinating syngeneic malignant cells treated with a lethal dose of the putative ICD-inducer, followed by the contralateral injection of the same living malignant cells. Subsequent rejection of the tumor indicates ICD. As a confirmatory experiment, preestablished tumors are treated *in vivo* with the putative ICD-inducer. Therapy response can be compared between immunocompetent and immunodeficient mice, whereby the latter respond suboptimally to ICD induction (Kepp et al., 2014). According to this protocol, several chemotherapeutics such as doxorubicin (among other anthracyclines) (Sistigu et al., 2014) and oxaliplatin, specific forms of radiation therapy (Apetoh et al., 2007), and the sole ligation of some PRR, e.g., by cytosolic RNAs (Duewell et al., 2014; Yatim et al., 2015) have proved to induce immunogenic forms of programmed cell death. Regardless of the broad spectrum of ICD-inducers and the diverse downstream signaling pathways, some reoccurring molecular features of ICD have been identified: the secretion of ATP, exposure of Calreticulin on the surface of the dying cell, and release of HMGB1 (Kepp et al., 2014).

Mechanistically, during immunogenic cell death, autophagic processes may relocalize vesicular ATP stores and secrete ATP by opening pannexin 1 channels. Extracellular ATP acts as a “find-me-signal” for macrophage and DC precursors. ATP binding to purinergic receptors may activate the NLRP3 inflammasome, resulting in IL-1β and IL-18 secretion (Chekeni et al., 2010; Kroemer et al., 2013). Consistently, autophagy-deficient tumor cells secreted less ATP upon chemotherapy-induced cell death, correlating with less immune infiltration and a reduced immune response, which could be restored by inhibiting extracellular enzymatic ATP-degradation (Michaud et al., 2011).

Calreticulin can be exposed to the cell surface when, e.g., chemotherapeutics trigger an endoplasmatic reticulum stress response. This stress response involves eIF α phosphorylation and subsequent activation of caspase-8, leading to the transport of calreticulin from the endoplasmic reticulum onto the plasma membrane (Panaretakis et al., 2009). This occurs before cells display any visible signs of apoptosis as the exposure of calreticulin precedes phosphatidylserine exposure in ICD. Though both convey an “eat-me-signal” to phagocytic cells. In contrast to phosphatidylserin, calreticulin is considered a hallmark of ICD as it promotes antigen uptake, stimulates DCs to produce inflammatory cytokines, and enhances T cell priming (Kroemer et al., 2013; Obeid et al., 2007).

High mobility group box protein 1 (HMGB1) is another hallmark of ICD. Usually bound to chromatin within the cell, HMGB1 is released upon primary or postapoptotic necrosis when the plasma membrane ruptures and, thus, constitutes another “danger-signal” (Kroemer et al., 2013; Scaffidi, Misteli, & Bianchi, 2002). Activating the TLR4 pathway, HMGB1 enhances the cross-presentation of dying cell-derived antigens on DCs by delaying their degradation in phagosomes. Significantly, in a murine cancer model, this pathway contributed to the effectiveness of some systemic chemotherapies and ionizing radiation (Apetoh et al., 2007).

However, beyond exposing preformed “constitutive DAMPs” (cDAMPs) to the immune system, cancer cells under stress also produce “inducible DAMPs” (iDAMPs) through transcriptional changes, post-translational modifications, de-shielding or transport into other compartments. Consequently, iDAMPs activate several innate immune pathways in their microenvironment (Yatim et al., 2017). To therapeutically bolster anti-cancer immunity, a comprehensive understanding of the immunogenic factors released by cells under stress and the respective upstream pathways is needed. Herein, extracellular vesicles released by tumor cells have recently attracted much interest for their ability to modulate the anticancer immune response.

3.4. Tumor-derived extracellular vesicles modulate cancer immunity

Extracellular vesicles (EVs) are nano-size intercellular communication devices carrying nucleic acids and proteins in a lipid bilayer, that regulate numerous immune functions. The following section will highlight the molecular basis of EV-mediated intercellular communication and its role in cancer immunology.

EVs encompass a heterogeneous group of membrane-enclosed structures emitted by all cells. Early in their life cycle, their biogenesis pathway separates EVs into subgroups. Exosomes emerge by inward-budding of the endosomal membrane and are released by the fusion of multivesicular endosomes (MVE) with the plasma membrane. Microvesicles, in contrast, are directly shed from the plasma membrane (van Niel, D'Angelo, & Raposo, 2018). Currently, there is no consensus on markers that could ultimately separate the EVs of different biogenesis, so EVs are commonly described as small, medium, or large.

During EV biogenesis, the EV's prospective cargo is targeted to the membrane, clustering at the site where a vesicle will bud and ultimately fissure (van Niel et al., 2018). In particular, loading of RNAs into EVs is a regulated process that can be aided by tetraspanin-enriched microdomains sequestering RNA-binding proteins (RBPs), like major vault protein and Y-box-binding protein 1 (Perez-Hernandez et al., 2013; Shurtleff et al., 2017; Teng et al., 2017), or the miRNA-induced silencing complex (Gibbings, Ciaudo, Erhardt, & Voinnet, 2009). mRNAs may be targeted in a sequence-specific manner into tumor-derived microvesicles. This mRNA loading depends on conserved sequences at the mRNA's 3' UTR serving as EV-zipcode, though details of this mechanism still need to be elucidated (Bolukbasi et al., 2012). In general, RNAs that are small, non-coding, highly abundant in the cytosol, and able to associate with membranes or RNA-binding proteins (RBPs) are likely to be incorporated into nascent EVs (O'Brien, Breyne, Ughetto, Laurent, & Breakefield, 2020).

In the case of exosomes, after loading with specific cargo, intraluminal vesicles (ILV) bud into MVEs via several mechanisms. One of them depends on the endosomal sorting complex required for transport (ESCRT). Herein, ESCRT-0 and ESCRT-I cluster ubiquitylated transmembrane cargo in the limiting membrane of the MVE (Tamai et al., 2010), then recruit ESCRT-II and ESCRT-III for budding and fissuring of ILVs into the MVE. Further, ESCRT-independent mechanisms of exosome biogenesis depend on ceramide or cone-shaped tetraspanins, like CD81, that cluster in microdomains with cholesterol curving the endosomal membrane inwards (Zimmerman et al., 2016). When the MVE fuses with

the plasma membrane, exosomes are released from their originating cell. Therefore, MVEs are transported along the cytoskeleton fueled by molecular motor molecules and regulated by small GTPases, such as Rab27a, that dock them at the plasma membrane (Ostrowski et al., 2010; Sinha et al., 2016). The following fusion of the endosomal and plasma membrane is mediated by SNARE proteins, releasing the ILVs into the extracellular space (Jahn & Scheller, 2006). In contrast, microvesicle budding from the plasma membrane occurs via cargo clustering and local disruption of the phospholipid asymmetry by Ca2+-dependent aminophospholipid translocases, among other mechanisms (Piccin, Murphy, & Smith, 2007). Their fission is performed by actin and myosin contraction and directly releases the microvesicle to the extracellular space (D'Souza-Schorey & Clancy, 2012). During this microvesicle biogenesis, transmembrane proteins, like MHC, keep their topology with the same part facing outside when located on the plasma membrane or the EV (van Niel et al., 2018).

EVs must convey their molecular signal through interaction with their target cell to facilitate intercellular communication. For antigen presentation and signaling via membrane-bound receptors, this interaction may consist of simply binding to the cell surface (van Niel et al., 2018). However, many functions of EVs require the transfer of vesicular content into the cytosol of the target cell. The EV membrane can fuse with the plasma membrane directly or with the endosomal membrane after being taken up through various endocytic routes. Herein, EVs deliver functional molecules to the recipient cell, protecting them from degradation by extracellular enzymes and intracellular lysosomes (Mulcahy, Pink, & Carter, 2014). In particular, macropinocytosis has been linked to the cytosolic delivery of nucleic acids (Desai, Hunter, & Kapustin, 2019).

Notably, EVs derived from malignant cells potentially promote disease progression. Tumor-derived EVs support the physical expansion of the tumor by supporting invasive growth, preforming metastatic niches, and suppressing immune responses at multiple levels. On tumor-derived EVs, the immune checkpoint ligand PD-L1 is upregulated in the presence of IFNγ and inhibits cytotoxic T cell activity (G. Chen et al., 2018; Ricklefs et al., 2018). The abundance of this EV-associated PD-L1 in the circulation correlates with response to immune checkpoint inhibition in melanoma patients (G. Chen et al., 2018; Serratì et al., 2022). Other mechanisms of tumor-derived EVs to suppress antitumor T cell responses are EV-bound Fas-ligand mediated apoptosis of lymphocytes (Andreola et al., 2002) or enhanced proliferation and immunosuppressive capacity of regulatory T cells (Szajnik, Czystowska, Szczepanski, Mandapathil, & Whiteside, 2010). Also, tumor-derived EVs can

inhibit the cross-presentation capability of DCs by triggering the expression of the ectonucleotidase CD73 immune checkpoint (Salimu et al., 2017).

On the other hand, EV composition and biological function can change drastically during treatment, reflecting the current state of their originating cells. For instance, breast cancer cells treated with ionizing radiation or topotecan, both known to induce DNA-double-strand breaks, allegedly shuttle tumor DNA via EVs, thereby activating the STING pathway and IFN-I production in host cells and culminating in T cell responses against the tumor (J. M. Diamond et al., 2018; Kitai et al., 2017). However, if DNA is loaded into small EVs is still disputed in the field, and EV preparations may co-isolate DNA that is secreted by EV-independent mechanisms (Jeppesen et al., 2019).

Viral and endogenous 3pRNAs can be transferred via EVs that activate pattern recognition in recipient cells (Baglio et al., 2016; Nabet et al., 2017). Interestingly, under specific conditions in cancer, stromal cells may upregulate the Pol-3-driven transcription of triphosphorylated RNA (specifically RN7SL1), exceeding the shielding capacity of specific RNA-binding proteins and being loaded into EVs. Transfer of this unshielded 3pRNA may activate RIG-I in tumor cells and initiate inflammatory immune responses (Nabet et al., 2017). Hence, cancer-derived EVs can signal “danger” to neighboring immune cells by transferring immunogenic nucleic acids with consequential effects on the immune response against cancer.

In addition to the transfer of danger signals, EVs from tumor cells may serve as relevant sources of antigens for cross-presentation. Accordingly, if bound to EVs, the artificial tumor antigen ovalbumin (OVA) triggers specific CD8+ T cells to expand and protect tumor-bearing mice more effectively than soluble OVA (Zeelenberg et al., 2008). Another study indicated that tumor EVs are more immunogenic than irradiated whole tumor cells, apoptotic bodies, or tumor lysates (Wolfers et al., 2001). Potentially, reactive oxygen species or redox enzymes carried within EVs may alkalinize the DC’s phagosome and, thus, promote the loading of tumor antigens onto MHC-I for CD8+ T cell cross-priming (Battisti et al., 2017). The EV’s role as an antigen vehicle may also be based on the capability of DCs for selective uptake, e.g., via binding phosphatidylserine on the EV surface or tetraspanin/integrin interactions (Mulcahy et al., 2014).

In conclusion, tumor cell-derived EVs may threaten or aid cancer patients depending on the releasing cell type and its physiological state, mediated by their molecular composition. EVs transfer tumor antigens (Wolfers et al., 2001; Zeelenberg et al., 2008) and under certain

circumstances immunogenic nucleic acids that promote T cell cross-priming (J. M. Diamond et al., 2018; Kitai et al., 2017). Thus, tumor-derived EVs might be used as personalized anticancer vaccines. Given this potential of targeted delivery of antigens and immunomodulatory molecules, therapeutic EVs are currently tested in multiple clinical trials (Marar, Starich, & Wirtz, 2021).

3.5. Harnessing innate immune signaling to improve immunotherapies

Immunotherapy against cancer marks a significant “breakthrough,” as designated by the Science magazine in 2013 (Couzin-Frankel, 2013). Its novelty consists in mobilizing an immune response and targeting immunosuppression rather than directly aiming at the tumor’s mere viability. The duration of this immune response may extend beyond immunotherapy administration, possibly providing long-lasting immunity.

Naturally, a multitude of immune checkpoints helps to maintain self-tolerance but is regularly exploited by tumors to suppress anti-cancer immunity. CTLA4 competes with the T cell’s costimulatory receptor CD28, limiting T cell priming. PD-1, upregulated upon continuous antigen-stimulation without adequate $CD4^+$ T-cell help, marks $CD8^+$ T cell exhaustion (Zappasodi et al., 2018). The immune checkpoint inhibiting monoclonal antibodies anti-CTLA4 (e.g., ipilimumab), anti-PD-1 (e.g., pembrolizumab), and anti-PD-L1 (e.g., atezolizumab) have been approved by the FDA for an extending spectrum of oncological indications. However, only a fraction of patients responds to immune checkpoint blockade (ICB) (Brahmer et al., 2012; Hodi et al., 2010).

These ICB-unresponsive “cold” tumors are characterized by pauce and dysbalanced immune infiltration. Their microenvironment is characterized by macrophages, MDSCs, and Tregs over antitumor effectors such as $CD8^+$ cytotoxic T cells, $CD4^+$ Th1-polarized helper T cells, and NK cells. Further, immunosuppressive cytokine milieus and metabolic stress can thwart an effective immune response, even if reinforced by ICB. Thus, strategies to convert “cold” into “hot” T-cell-inflamed tumors are sought for (Duan, Zhang, Zheng, & Zhang, 2020). Notably, in many cases, T-cell recruitment and activation crucially depend on IFN-I release and signaling events downstream of IFN-sensing (Gajewski, 2015). Therefore, targeting innate immune signaling in the tumor or its microenvironment promises to overcome ICB therapy resistance.

Though not much considered in the past, targeting innate immune signaling is also deployed by several conventional cancer therapies (Galluzzi, Buque, Kepp, Zitvogel, & Kroemer, 2015; Z. Liu, Han, & Fu, 2020; Zappasodi et al., 2018). Radiotherapy (RT), eventually activating such innate immune signaling, is frequently used to treat cancer patients. Beyond the direct killing of tumor cells, ionizing radiation potentially releases DAMPs, induces IFN-I release, and increases cross-presentation by activated DCs and MHC-I upregulation in tumor cells. In some cases, this results in remission at distant tumor sites, called the abscopal effect, which has been attributed to RT-mediated

systemic immune responses (Apetoh et al., 2007; Lee et al., 2009; Reits et al., 2006). In murine tumor models, STING signaling in DCs was found to be required to induce adaptive immunity upon irradiation (Deng et al., 2014). Interestingly, the EVs from irradiated tumors have been found to transfer IFN-I stimulatory dsDNA (J. M. Diamond et al., 2018). Such damaged nuclear or mitochondrial DNA frequently accumulates in the tumor's cytosol due to genome instability, irradiation, or genotoxic chemotherapy.

The synergy of radiotherapy and anti-CTLA4 to generate a systemic immune response against murine melanoma is governed by tumor-intrinsic RIG-I signaling (Poeck et al., 2021). Clinically, in generally ICB-resistant, microsatellite-stable colon and pancreatic carcinomas, the abscopal response to combined radiotherapy and ICB correlates with potentially immunogenic retroviral RNA expression in irradiated tumor cells (Parikh et al., 2021). Further, immunogenic dsRNA is therapeutically upregulated by DNA methyltransferase inhibitors, such as the common antiproliferative drug 5-azacytidine, correlating with endogenous retrovirus expression (Chiappinelli et al., 2015). Induction of an antiviral response through TLR3 and RLR activation in tumor cells, subsequent apoptosis, and auto-/ paracrine IFN-I sensing significantly enhances anti-CTLA4 therapy (Chiappinelli et al., 2015). Similarly, the infection of tumors with the Newcastle disease virus (NDV), an alleged RIG-I ligand, elicits infiltration by antigen-specific lymphocytes of local and distant, uninfected sites, thereby delaying tumor growth. NDV's synergism with anti-CTLA4 occurred irrespective of intrinsic tumor cell lysis but depended entirely on IFN-I (Fournier, Wilden, & Schirrmacher, 2012; Zamarin et al., 2014). Consistently, synthetic RNAs targeting RLRs in pancreatic cancer elicit a highly immunogenic form of cell death *in vitro* and *in vivo* (Duewell et al., 2014). RIG-I activation in malignant cells and the tumor microenvironment enhances cross-priming, tumor-specific cytotoxic T-cell infiltration, and the MHC-I antigen processing and presentation machinery. This tumor intrinsic RIG-I activation synergizes with checkpoint blockade in murine tumor models and correlates with improved melanoma patients' responses to ICB therapy (Heidegger, Wintges, et al., 2019; Such et al., 2020). Different RIG-I ligands are being tested in phase I/II clinical trials with intralesional injection into advanced and refractory solid tumors as single agents or in combination with ICB (Iurescia, Fioretti, & Rinaldi, 2020).

Recent preclinical and clinical data suggest that harnessing innate immune sensing in malignant and non-malignant cells may strengthen current immunotherapies, including ICB. A promising strategy comprises targeting tumor-intrinsic RIG-I and using the hereby released tumor-derived extracellular vesicles.

4. Objectives

In the last decade, cancer patients for whom no promising therapies existed before experienced long-term responses to immunotherapy. Yet a relatively small number of patients benefit from this novel approach. Thus, mechanisms that drive therapy response and resistance may provide critical insights to extend the benefits of immunotherapy to more patients, overcoming immunologically “cold” tumors and the sizeable interindividual heterogeneity of therapy response.

IFN-I induction in the tumor microenvironment is crucial to adaptive antitumor immune responses. As a significant source of IFN-I, RIG-I/MAVS (and cGAS/STING) signaling presents a promising target. RIG-I activation combines immunogenic cell death and cell death-independent stress signals cumulating in an “antiviral response” signature that can predict ICB response. However, little is known about the biogenesis of immunogenic signals propagated by RIG-I-activated tumor cells, their molecular composition, transfer, and the targeted pathways in recipient cells. More detailed knowledge of how tumor-intrinsic RIG-I signaling elicits T cell-based antitumor immunity could enable precise therapeutic targeting of these mechanisms to improve current immunotherapies. Hence, this work aimed to elucidate:

a) How does RIG-I activation in tumor cells translate into immunogenic cell death?
b) Do EVs generated upon tumor-intrinsic RIG-I signaling prime anti-neoplastic immunity? What are the mechanisms underlying immunostimulation by such EVs?
c) Do RIG-I-induced programmed cell death and immunostimulatory EVs synergize with ICB?

5. Methods

Beyond referring to the material and method sections in the publications that form part of this dissertation, the following section provides an overview of the main experimental settings used to answer the research questions raised above.

To investigate the role of tumor-intrinsic RIG-I activation on immunogenic cell death and immunogenic EV release, the cell lines of murine melanoma B16 expressing the artificial tumor antigen ovalbumin (B16.OVA), murine melanoma B16-F10 without such artificial tumor antigen, murine pancreatic carcinoma Panc02, murine mammary carcinoma 4T1, murine colon carcinoma C26, murine fibroblasts NIH3T3 were used. To study the impact of cytosolic nucleic acid sensing and downstream events on immunostimulation, cells were transfected with a synthetic RIG-I ligand, *in vitro* transcribed 5'-triphosphorylated RNA (3pRNA), a sequence-identical non-triphosphorylated RNA (synRNA), a cGAS ligand, non-CpG double-stranded DNA oligonucleotide (interferon stimulatory DNA, ISD), or exposed to recombinant IFN-I. Unintended co-isolation of 3pRNA liposomes was assessed by testing "mock-EV" preparations from cell-free cultures. After 48 hours of incubation of treated or untreated cells, easily detachable dead cells were harvested and washed to be applied in subsequent experiments. For EV preparations, 24 hours after transfection, the supernatant was collected, cell debris was removed by centrifugation at 400 G for 5 min, and filtered through a 220 nm PVDF membrane. Then, EVs released from tumor cells were enriched via precipitation (using "total exosome isolation (from cell media) reagent" from Thermo Fisher) or size exclusion chromatography (using "Exo spin" from Cell GS). To separate EV subsets by differential ultracentrifugation, sequential centrifugation with 2,000 G for 20 min, 10,000 G for 40 min, and 100,000 G for 90 min was applied. To characterize EV-preparations, according to MISEV2018 guidelines (Thery et al., 2018), they were visualized via electron microscopy, quantified via nanoparticle tracking analysis, assessed for the canonical EV markers Alix, HSP70, CD81, CD63, and for the absence of intracellular proteins, not associated with the endosome or the plasma membrane, cytochrome c (mitochondria) and calnexin (endoplasmatic reticulum). Detection of tumor antigens OVA, gp100, and melan A in EV preparations was performed by western blot. Here, B16 cells succumbing to RIG-I-induced cell death will be referred to as 3p-B16, EV-preparations derived from RIG-I-activated cells as RIG-I-EVs and EV-preparations from cells cultured under steady-state conditions as Ctrl-Evs.

To establish the *in vivo* immunogenicity of tumor-intrinsic RIG-I targeting, mice were inoculated with 3p-B16 and vehicle or RIG-I-EVs and Ctrl-EVs. The inoculation was repeated after seven days, and the immune response was analyzed on day fourteen after the first inoculation. To quantify the activation of cytotoxic T cells, draining lymph nodes or spleen were explanted and cocultured with the specific tumor antigen ovalbumin (OVA) for 48 hours. IFN-γ production by $CD8^+$ T cells was then assessed by flow cytometry and compared against control groups that received cells or EVs from untreated cultures or vehicle only. Our publication “In Vivo Immunogenicity Screening of Tumor-Derived Extracellular Vesicles by Flow Cytometry of Splenic T Cells” describes and discusses the strengths and limitations of this method in more detail (Stritzke, Poeck, & Heidegger, 2021). Additionally, circulating T cells in the peripheral blood were analyzed regarding activation and T cell receptor specificity using a tetramer stain for flow cytometry. This experiment was also performed with genetically engineered melanoma cells or gene-deficient mice, assessing the requirement of distinct signaling pathways in the tumor cells and the host (or specific immune cells). In our tumor models, gene defects in immune or EV biogenesis-related pathways were induced by CRISPR-Cas9-mediated somatic mutagenesis and were confirmed by rtPCR and western blot. EV-immunizations were also performed in MAVS-($Mavs^{-/-}$) and STING-deficient ($Sting^{gt/gt}$) recipients, in mice treated with an IFN-I receptor blocking antibody anti-IFNaR1 and in mice with a conditional genetic deficiency of IFNaR1 in $CD11c^+$ DCs (CD11c-Cre $Ifnar^{fl/fl}$) or $LysM^+$ macrophages (LysM-Cre $Ifnar^{fl/fl}$).

Further, mice bearing a subcutaneously implanted tumor were treated repeatedly with RIG-I-stimulated tumor cells or their EV-preparations to test their antitumor efficacy. Some mice were injected intraperitoneally with anti-CD8a or anti-NK1.1 depleting antibodies. Alternatively, melanoma cells were implanted into mice after receiving prophylactic vaccinations with identical dead tumor cells. Assessing the formation of immune memory in complete responders, mice were rechallenged subcutaneously with identical tumor cells at the contralateral flank. To address the potential synergism of RIG-I-induced EVs with established ICB, the combination of EVs plus dual ICB with anti-CTLA4 and anti-PD1 was compared against EV-therapy or dual ICB in a murine model with pre-established tumors. In all settings, tumor growth and survival were regularly measured. Tumor size was approximated by caliper measurement of its superficial expansion using the formula for ellipsoid volumes (volume = π / 6 x [(length + width) / 2] ^{3}). The survival of mice was limited when their tumor reached a predefined critical size in compliance with ethics guidelines. Beyond overall growth or regression, tumor-infiltrating immune cells were analyzed via flow

cytometry of EV-treated tumor tissue, capturing density, cellular subtypes, and activation state of antigen-presenting cells, NK cells, and T cells.

Complementary to *in vivo* assays, BMDCs were analyzed *in vitro* upon cocultivation with 3p-B16, immunostimulatory (is)EVs, and Ctrl-EVs since activation and costimulation by antigen-presenting cells pose prerequisites for T cell responses. After coculture with EVs, murine BMDCs' and human PBMCs' release of IFN-β, CXCL-10, and other cytokines was quantified via ELISA, and the expression of the costimulatory factor CD86 and cross-presentation of an OVA-specific epitope, SIINFEKL, was determined via flow cytometry. Required signaling pathways in tumor cells and antigen-presenting cells for their ability to induce an adaptive immune response were analyzed using genetic engineering, as described above. Uptake by dendritic cells and intracellular delivery of EVs were visualized by fluorescent microscopy and semi-quantitatively measured by flow cytometry. Pretreating BMDCs tested the role of specific uptake routes with the inhibitors dynasore (Clathrin- and caveolin-dependent endocytosis) and amiloride (macropinocytosis), D-mannose or EDTA (both C-type lectin receptor-mediated endocytosis).

Our results suggest a critical role for the nucleic acid cargo within RIG-I-EV-mediated immunity. RNA and DNA from EVs were isolated and transfected into BMDCs, assessing their contribution to DC activation measured by IFN-β release. Applying the triphosphate cleaving enzyme alkaline phosphatase quantified the specific contribution of 3pRNA to RIG-I-EVs' immunogenicity. Single EV flow cytometry visualized the incorporation of fluorescently labeled 3pRNA into EVs after their previous transfection into tumor cells *in vitro*. Further, next-generation sequencing of small non-coding RNAs inside EVs was performed, analyzing the shift in EV cargo RNA subtypes and individual transcripts upon aberrant tumor intrinsic RIG-I signaling. Cumulative U1 and U2 RNA transcripts, referenced to the library RNAcentral (Consortium et al., 2015), were normalized to overall library size and compared between conditions.

Correlating our findings with clinical outcomes, the overall survival of 456 melanoma patients from the TCGA databank was stratified by transcriptional activity of a previously described set of genes associated with tumor EV secretion (Hurwitz et al., 2016) and the expression of *DDX58* (RIG-I). Also, therapy response to anti-PD1 and anti-CTLA4 checkpoint blockade was mapped to the transcriptional activity of clinical melanoma samples.

6. Summary of selected original publications

6.1. "Targeting intrinsic RIG-I signaling turns melanoma cells into type I interferon-releasing cellular antitumor vaccines"

Here, we show that tumor-intrinsic RIG-I signaling triggers immunogenic cancer cell death.

Transfecting murine melanoma cells, B16.OVA, with 5'-triphosposphorylated RNA (3pRNA) *in vitro*, led to RIG-I-dependent cell death. Such RIG-I activated B16.OVA cells induced dendritic cell maturation and cross-presentation of tumor antigens, activating and expanding tumor antigen-specific T cells *in vivo*. Inoculating mice with RIG-I-activated B16 undergoing ICD conferred effective antitumor immunity against the subsequent challenge with viable probes of the same cancer cells via $CD8^+$ T cells and $NK1.1^+$ NK cells, even in the absence of the artificial tumor antigen ovalbumin.

Consistent with the common conception of IFN-I as essential to initiate adaptive immune responses against cancer, dendritic cell activation and subsequent T cell priming in response to tumor cells undergoing RIG-I-induced cell death depended on Interferon alpha and beta Receptor 1 (IFNaR1) signaling in host cells. RIG-I activation in tumor cells provided significant amounts of IFN-I, and, consequently, RIG-I activated tumor cells with defective transcription factors Interferon regulatory factors 3 and 7 (Irf3/7) were less immunogenic. In contrast, NLRP3-dependent inflammasome formation in host cells was dispensable for activating $CD8^+$ T cells *in vivo* despite the abundant release of hallmark DAMPS like ATP. Adding to the tumor-autonomous IFN-I production, the immunogenicity of RIG-I activated tumor cells based on functional MAVS signaling in the host cells, whereas STING was dispensable, suggesting a transfer of immunostimulatory RNA from dying tumor cells.

In contrast to the RIG-I agonist 3pRNA, oxaliplatin, a bona fide ICD inducer, neither stimulated tumor-derived IFN-I nor did its induction of cell death and release of DAMPS rely on tumor intrinsic RIG-I, suggesting a different mechanism of ICD.

In summary, targeting tumor intrinsic RIG-I triggers immunogenic programmed cell death, thereby turning tumor cells into an IFN-I-producing cellular vaccine against individual cancer antigens.

Florian Stritzke, the co-first author of “Targeting intrinsic RIG-I signaling turns melanoma cells into type I interferon-releasing cellular antitumor vaccines,” did animal experiments, visualized, and analyzed results, and reviewed the manuscript.

6.2. “Harnessing nucleic acid sensors in tumor cells to reprogram biogenesis and RNA cargo of extracellular vesicles for T-cell-mediated cancer immunotherapy”

(Manuscript under revision in Cell Reports Medicine)

Here, we show that RIG-I governs tumor-derived extracellular vesicles' composition and immunomodulatory function.

Similar to whole cells after RIG-I-induced cell death, EVs released during the RIG-I pathway activation mediated dendritic cell maturation, the release of IFN-I, and T cell cross-priming. In a murine melanoma model, RIG-I-induced immunostimulatory (is)EVs triggered protective antitumor immune responses by expanding systemic tumor antigen-specific T cells as well as activating and accumulating T and NK cells in the tumor microenvironment. Importantly, isEVs treatment synergized with anti-CTLA4 plus anti-PD1.

Tumor-intrinsic RIG-I signaling significantly enhanced EV’s immunogenicity but did not impact the quantity of EV biogenesis nor the expression of canonical EV markers. Tumor intrinsic cGAS/STING signaling, though, resulted in poorly immunostimulatory EVs. Tumor-intrinsic transcription factors IRF3/7 facilitated isEV biogenesis, whereas cell death execution via Caspase-3 or MLKL was dispensable. Rab27a, a small GTPase involved in vesicle trafficking and membrane fusion, significantly contributed to the number of released EVs and the EV-mediated IFN-I response. Tumor-derived isEVs were found in different preparations, including precipitation, size-exclusion chromatography, and differential ultracentrifugation, diminishing the potential of confounding effects through co-isolation.

Tumor-derived EVs were actively taken up by dendritic cells via endocytosis and delivered into cytosolic compartments, as visualized by fluorescence microscopy. Specifically, isEV uptake into DCs via macropinocytosis and host cytosolic nucleic acid receptor signaling, mainly via MAVS, conveyed IFN-I production. Transfection of RNA isolated from isEVs was sufficient to induce IFN-I, whereas RNA from EVs of untreated tumor cell cultures did not induce IFN-I. STING signaling in the host and isEV-DNA transfection only had marginal effects on IFN-I production. IFN-I sensing in DCs or macrophages was required to activate T cells in response to isEV treatment.

After transfection into cancer cells, exogenous, fluorescently labeled 3pRNA was detected within a small fraction of EVs via specialized flow cytometry, implying a potential role in the immunostimulatory cargo of isEVs. However, triphosphate inactivating alkaline

phosphatase treatment reduced but did not abolish isEV-RNA immunogenicity, demonstrating a role for endogenous non-triphosphorylated RNAs. Tumor-intrinsic RIG-I signaling governed EVs' endogenous RNA cargo composition, as evidenced by next-generation sequencing. Small nuclear (sn)RNAs and small nucleolar (sno)RNAs were differentially regulated with a particular increase of U1 and U2 spliceosomal RNAs in isEVs, which have been implicated as endogenous RLR-ligands in cancer (Ranoa et al., 2016).

Addressing the applicability of these findings to the human situation, the exposure of peripheral blood mononuclear cells to isEVs from human melanoma resulted in the production of IFN-I and the IFN-I-induced chemokine CXCL10 by monocytes. Like murine B16 EVs, human melanoma EVs carried tumor antigens. HLA-matched DCs exposed to isEVs cross-primed and activated tumor antigen-specific T cells, as reported by our collaborators. In a retrospective analysis of melanoma patients from the TCGA, high expression of a gene set, which has been linked to EV secretion, was associated with reduced overall survival. However, concomitantly high expression of *DDX58* (encoding RIG-I) within this unfavorable cohort was associated with improved survival. Concomitantly enhanced *DDX58* and EV pathway gene transcription further showed a trend toward a durable response to anti-CTLA4 and anti-PD1 immunotherapy.

In summary, tumor-intrinsic RIG-I governs the biogenesis of immunogenic EVs that reprogramme the tumor microenvironment, trigger a potent antitumor T cell response, and synergize with ICB.

Florian Stritzke, the co-first author of "Reprogramming biogenesis and immunomodulatory function of tumor-derived extracellular vesicles by targeting the RIG-I pathway," designed the research and did most experiments, in particular, murine EV cell culture and animal experiments, visualized, analyzed, and interpreted results, and wrote the manuscript.

6.3. “In Vivo Immunogenicity Screening of Tumor-Derived Extracellular Vesicles by Flow Cytometry of Splenic T Cells”

Here, we describe a flow cytometry-based screening method to evaluate EVs' *in vivo* immunogenicity emerging under various conditions.

First, EVs were collected from *in vitro* cultures of murine cancers under steady-state or experimental conditions, here oxaliplatin chemotherapy exposure. After adequate incubation, the EVs accumulating in the supernatant were enriched, e.g., using a precipitation-based kit. Immunization of syngeneic mice with EV preparations was performed twice, followed by the explantation of the draining lymph nodes and the spleen to analyze the immune response locally and systemically. Tumor-reactive T cells were identified by restimulation with a known tumor antigen. Finally, immune cells’ surface markers, like CD8, and secretory proteins, like IFN-γ, were stained and measured through flow cytometry. Prospectively, combining genetic engineering of tumor cells and recipient animals with variations of this screening method may unveil critical and potentially actionable insights into the mechanisms underlying EVs' immunogenicity.

The co-first author of “In Vivo Immunogenicity Screening of Tumor-Derived Extracellular Vesicles by Flow Cytometry of Splenic T Cells,” Florian Stritzke designed the research, analyzed, and interpreted the results, and wrote the manuscript.

7. Discussion

RIG-I regulates numerous cell death and immune pathways, critically impacting cancer immunosurveillance and therapy response to checkpoint inhibition with anti-CTLA-4 and its combination with anti-PD-1(Duewell et al., 2014; Heidegger, Wintges, et al., 2019). The underlying mechanisms that turn cancer cells immunogenic long remained elusive. Rather than the mode of cell death execution (apoptosis, necroptosis, necrosis, etc.), specific inflammatory signaling events apparently drive the immunogenicity of RIG-I activation (Yatim et al., 2015). Specifically, RIG-I-induced ICD and release of isEVs require IRF3/7 in the tumor cell, mediating IFN-I production. The biogenesis of isEVs involves significant auto-/paracrine IFN-I signaling. Such IFN-I signaling can initiate a feedback loop stimulating the expression of interferon-stimulated genes, including RIG-I and STING (Y. Liu et al., 2016), potentially further enhancing cytosolic nucleic acid sensing and activation of consecutive pathways. In our study, tumor-intrinsic cGAS/STING's role in isEV biogenesis differs between species and cell types. Upon RIG-I targeting, STING surprisingly contributes to the biogenesis of B16 isEVs. Further, cGAS/STING activation alone eventually produces isEVs, too, whereas to a lesser degree, which the faint cGAS/STING pathway may explain in B16 (Heidegger, Wintges, et al., 2019). Consistent with several other studies, this finding suggests crosstalk between cytosolic RIG-I/MAVS and cGAS/STING signaling (Zevini, Olagnier, & Hiscott, 2017). In summary, sensing immunostimulatory cytosolic nucleic acids triggers distinct tumor-intrinsic pathways with consequential immunomodulatory effects.

IFN-I is well known to play a prominent role in the innate immune sensing of cancer (M. S. Diamond et al., 2011; Fuertes et al., 2011). Following tumor-intrinsic RIG-I activation, IFN-I mediates $CD103^+$ dendritic cells to express costimulatory molecules, cross-present tumor antigens, and prime $CD8^+$ T cells (Bek et al., 2019; Heidegger, Kreppel, et al., 2019; Heidegger, Wintges, et al., 2019), Fig. 1. With this, host IFN-I critically adds to the tumor-derived IFN-I. Like RIG-I-induced ICD, isEVs require host MAVS signaling and STING to elicit IFN-I production in response to immunostimulatory nucleic acid transfer. Endogenous RIG-I-activating RNA in the tumor cell's cytosol has been reported to increase during conditions of genotoxic stress, like chemotherapy and radiation (Ranoa et al., 2016). Interestingly, the same genotoxic treatments produce isEVs with the capacity to trigger an IFN-I response (J. M. Diamond et al., 2018; Kitai et al., 2017). Moreover, infection of macrophages with the intracellular bacterium Listeria monocytogenes results in STING-mediated loading of immunostimulatory nucleic acids into EVs (Nandakumar et al., 2019).

Together with our results, this evidence suggests a conserved mechanism in mammalian cells to generate isEVs when encountering an accumulation of immunostimulatory cytosolic nucleic acids during cellular stress, including genotoxicity or intracellular pathogenic infection.

Notably, sustained interferon signaling in tumor cells has also been linked to resistance to immunotherapy by upregulating PDL1 and other immunosuppressive mechanisms (Benci et al., 2016). In breast cancer cells, an interferon-related DNA-damage resistance signature (IRDS) associate with therapeutic failure of chemotherapy and radiation (Weichselbaum et al., 2008). Specifically, breast cancer cells showing a constitutional IRDS can trigger the production of stromal EVs containing the RIG-I ligand RN7SL1 that may, under certain circumstances, promote a more aggressive cancer phenotype (Nabet et al., 2017). However, dose and duration are decisive regarding the effects of interferon. Low-level type I interferon mediates long-term transcriptional changes through unphosphorylated IFN-stimulated gene factor 3, corresponding to the potentially detrimental IRDS (Cheon & Stark, 2009). Conversely, treatment of triple-negative breast cancer cells with IFN-β at a dose that induces robust phosphorylation of IFN-stimulated gene factor 3 has shown to reduce stem cell properties (Doherty et al., 2017). Clinically, basal-like breast cancers can be classified by IFN/STAT-activated gene expression marking an immune-activated, relatively beneficial subtype, in contrast to an immunosuppressed subtype with poor prognosis (Burstein et al., 2015; S. Liu et al., 2012). Consistent with the context-dependent dichotomy of interferon, RN7SL1 delivered by CAR-T cell-derived EVs to immune cells, instead of stromal EVs to breast cancer cells, constrains myeloid-derived suppressor cell development and enhances costimulation and antigen presentation by DCs (Johnson et al., 2021). The dichotomy following danger signaling and interferon production seems plausible, considering the evolutionary need to balance eliminating potentially dangerous cells against the risk of autoimmune disease upon persistent sublime danger signals. Evidently, the intensity and duration of the initiating stimulus, as well as the sensing cell type, play a pivotal role (Vanpouille-Box, Demaria, Formenti, & Galluzzi, 2018). In our studies, EVs from cancer cells with acute RIG-I activation have an immunostimulatory effect and reduce tumor growth. However, we cannot rule out that an altered intensity and duration of RIG-I activation will yield different EV properties. Hence, the mechanisms of the interferon-governed junction toward cancer immunosurveillance require further investigation.

Although EVs are well-known to be a source of tumor antigens for cross-priming (Wolfers et al., 2001; Zeelenberg et al., 2008), the EV components that translate antigen exposure into effective anti-tumor immunity are largely unknown. In our model, RIG-I-induced isEVs

carry exogenous 3pRNA primarily transfected into the melanoma cell as well as RIG-I-induced endogenous immunostimulatory RNAs. The loading of previously transfected RNAs demonstrates EVs' principal capability to serve as drug vehicles for RNA-based therapies without manipulating purified EVs, like electroporation (O'Brien et al., 2020). However, in our setting, the loading efficacy of transfected RNA was very low, as indicated by single EV flow cytometry, and would need to be optimized to deliver exogenously transcribed, therapeutic RNAs. Further, upon targeting tumor-intrinsic RIG-I, the cargo of endogenous, small non-coding RNAs within EVs shifts significantly. If bearing an uncapped 5'-triphosphate moiety or complex secondary structures, these RNAs may activate RIG-I-like receptors in EV-recipient cells. However, the individual contribution of specific RNA sequences to RIG-I-EV immunogenicity remains to be identified. One study implied that small nuclear RNAs might leak into the cytosol during cellular stress in tumor cells. They can bind and activate RIG-I culminating in IFN-I production and cell death upon chemotherapy and ionizing radiation (Ranoa et al., 2016). Significantly, two RNAs that facilitate this process, spliceosomal snRNA U1 and U2, were enriched in RIG-I-EVs, too. Another endogenous RIG-I ligand, RN7SL1, following transcriptional upregulation through NOTCH-MYC signaling in stromal cells, reportedly exceeds the shielding capacity of RNA binding proteins (RBPs) and is sorted into EVs (J. M. Diamond et al., 2018). Moreover, endogenous retroviruses might provide a source of RLR-ligands as they have also been upregulated by DNA methyltransferase inhibitor 5-azacytidine treatment. This overexpression of endogenous retroviruses, usually silenced in somatic cells, activates cytosolic RNA sensors and triggers an antiviral defense pathway increasing susceptibility against anti-CTLA4 (Chiappinelli et al., 2015). Whether nucleic acid loading into isEVs is a directed process or a stochastic event to date is still unclear. Future studies will need to determine the origins of immunostimulatory RNA and the mechanisms of its loading into isEVs. Considering the RIG-I prevalence inside EVs, one hypothesis consists of specific RNA-protein complex incorporation into EVs, albeit RIG-I is found in EV preparations regardless of activation status in the parental cell. Beyond the transfer of antigens, RIG-I-EVs shuttled immunomodulatory proteins, including RBPs and beyond, which deserves future investigation.

Active uptake of fragments from dying cells and EVs precedes tumor-specific immunity. In RIG-I-induced ICD, calreticulin is exposed on the outer membrane, known to promote phagocytosis by dendritic cells (Obeid et al., 2007). Diverse endocytic pathways can mediate EV uptake into murine BMDCs, but only macropinocytosis facilitates the IFN-I response to isEVs. Hence, engulfment of isEVs through macropinocytosis seems to deliver

immunostimulatory nucleic acids into the cytosol of myeloid cells, where innate nucleic acid receptors are typically located, Fig. 1. This requirement for macropinocytosis is consistent with earlier reports about macropinocytosis as a therapeutic nucleic acids delivery route (Desai et al., 2019). Notably, EV uptake is unaffected by RIG-I signaling in the EV's parental cell. Targeted delivery of tumor-derived DAMPs to the proper cellular compartment in the correct cell type at the right time has an evident impact on the anti-tumor immune response. Potentially, reprogramming tumor-derived EVs may target and restimulate the exact immune cell subsets previously subjected to tumor-mediated immunosuppression. However, EV-mediated communication in the tumor microenvironment is likely multidirectional and, thus, far more complex than our *in vitro* experiments reflect. Therefore, mapping the routes of immunostimulatory EVs during RIG-I activating therapies *in vivo* should unveil additional and more nuanced insights.

The immune landscape of the tumor changes significantly upon the injection of RIG-I-EVs. $CD103^+$ cDC1s populate the tumor microenvironment more densely, clinically associated with favorable outcomes in anti-PD1 treatment (Barry et al., 2018; Bottcher et al., 2018). Dendritic cells express the maturation markers MHC-II and costimulatory CD86 at higher levels, Fig. 1. Activated, IFN-γ-producing T and NK cells become more abundant in the tumor, which is an independent favorable prognostic factor (Naito et al., 1998; Schumacher et al., 2001). Likewise, NK cells can be activated by RIG-I-EVs (Dassler-Plenker et al., 2016), and, in our model, NK cells are required for RIG-I-EV-mediated antitumor immunity. As reported elsewhere, these activated NK cells may trigger the infiltration, differentiation, and survival of cDC1s, thus increasing the tumor's susceptibility to immune checkpoint blockade (Barry et al., 2018; Bottcher et al., 2018). Whether NK cells in our model facilitate the RIG-I-EV-induced T cell response or exert antitumor activity independent of T cells remains to be determined.

Being linked to disease progression through therapy resistance, preformation of metastatic niches, and suppression of immune responses, tumor-derived EVs have been mainly regarded as adversarial to overall prognosis and response to immunotherapy (Zomer & van Rheenen, 2016). Contrasting with the common conception of EVs, interfering with multivesicular endosome membrane fusion at the final steps of exosome release, gene silencing of Rab27a reduces the quantity of EVs released from B16.OVA. Notably, exposing $Rab27a^{-/-}$ B16.OVA to RIG-I agonist *in vivo* results in less antigen-specific T cell activation and unrestricted tumor growth at distant sites compared with 3pRNA treatment of WT B16.OVA, indicating a role for isEVs in the systemic antitumor immune response upon locally RIG-I activating therapies. However, the translation of isEVs needs to account for

the stromal compartment of the TME. Tumor-stroma interactions can reportedly induce EVs promoting an aggressive cancer phenotype (Nabet et al., 2017). EVs from cancer-associated fibroblasts have been shown to induce PD-L1 expression, potentially suppressing tumor-infiltrating immune cells *in vivo (Dou et al., 2020)*. Significantly, our *ex vivo* cocultures with tumor-associated fibroblasts did not impair isEV biogenesis. We do not see a dominant immunosuppressive effect of the TME on tumor-derived EVs, given the caveat that our models may not capture the complex cancer-promoting evolution of tumor-stroma interactions in cancer patients.

Evaluating the clinical relevance of intratumoral isEV biogenesis, using retrospective data from the TCGA, high EV pathway activity, according to a predefined gene set (Hurwitz et al., 2016), associated with shortened overall survival, in line with the popular conception of EVs as cancer-promoting. However, in the high EV pathway activity subgroup, patients with an increased transcription rate of *DDX58* (RIG-I) lived significantly longer than patients with low *DDX58* transcription, compatible with our isEV hypothesis. Further, a trend toward a durable response to anti-PD-1 and anti-CTLA4 ICB was observed in melanoma patients with high EV pathway and high *DDX58* transcription. A limitation to conclusions drawn from these retrospective clinical data is our preliminary understanding of EV biogenesis, as designated EV pathways overlap with other functions like intracellular trafficking of vesicles as endocytosis. In melanoma, *DDX58* expression per se has been linked to the expression of the antigen processing and presentation machinery in the tumor. In contrast, its downregulation was associated with non-responsiveness to ICB. Consistently, *ex vivo*, intratumoral RIG-I activation synergized with anti-PD-1 and anti-TIGIT in boosting T cell effector function (Such et al., 2020). In a retrospective cohort of melanoma patients, *DDX58* expression was associated with durable response and prolonged survival upon anti-CTLA4 therapy. In a murine melanoma model, intratumoral activation of RIG-I synergized with intratumoral activation of RIG-I synergized with anti-CTLA4 and its combination with anti-PD1 (Heidegger, Wintges, et al., 2019). Despite the immunostimulatory potential of EVs, their relative contribution to patients' T cell responses against RIG-I-activated tumor cells remains to be determined.

Throughout different contexts, RIG-I signaling in tumor cells triggers isEV biogenesis. For the translation of isEVs into clinical application, a thorough investigation of how RIG-I signaling does or does not impact the adverse and immunosuppressive functions of tumor-derived EVs will be critical. Based on a cumulating body of evidence, we here introduce reprogramming EV biogenesis from autologous tumor tissue under precisely defined molecular conditions as a therapeutic strategy against cancer.

Cytosolic nucleic acid-sensing emerges as a significant regulator in conventional cancer therapy and immunotherapy. cGAS/STING signaling in myeloid cells contributes to anti-CTLA-4 plus anti-PDL1 (Schadt et al., 2019), and previous research of our group identified RIG-I/MAVS to govern the response towards anti-CTLA4 alone or together with anti-PD1 (Heidegger, Wintges, et al., 2019). Irradiation (J. M. Diamond et al., 2018; Ranoa et al., 2016), demethylating agents, and chemotherapies (Chiappinelli et al., 2015) can activate cytosolic nucleic acid receptors, thereby enhancing the effect of ICB (Poeck et al., 2021). Herein, under certain circumstances, endogenous immunostimulatory nucleic acids can activate innate immune receptors through transcriptional upregulation, evasion of shielding proteins, specific packaging into EVs, and hitherto unknown mechanisms (O'Brien et al., 2020). Hence, investigating the role of cytosolic nucleic acid receptors in cancer immunosurveillance opens promising translational opportunities. These opportunities may include expanding the benefits of ICB to more patients and the precise prediction of individual therapy responses. Depending on molecular characteristics and immune infiltration of individual tumors, the strategic combination of RIG-I activating therapies or autologous cancer vaccines with specific immunotherapies might be more effective than each monotherapy.

In summary, our results identify tumor-intrinsic RIG-I signaling to:

a) Induce IFN-I-dependent immunogenic programmed tumor cell death,
b) alter the composition and thus the immunomodulatory function of tumor-derived EVs, turning them into personalized anticancer vaccines,
c) critically regulate therapy response to immune checkpoint blockade.

Ultimately, exploiting cytosolic nucleic acid sensing in the tumor and its microenvironment is a promising strategy to improve cancer immunosurveillance.

Fig. 1: Schematic overview of findings on RIG-I-induced mechanisms supporting cancer immunosurveillance.

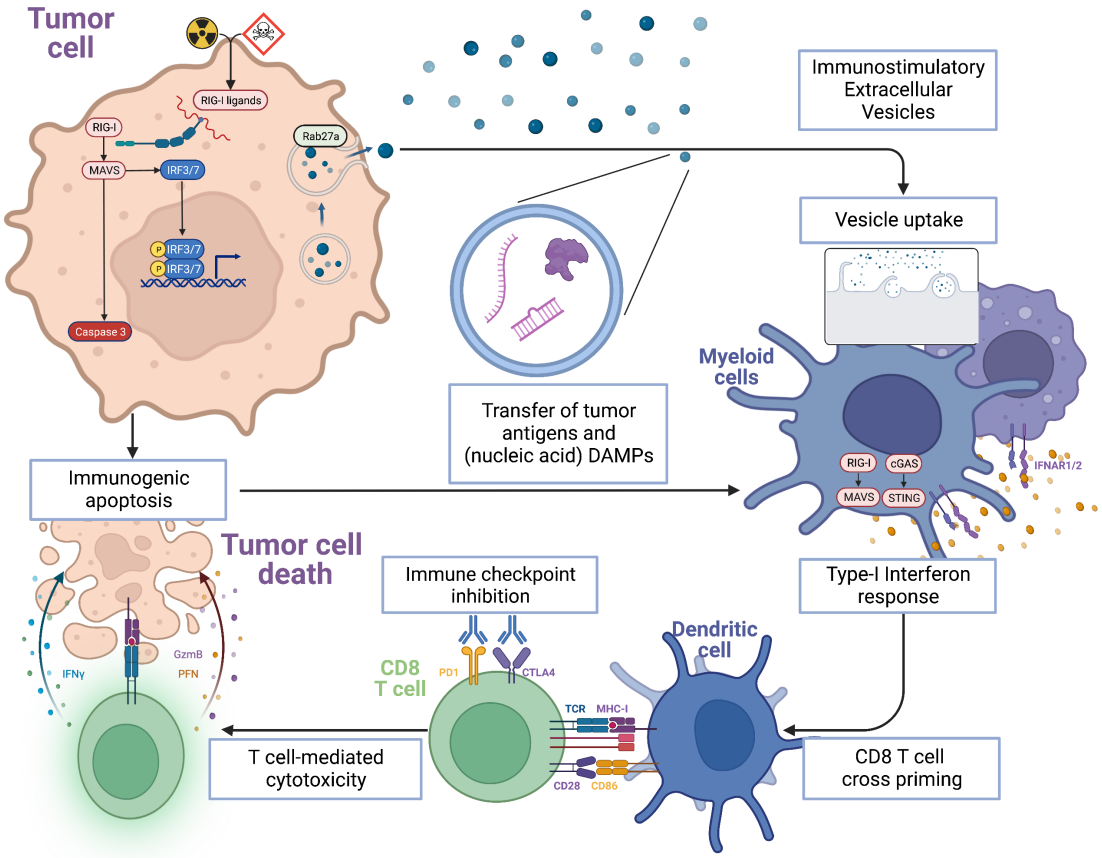

Tumor-intrinsic RIG-I signaling via adapter protein MAVS and IRF transcription factors induces Caspase-3-dependent immunogenic apoptosis and the generation of immunostimulatory EVs. Hereby, tumor antigens and DAMPs are released. The uptake of immunostimulatory EVs by macropinocytosis and cytosolic nucleic acid sensing mediates substantial IFN-I release. In the following type-I interferon response, antigen-presenting cells are activated, and prime tumor antigen-specific T cells. These RIG-I-induced mechanisms result in an anti-tumor T cell response enhancing local and systemic cancer immunosurveillance.

8. List of abbreviations

ATP	Adenosine triphosphate
Batf3	Basic leucine zipper transcription factor ATF-like 3
BMDC	Bone marrow-derived dendritic cell
CARD	Caspase recruitment and activation domain
Caspase	Cysteinyl-aspartate specific protease
CCL	C-C motif chemokine ligand
CD	Cluster of differentiation
cDC1	Conventional dendritic cell type 1
cGAS	Cyclic GMP–AMP (cGAMP) synthase
CRISPR	Clustered regularly interspaced short palindromic repeats
CTLA4	Cytotoxic T-lymphocyte-associated Protein 4
CXCL	C-X-C motif chemokine ligand
DAMP	Danger-associated molecular pattern
Dxd58	DExD/H-box helicase 58 (gene encoding RIG-I)
DC	Dendritic cell
ELISA	Enzyme-linked immunosorbent assay
ESCRT	Endosomal sorting complex required for transport
EV	Extracellular vesicle
FLT3L	FMS-like tyrosine kinase 3 ligand
HLA	Human leukocyte antigen
HMGB1	High mobility group box 1
ICD	Immunogenic cell death
IFN	Interferon
IFN-I	Type-I interferon
IFNaR	Type-I interferon receptor
IL	Interleukin
ILV	Intraluminal vesicles
IRDS	Interferon-related DNA-damage resistance signature
IRF	Interferon regulatory factor
isEV	Immunostimulatory EV
LGP2	Laboratory of Genetics and Physiology 2

MAVS	Mitochondrial antiviral-signaling protein
MDA5	Melanoma differentiation-associated protein 5
MHC-I / -II	Major histocompatibility complex class I / class II
MVE	Multivesicular endosome
NF-κb	Nuclear factor kappa B
NKG2D	Natural killer group 2D
NLRP3	NOD-, LRR- and pyrin domain-containing protein 3
OVA	Ovalbumin
PAMP	Pathogen-associated molecular pattern
Pol-3	RNA polymerase III
PD1	Programmed cell death protein 1
PRR	Pattern recognition receptor
Rab27a	Ras-related protein 27a
RAG2	Recombination activating gene 2
RBP	RNA-binding proteins
RIG-I	Retinoic acid inducible gene I
RLR	RIG-I like receptor
STING	Stimulator of interferon genes
STAT1	Signal transducer and activator of transcription 1
TBK1	TANK-binding kinase 1
TCGA	The Cancer Genome Atlas
Th1	Type 1 T helper
Treg	Regulatory T cell
TLR	Toll-like receptors
TNF	Tumor necrosis factor
WT	Wild-type
XCL	X-C motif chemokine ligand

9. References

Ablasser, A., Bauernfeind, F., Hartmann, G., Latz, E., Fitzgerald, K. A., & Hornung, V. (2009). RIG-I-dependent sensing of poly(dA:dT) through the induction of an RNA polymerase III-transcribed RNA intermediate. *Nat Immunol, 10*(10), 1065-1072. doi:10.1038/ni.1779

Ahn, J., Xia, T., Konno, H., Konno, K., Ruiz, P., & Barber, G. N. (2014). Inflammation-driven carcinogenesis is mediated through STING. *Nat Commun, 5*, 5166. doi:10.1038/ncomms6166

Albert, M. L., Sauter, B., & Bhardwaj, N. (1998). Dendritic cells acquire antigen from apoptotic cells and induce class I-restricted CTLs. *Nature, 392*(6671), 86-89. doi:10.1038/32183

Amarante-Mendes, G. P., Adjemian, S., Branco, L. M., Zanetti, L. C., Weinlich, R., & Bortoluci, K. R. (2018). Pattern Recognition Receptors and the Host Cell Death Molecular Machinery. *Front Immunol, 9*, 2379. doi:10.3389/fimmu.2018.02379

Andreola, G., Rivoltini, L., Castelli, C., Huber, V., Perego, P., Deho, P., . . . Fais, S. (2002). Induction of lymphocyte apoptosis by tumor cell secretion of FasL-bearing microvesicles. *J Exp Med, 195*(10), 1303-1316. doi:10.1084/jem.20011624

Apetoh, L., Ghiringhelli, F., Tesniere, A., Obeid, M., Ortiz, C., Criollo, A., . . . Zitvogel, L. (2007). Toll-like receptor 4-dependent contribution of the immune system to anticancer chemotherapy and radiotherapy. *Nat Med, 13*(9), 1050-1059. doi:10.1038/nm1622

Baglio, S. R., van Eijndhoven, M. A., Koppers-Lalic, D., Berenguer, J., Lougheed, S. M., Gibbs, S., . . . Pegtel, D. M. (2016). Sensing of latent EBV infection through exosomal transfer of 5'pppRNA. *Proc Natl Acad Sci U S A, 113*(5), E587-596. doi:10.1073/pnas.1518130113

Balachandran, V. P., Luksza, M., Zhao, J. N., Makarov, V., Moral, J. A., Remark, R., . . . Leach, S. D. (2017). Identification of unique neoantigen qualities in long-term survivors of pancreatic cancer. *Nature, 551*(7681), 512-516. doi:10.1038/nature24462

Barry, K. C., Hsu, J., Broz, M. L., Cueto, F. J., Binnewies, M., Combes, A. J., . . . Krummel, M. F. (2018). A natural killer-dendritic cell axis defines checkpoint therapy-responsive tumor microenvironments. *Nat Med, 24*(8), 1178-1191. doi:10.1038/s41591-018-0085-8

Battisti, F., Napoletano, C., Rahimi Koshkaki, H., Belleudi, F., Zizzari, I. G., Ruscito, I., . . . Rughetti, A. (2017). Tumor-Derived Microvesicles Modulate Antigen Cross-Processing via Reactive Oxygen Species-Mediated Alkalinization of Phagosomal Compartment in Dendritic Cells. *Front Immunol, 8*, 1179. doi:10.3389/fimmu.2017.01179

Bek, S., Stritzke, F., Wintges, A., Nedelko, T., Bohmer, D. F. R., Fischer, J. C., . . . Heidegger, S. (2019). Targeting intrinsic RIG-I signaling turns melanoma cells into

type I interferon-releasing cellular antitumor vaccines. *Oncoimmunology, 8*(4), e1570779. doi:10.1080/2162402X.2019.1570779

Benci, J. L., Xu, B., Qiu, Y., Wu, T. J., Dada, H., Twyman-Saint Victor, C., . . . Minn, A. J. (2016). Tumor Interferon Signaling Regulates a Multigenic Resistance Program to Immune Checkpoint Blockade. *Cell, 167*(6), 1540-1554 e1512. doi:10.1016/j.cell.2016.11.022

Besch, R., Poeck, H., Hohenauer, T., Senft, D., Hacker, G., Berking, C., . . . Hartmann, G. (2009). Proapoptotic signaling induced by RIG-I and MDA-5 results in type I interferon-independent apoptosis in human melanoma cells. *J Clin Invest, 119*(8), 2399-2411. doi:10.1172/JCI37155

Bolukbasi, M. F., Mizrak, A., Ozdener, G. B., Madlener, S., Strobel, T., Erkan, E. P., . . . Saydam, O. (2012). miR-1289 and "Zipcode"-like Sequence Enrich mRNAs in Microvesicles. *Mol Ther Nucleic Acids, 1*, e10. doi:10.1038/mtna.2011.2

Bottcher, J. P., Bonavita, E., Chakravarty, P., Blees, H., Cabeza-Cabrerizo, M., Sammicheli, S., . . . Reis e Sousa, C. (2018). NK Cells Stimulate Recruitment of cDC1 into the Tumor Microenvironment Promoting Cancer Immune Control. *Cell, 172*(5), 1022-1037 e1014. doi:10.1016/j.cell.2018.01.004

Bottcher, J. P., & Reis e Sousa, C. (2018). The Role of Type 1 Conventional Dendritic Cells in Cancer Immunity. *Trends Cancer, 4*(11), 784-792. doi:10.1016/j.trecan.2018.09.001

Brahmer, J. R., Tykodi, S. S., Chow, L. Q., Hwu, W. J., Topalian, S. L., Hwu, P., . . . Wigginton, J. M. (2012). Safety and activity of anti-PD-L1 antibody in patients with advanced cancer. *N Engl J Med, 366*(26), 2455-2465. doi:10.1056/NEJMoa1200694

Broz, M. L., Binnewies, M., Boldajipour, B., Nelson, A. E., Pollack, J. L., Erle, D. J., . . . Krummel, M. F. (2014). Dissecting the tumor myeloid compartment reveals rare activating antigen-presenting cells critical for T cell immunity. *Cancer Cell, 26*(5), 638-652. doi:10.1016/j.ccell.2014.09.007

Bu, Y., Liu, F., Jia, Q. A., & Yu, S. N. (2016). Decreased Expression of TMEM173 Predicts Poor Prognosis in Patients with Hepatocellular Carcinoma. *PLoS One, 11*(11), e0165681. doi:10.1371/journal.pone.0165681

Burnet, F. M. (1967). Immunological aspects of malignant disease. *Lancet, 1*(7501), 1171-1174. doi:10.1016/s0140-6736(67)92837-1

Burstein, M. D., Tsimelzon, A., Poage, G. M., Covington, K. R., Contreras, A., Fuqua, S. A. W., . . . Brown, P. H. (2015). Comprehensive Genomic Analysis Identifies Novel Subtypes and Targets of Triple-Negative Breast Cancer. *Clinical Cancer Research, 21*(7), 1688-1698. doi:10.1158/1078-0432.ccr-14-0432

Chekeni, F. B., Elliott, M. R., Sandilos, J. K., Walk, S. F., Kinchen, J. M., Lazarowski, E. R., . . . Ravichandran, K. S. (2010). Pannexin 1 channels mediate 'find-me' signal release and membrane permeability during apoptosis. *Nature, 467*(7317), 863-867. doi:10.1038/nature09413

Chen, G., Huang, A. C., Zhang, W., Zhang, G., Wu, M., Xu, W., . . . Guo, W. (2018). Exosomal PD-L1 contributes to immunosuppression and is associated with anti-PD-1 response. *Nature, 560*(7718), 382-386. doi:10.1038/s41586-018-0392-8

Chen, Q., Boire, A., Jin, X., Valiente, M., Er, E. E., Lopez-Soto, A., . . . Massague, J. (2016). Carcinoma-astrocyte gap junctions promote brain metastasis by cGAMP transfer. *Nature, 533*(7604), 493-498. doi:10.1038/nature18268

Cheon, H., & Stark, G. R. (2009). Unphosphorylated STAT1 prolongs the expression of interferon-induced immune regulatory genes. *Proceedings of the National Academy of Sciences, 106*(23), 9373-9378. doi:10.1073/pnas.0903487106

Chiang, J. J., Sparrer, K. M. J., van Gent, M., Lassig, C., Huang, T., Osterrieder, N., . . . Gack, M. U. (2018). Viral unmasking of cellular 5S rRNA pseudogene transcripts induces RIG-I-mediated immunity. *Nat Immunol, 19*(1), 53-62. doi:10.1038/s41590-017-0005-y

Chiappinelli, K. B., Strissel, P. L., Desrichard, A., Li, H., Henke, C., Akman, B., . . . Strick, R. (2015). Inhibiting DNA Methylation Causes an Interferon Response in Cancer via dsRNA Including Endogenous Retroviruses. *Cell, 162*(5), 974-986. doi:10.1016/j.cell.2015.07.011

Chiu, Y. H., Macmillan, J. B., & Chen, Z. J. (2009). RNA polymerase III detects cytosolic DNA and induces type I interferons through the RIG-I pathway. *Cell, 138*(3), 576-591. doi:10.1016/j.cell.2009.06.015

Consortium, R. N., Petrov, A. I., Kay, S. J. E., Gibson, R., Kulesha, E., Staines, D., . . . Pruitt, K. D. (2015). RNAcentral: an international database of ncRNA sequences. *Nucleic Acids Res, 43*(Database issue), D123-129. doi:10.1093/nar/gku991

Couzin-Frankel, J. (2013). Breakthrough of the year 2013. Cancer immunotherapy. *Science, 342*(6165), 1432-1433. doi:10.1126/science.342.6165.1432

D'Souza-Schorey, C., & Clancy, J. W. (2012). Tumor-derived microvesicles: shedding light on novel microenvironment modulators and prospective cancer biomarkers. *Genes & Development, 26*(12), 1287-1299. doi:10.1101/gad.192351.112

Dassler-Plenker, J., Reiners, K. S., van den Boorn, J. G., Hansen, H. P., Putschli, B., Barnert, S., . . . Coch, C. (2016). RIG-I activation induces the release of extracellular vesicles with antitumor activity. *Oncoimmunology, 5*(10), e1219827. doi:10.1080/2162402X.2016.1219827

Demaria, O., De Gassart, A., Coso, S., Gestermann, N., Di Domizio, J., Flatz, L., . . . Gilliet, M. (2015). STING activation of tumor endothelial cells initiates spontaneous and therapeutic antitumor immunity. *Proc Natl Acad Sci U S A, 112*(50), 15408-15413. doi:10.1073/pnas.1512832112

Deng, L., Liang, H., Xu, M., Yang, X., Burnette, B., Arina, A., . . . Weichselbaum, R. R. (2014). STING-Dependent Cytosolic DNA Sensing Promotes Radiation-Induced Type I Interferon-Dependent Antitumor Immunity in Immunogenic Tumors. *Immunity, 41*(5), 843-852. doi:10.1016/j.immuni.2014.10.019

Desai, A. S., Hunter, M. R., & Kapustin, A. N. (2019). Using macropinocytosis for intracellular delivery of therapeutic nucleic acids to tumour cells. *Philos Trans R Soc Lond B Biol Sci, 374*(1765), 20180156. doi:10.1098/rstb.2018.0156

Diamond, J. M., Vanpouille-Box, C., Spada, S., Rudqvist, N. P., Chapman, J. R., Ueberheide, B. M., . . . Demaria, S. (2018). Exosomes Shuttle TREX1-Sensitive IFN-Stimulatory dsDNA from Irradiated Cancer Cells to DCs. *Cancer Immunol Res, 6*(8), 910-920. doi:10.1158/2326-6066.CIR-17-0581

Diamond, M. S., Kinder, M., Matsushita, H., Mashayekhi, M., Dunn, G. P., Archambault, J. M., . . . Schreiber, R. D. (2011). Type I interferon is selectively required by dendritic cells for immune rejection of tumors. *J Exp Med, 208*(10), 1989-2003. doi:10.1084/jem.20101158

Doherty, M. R., Cheon, H., Junk, D. J., Vinayak, S., Varadan, V., Telli, M. L., . . . Jackson, M. W. (2017). Interferon-beta represses cancer stem cell properties in triple-negative breast cancer. *Proceedings of the National Academy of Sciences, 114*(52), 13792-13797. doi:10.1073/pnas.1713728114

Dou, D., Ren, X., Han, M., Xu, X., Ge, X., Gu, Y., & Wang, X. (2020). Cancer-Associated Fibroblasts-Derived Exosomes Suppress Immune Cell Function in Breast Cancer via the miR-92/PD-L1 Pathway. *Front Immunol, 11*, 2026. doi:10.3389/fimmu.2020.02026

Duan, Q., Zhang, H., Zheng, J., & Zhang, L. (2020). Turning Cold into Hot: Firing up the Tumor Microenvironment. *Trends Cancer, 6*(7), 605-618. doi:10.1016/j.trecan.2020.02.022

Duewell, P., Steger, A., Lohr, H., Bourhis, H., Hoelz, H., Kirchleitner, S. V., . . . Schnurr, M. (2014). RIG-I-like helicases induce immunogenic cell death of pancreatic cancer cells and sensitize tumors toward killing by CD8(+) T cells. *Cell Death Differ, 21*(12), 1825-1837. doi:10.1038/cdd.2014.96

Dunn, G. P., Old, L. J., & Schreiber, R. D. (2004). The three Es of cancer immunoediting. *Annu Rev Immunol, 22*, 329-360. doi:10.1146/annurev.immunol.22.012703.104803

Ehrlich, P. (1909). Ueber den jetzigen Stand der Karzinomforschung. *Ned Tijdschr Geneeskd, 5*, 273–290.

Fournier, P., Wilden, H., & Schirrmacher, V. (2012). Importance of retinoic acid-inducible gene I and of receptor for type I interferon for cellular resistance to infection by Newcastle disease virus. *Int J Oncol, 40*(1), 287-298. doi:10.3892/ijo.2011.1222

Fuertes, M. B., Kacha, A. K., Kline, J., Woo, S. R., Kranz, D. M., Murphy, K. M., & Gajewski, T. F. (2011). Host type I IFN signals are required for antitumor CD8+ T cell responses through CD8{alpha}+ dendritic cells. *J Exp Med, 208*(10), 2005-2016. doi:10.1084/jem.20101159

Gajewski, T. F. (2015). The Next Hurdle in Cancer Immunotherapy: Overcoming the Non-T-Cell-Inflamed Tumor Microenvironment. *Semin Oncol, 42*(4), 663-671. doi:10.1053/j.seminoncol.2015.05.011

Galluzzi, L., Buque, A., Kepp, O., Zitvogel, L., & Kroemer, G. (2015). Immunological Effects of Conventional Chemotherapy and Targeted Anticancer Agents. *Cancer Cell, 28*(6), 690-714. doi:10.1016/j.ccell.2015.10.012

Galluzzi, L., Buque, A., Kepp, O., Zitvogel, L., & Kroemer, G. (2017). Immunogenic cell death in cancer and infectious disease. *Nat Rev Immunol, 17*(2), 97-111. doi:10.1038/nri.2016.107

Gardner, A., & Ruffell, B. (2016). Dendritic Cells and Cancer Immunity. *Trends Immunol, 37*(12), 855-865. doi:10.1016/j.it.2016.09.006

Gibbings, D. J., Ciaudo, C., Erhardt, M., & Voinnet, O. (2009). Multivesicular bodies associate with components of miRNA effector complexes and modulate miRNA activity. *Nat Cell Biol, 11*(9), 1143-1149. doi:10.1038/ncb1929

Gubin, M. M., Zhang, X., Schuster, H., Caron, E., Ward, J. P., Noguchi, T., . . . Schreiber, R. D. (2014). Checkpoint blockade cancer immunotherapy targets tumour-specific mutant antigens. *Nature, 515*(7528), 577-581. doi:10.1038/nature13988

Hanahan, D., & Weinberg, R. A. (2011). Hallmarks of cancer: the next generation. *Cell, 144*(5), 646-674. doi:10.1016/j.cell.2011.02.013

Harding, F. A., McArthur, J. G., Gross, J. A., Raulet, D. H., & Allison, J. P. (1992). CD28-mediated signalling co-stimulates murine T cells and prevents induction of anergy in T-cell clones. *Nature, 356*(6370), 607-609. doi:10.1038/356607a0

Harding, S. M., Benci, J. L., Irianto, J., Discher, D. E., Minn, A. J., & Greenberg, R. A. (2017). Mitotic progression following DNA damage enables pattern recognition within micronuclei. *Nature, 548*(7668), 466-470. doi:10.1038/nature23470

Heidegger, S., Kreppel, D., Bscheider, M., Stritzke, F., Nedelko, T., Wintges, A., . . . Poeck, H. (2019). RIG-I activating immunostimulatory RNA boosts the efficacy of anticancer vaccines and synergizes with immune checkpoint blockade. *EBioMedicine, 41*, 146-155. doi:10.1016/j.ebiom.2019.02.056

Heidegger, S., Wintges, A., Stritzke, F., Bek, S., Steiger, K., Koenig, P. A., . . . Poeck, H. (2019). RIG-I activation is critical for responsiveness to checkpoint blockade. *Sci Immunol, 4*(39), eaau8943. doi:10.1126/sciimmunol.aau8943

Hodi, F. S., O'Day, S. J., McDermott, D. F., Weber, R. W., Sosman, J. A., Haanen, J. B., . . . Urba, W. J. (2010). Improved survival with ipilimumab in patients with metastatic melanoma. *N Engl J Med, 363*(8), 711-723. doi:10.1056/NEJMoa1003466

Hornung, V., Ellegast, J., Kim, S., Brzozka, K., Jung, A., Kato, H., . . . Hartmann, G. (2006). 5'-Triphosphate RNA is the ligand for RIG-I. *Science, 314*(5801), 994-997. doi:10.1126/science.1132505

Hu, J., He, Y., Yan, M., Zhu, C., Ye, W., Zhu, H., . . . Zhang, Z. (2013). Dose dependent activation of retinoic acid-inducible gene-I promotes both proliferation and apoptosis signals in human head and neck squamous cell carcinoma. *PLoS One, 8*(3), e58273. doi:10.1371/journal.pone.0058273

Hurwitz, S. N., Rider, M. A., Bundy, J. L., Liu, X., Singh, R. K., & Meckes, D. G., Jr. (2016). Proteomic profiling of NCI-60 extracellular vesicles uncovers common protein cargo

and cancer type-specific biomarkers. *Oncotarget, 7*(52), 86999-87015. doi:10.18632/oncotarget.13569

International Agency for Research on Cancer, W. H. O. (2022). CANCER TOMORROW. Retrieved from https://gco.iarc.fr/tomorrow/en/dataviz/isotype?types=0&single_unit=500000

Iurescia, S., Fioretti, D., & Rinaldi, M. (2020). The Innate Immune Signalling Pathways: Turning RIG-I Sensor Activation Against Cancer. *Cancers (Basel), 12*(11), 3158. doi:10.3390/cancers12113158

Jager, E., Nagata, Y., Gnjatic, S., Wada, H., Stockert, E., Karbach, J., . . . Knuth, A. (2000). Monitoring CD8 T cell responses to NY-ESO-1: correlation of humoral and cellular immune responses. *Proc Natl Acad Sci U S A, 97*(9), 4760-4765. doi:10.1073/pnas.97.9.4760

Jahn, R., & Scheller, R. H. (2006). SNAREs — engines for membrane fusion. *Nature Reviews Molecular Cell Biology, 7*(9), 631-643. doi:10.1038/nrm2002

Janeway, C. A., Jr. (1992). The immune system evolved to discriminate infectious nonself from noninfectious self. *Immunol Today, 13*(1), 11-16. doi:10.1016/0167-5699(92)90198-G

Jeppesen, D. K., Fenix, A. M., Franklin, J. L., Higginbotham, J. N., Zhang, Q., Zimmerman, L. J., . . . Coffey, R. J. (2019). Reassessment of Exosome Composition. *Cell, 177*(2), 428-445.e418. doi:10.1016/j.cell.2019.02.029

Johnson, L. R., Lee, D. Y., Eacret, J. S., Ye, D., June, C. H., & Minn, A. J. (2021). The immunostimulatory RNA RN7SL1 enables CAR-T cells to enhance autonomous and endogenous immune function. *Cell, 184*(19), 4981-4995 e4914. doi:10.1016/j.cell.2021.08.004

Kawai, T., & Akira, S. (2010). The role of pattern-recognition receptors in innate immunity: update on Toll-like receptors. *Nat Immunol, 11*(5), 373-384. doi:10.1038/ni.1863

Kepp, O., Senovilla, L., Vitale, I., Vacchelli, E., Adjemian, S., Agostinis, P., . . . Galluzzi, L. (2014). Consensus guidelines for the detection of immunogenic cell death. *Oncoimmunology, 3*(9), e955691. doi:10.4161/21624011.2014.955691

Kitai, Y., Kawasaki, T., Sueyoshi, T., Kobiyama, K., Ishii, K. J., Zou, J., . . . Kawai, T. (2017). DNA-Containing Exosomes Derived from Cancer Cells Treated with Topotecan Activate a STING-Dependent Pathway and Reinforce Antitumor Immunity. *J Immunol, 198*(4), 1649-1659. doi:10.4049/jimmunol.1601694

Kroemer, G., Galluzzi, L., Kepp, O., & Zitvogel, L. (2013). Immunogenic cell death in cancer therapy. *Annu Rev Immunol, 31*, 51-72. doi:10.1146/annurev-immunol-032712-100008

Lafferty, K. J., & Cunningham, A. J. (1975). A new analysis of allogeneic interactions. *Aust J Exp Biol Med Sci, 53*(1), 27-42. doi:10.1038/icb.1975.3

Lee, Y., Auh, S. L., Wang, Y., Burnette, B., Wang, Y., Meng, Y., . . . Fu, Y. X. (2009). Therapeutic effects of ablative radiation on local tumor require CD8+ T cells:

changing strategies for cancer treatment. *Blood, 114*(3), 589-595. doi:10.1182/blood-2009-02-206870

Linsley, P. S., Greene, J. L., Brady, W., Bajorath, J., Ledbetter, J. A., & Peach, R. (1994). Human B7-1 (CD80) and B7-2 (CD86) bind with similar avidities but distinct kinetics to CD28 and CTLA-4 receptors. *Immunity, 1*(9), 793-801. doi:10.1016/s1074-7613(94)80021-9

Liu, S., Lachapelle, J., Leung, S., Gao, D., Foulkes, W. D., & Nielsen, T. O. (2012). CD8+ lymphocyte infiltration is an independent favorable prognostic indicator in basal-like breast cancer. *Breast Cancer Res, 14*(2), R48. doi:10.1186/bcr3148

Liu, Y., Goulet, M. L., Sze, A., Hadj, S. B., Belgnaoui, S. M., Lababidi, R. R., . . . Lin, R. (2016). RIG-I-Mediated STING Upregulation Restricts Herpes Simplex Virus 1 Infection. *J Virol, 90*(20), 9406-9419. doi:10.1128/JVI.00748-16

Liu, Z., Han, C., & Fu, Y. X. (2020). Targeting innate sensing in the tumor microenvironment to improve immunotherapy. *Cell Mol Immunol, 17*(1), 13-26. doi:10.1038/s41423-019-0341-y

Mackenzie, K. J., Carroll, P., Martin, C. A., Murina, O., Fluteau, A., Simpson, D. J., . . . Jackson, A. P. (2017). cGAS surveillance of micronuclei links genome instability to innate immunity. *Nature, 548*(7668), 461-465. doi:10.1038/nature23449

Marar, C., Starich, B., & Wirtz, D. (2021). Extracellular vesicles in immunomodulation and tumor progression. *Nat Immunol, 22*(5), 560-570. doi:10.1038/s41590-021-00899-0

Marcus, A., Mao, A. J., Lensink-Vasan, M., Wang, L., Vance, R. E., & Raulet, D. H. (2018). Tumor-Derived cGAMP Triggers a STING-Mediated Interferon Response in Non-tumor Cells to Activate the NK Cell Response. *Immunity, 49*(4), 754-763 e754. doi:10.1016/j.immuni.2018.09.016

Matzinger, P. (1994). Tolerance, danger, and the extended family. *Annu Rev Immunol, 12*, 991-1045. doi:10.1146/annurev.iy.12.040194.005015

Melief, C. J. (2008). Cancer immunotherapy by dendritic cells. *Immunity, 29*(3), 372-383. doi:10.1016/j.immuni.2008.08.004

Mellman, I., Coukos, G., & Dranoff, G. (2011). Cancer immunotherapy comes of age. *Nature, 480*(7378), 480-489. doi:10.1038/nature10673

Michallet, M. C., Meylan, E., Ermolaeva, M. A., Vazquez, J., Rebsamen, M., Curran, J., . . . Tschopp, J. (2008). TRADD protein is an essential component of the RIG-like helicase antiviral pathway. *Immunity, 28*(5), 651-661. doi:10.1016/j.immuni.2008.03.013

Michaud, M., Martins, I., Sukkurwala, A. Q., Adjemian, S., Ma, Y., Pellegatti, P., . . . Kroemer, G. (2011). Autophagy-dependent anticancer immune responses induced by chemotherapeutic agents in mice. *Science, 334*(6062), 1573-1577. doi:10.1126/science.1208347

Morelli, A. E., Larregina, A. T., Shufesky, W. J., Sullivan, M. L., Stolz, D. B., Papworth, G. D., . . . Thomson, A. W. (2004). Endocytosis, intracellular sorting, and processing of

exosomes by dendritic cells. *Blood, 104*(10), 3257-3266. doi:10.1182/blood-2004-03-0824

Mulcahy, L. A., Pink, R. C., & Carter, D. R. (2014). Routes and mechanisms of extracellular vesicle uptake. *J Extracell Vesicles, 3*. doi:10.3402/jev.v3.24641

Nabet, B. Y., Qiu, Y., Shabason, J. E., Wu, T. J., Yoon, T., Kim, B. C., . . . Minn, A. J. (2017). Exosome RNA Unshielding Couples Stromal Activation to Pattern Recognition Receptor Signaling in Cancer. *Cell, 170*(2), 352-366 e313. doi:10.1016/j.cell.2017.06.031

Naito, Y., Saito, K., Shiiba, K., Ohuchi, A., Saigenji, K., Nagura, H., & Ohtani, H. (1998). CD8+ T cells infiltrated within cancer cell nests as a prognostic factor in human colorectal cancer. *Cancer Res, 58*(16), 3491-3494. doi:58(16):3491-4

Nandakumar, R., Tschismarov, R., Meissner, F., Prabakaran, T., Krissanaprasit, A., Farahani, E., . . . Paludan, S. R. (2019). Intracellular bacteria engage a STING-TBK1-MVB12b pathway to enable paracrine cGAS-STING signalling. *Nat Microbiol, 4*(4), 701-713. doi:10.1038/s41564-019-0367-z

O'Brien, K., Breyne, K., Ughetto, S., Laurent, L. C., & Breakefield, X. O. (2020). RNA delivery by extracellular vesicles in mammalian cells and its applications. *Nat Rev Mol Cell Biol, 21*(10), 585-606. doi:10.1038/s41580-020-0251-y

Obeid, M., Tesniere, A., Ghiringhelli, F., Fimia, G. M., Apetoh, L., Perfettini, J. L., . . . Kroemer, G. (2007). Calreticulin exposure dictates the immunogenicity of cancer cell death. *Nat Med, 13*(1), 54-61. doi:10.1038/nm1523

Ostrowski, M., Carmo, N. B., Krumeich, S., Fanget, I., Raposo, G., Savina, A., . . . Thery, C. (2010). Rab27a and Rab27b control different steps of the exosome secretion pathway. *Nat Cell Biol, 12*(1), 19-30. doi:10.1038/ncb2000

Ott, P. A., Hu, Z., Keskin, D. B., Shukla, S. A., Sun, J., Bozym, D. J., . . . Wu, C. J. (2017). An immunogenic personal neoantigen vaccine for patients with melanoma. *Nature, 547*(7662), 217-221. doi:10.1038/nature22991

Paludan, S. R., Reinert, L. S., & Hornung, V. (2019). DNA-stimulated cell death: implications for host defence, inflammatory diseases and cancer. *Nat Rev Immunol, 19*(3), 141-153. doi:10.1038/s41577-018-0117-0

Panaretakis, T., Kepp, O., Brockmeier, U., Tesniere, A., Bjorklund, A. C., Chapman, D. C., . . . Kroemer, G. (2009). Mechanisms of pre-apoptotic calreticulin exposure in immunogenic cell death. *EMBO J, 28*(5), 578-590. doi:10.1038/emboj.2009.1

Parikh, A. R., Szabolcs, A., Allen, J. N., Clark, J. W., Wo, J. Y., Raabe, M., . . . Hong, T. S. (2021). Radiation therapy enhances immunotherapy response in microsatellite stable colorectal and pancreatic adenocarcinoma in a phase II trial. *Nat Cancer, 2*(11), 1124-1135. doi:10.1038/s43018-021-00269-7

Perez-Hernandez, D., Gutierrez-Vazquez, C., Jorge, I., Lopez-Martin, S., Ursa, A., Sanchez-Madrid, F., . . . Yanez-Mo, M. (2013). The intracellular interactome of tetraspanin-enriched microdomains reveals their function as sorting machineries toward exosomes. *J Biol Chem, 288*(17), 11649-11661. doi:10.1074/jbc.M112.445304

Piccin, A., Murphy, W. G., & Smith, O. P. (2007). Circulating microparticles: pathophysiology and clinical implications. *Blood Rev, 21*(3), 157-171. doi:10.1016/j.blre.2006.09.001

Pichlmair, A., Schulz, O., Tan, C. P., Naslund, T. I., Liljestrom, P., Weber, F., & Reis e Sousa, C. (2006). RIG-I-mediated antiviral responses to single-stranded RNA bearing 5'-phosphates. *Science, 314*(5801), 997-1001. doi:10.1126/science.1132998

Poeck, H., Bscheider, M., Gross, O., Finger, K., Roth, S., Rebsamen, M., . . . Ruland, J. (2010). Recognition of RNA virus by RIG-I results in activation of CARD9 and inflammasome signaling for interleukin 1 beta production. *Nat Immunol, 11*(1), 63-69. doi:10.1038/ni.1824

Poeck, H., Wintges, A., Dahl, S., Bassermann, F., Haas, T., & Heidegger, S. (2021). Tumor cell-intrinsic RIG-I signaling governs synergistic effects of immunogenic cancer therapies and checkpoint inhibitors in mice. *Eur J Immunol, 51*(6), 1531-1534. doi:10.1002/eji.202049158

Rajput, A., Kovalenko, A., Bogdanov, K., Yang, S. H., Kang, T. B., Kim, J. C., . . . Wallach, D. (2011). RIG-I RNA helicase activation of IRF3 transcription factor is negatively regulated by caspase-8-mediated cleavage of the RIP1 protein. *Immunity, 34*(3), 340-351. doi:10.1016/j.immuni.2010.12.018

Ranoa, D. R. E., Parekh, A. D., Pitroda, S. P., Huang, X., Darga, T., Wong, A. C., . . . Khodarev, N. N. (2016). Cancer therapies activate RIG-I-like receptor pathway through endogenous non-coding RNAs. *Oncotarget, 7*(18). doi:7:26496-26515

Rehwinkel, J., & Gack, M. U. (2020). RIG-I-like receptors: their regulation and roles in RNA sensing. *Nat Rev Immunol, 20*(9), 537-551. doi:10.1038/s41577-020-0288-3

Reits, E. A., Hodge, J. W., Herberts, C. A., Groothuis, T. A., Chakraborty, M., Wansley, E. K., . . . Neefjes, J. J. (2006). Radiation modulates the peptide repertoire, enhances MHC class I expression, and induces successful antitumor immunotherapy. *J Exp Med, 203*(5), 1259-1271. doi:10.1084/jem.20052494

Ricklefs, F. L., Alayo, Q., Krenzlin, H., Mahmoud, A. B., Speranza, M. C., Nakashima, H., . . . Chiocca, E. A. (2018). Immune evasion mediated by PD-L1 on glioblastoma-derived extracellular vesicles. *Sci Adv, 4*(3), eaar2766. doi:10.1126/sciadv.aar2766

Rizvi, N. A., Hellmann, M. D., Snyder, A., Kvistborg, P., Makarov, V., Havel, J. J., . . . Chan, T. A. (2015). Cancer immunology. Mutational landscape determines sensitivity to PD-1 blockade in non-small cell lung cancer. *Science, 348*(6230), 124-128. doi:10.1126/science.aaa1348

Sahin, U., Derhovanessian, E., Miller, M., Kloke, B. P., Simon, P., Lower, M., . . . Tureci, O. (2017). Personalized RNA mutanome vaccines mobilize poly-specific therapeutic immunity against cancer. *Nature, 547*(7662), 222-226. doi:10.1038/nature23003

Salimu, J., Webber, J., Gurney, M., Al-Taei, S., Clayton, A., & Tabi, Z. (2017). Dominant immunosuppression of dendritic cell function by prostate-cancer-derived exosomes. *Journal of Extracellular Vesicles, 6*(1), 1368823. doi:10.1080/20013078.2017.1368823

Scaffidi, P., Misteli, T., & Bianchi, M. E. (2002). Release of chromatin protein HMGB1 by necrotic cells triggers inflammation. *Nature, 418*(6894), 191-195. doi:10.1038/nature00858

Schadt, L., Sparano, C., Schweiger, N. A., Silina, K., Cecconi, V., Lucchiari, G., . . . van den Broek, M. (2019). Cancer-Cell-Intrinsic cGAS Expression Mediates Tumor Immunogenicity. *Cell Rep, 29*(5), 1236-1248 e1237. doi:10.1016/j.celrep.2019.09.065

Schock, S. N., Chandra, N. V., Sun, Y., Irie, T., Kitagawa, Y., Gotoh, B., . . . Winoto, A. (2017). Induction of necroptotic cell death by viral activation of the RIG-I or STING pathway. *Cell Death Differ, 24*(4), 615-625. doi:10.1038/cdd.2016.153

Schoggins, J. W. (2015). A Sense of Self: RIG-I's Tolerance to Host RNA. *Immunity, 43*(1), 1-2. doi:10.1016/j.immuni.2015.06.022

Schumacher, K., Haensch, W., Roefzaad, C., & Schlag, P. M. (2001). Prognostic significance of activated CD8(+) T cell infiltrations within esophageal carcinomas. *Cancer Res, 61*(10), 3932-3936. doi:61(10):3932-6

Serratì, S., Guida, M., Di Fonte, R., De Summa, S., Strippoli, S., Iacobazzi, R. M., . . . Azzariti, A. (2022). Circulating extracellular vesicles expressing PD1 and PD-L1 predict response and mediate resistance to checkpoint inhibitors immunotherapy in metastatic melanoma. *Mol Cancer, 21*(1). doi:10.1186/s12943-021-01490-9

Shurtleff, M. J., Yao, J., Qin, Y., Nottingham, R. M., Temoche-Diaz, M. M., Schekman, R., & Lambowitz, A. M. (2017). Broad role for YBX1 in defining the small noncoding RNA composition of exosomes. *Proc Natl Acad Sci U S A, 114*(43), E8987-E8995. doi:10.1073/pnas.1712108114

Sinha, S., Hoshino, D., Hong, N. H., Kirkbride, K. C., Grega-Larson, N. E., Seiki, M., . . . Weaver, A. M. (2016). Cortactin promotes exosome secretion by controlling branched actin dynamics. *Journal of Cell Biology, 214*(2), 197-213. doi:10.1083/jcb.201601025

Sistigu, A., Yamazaki, T., Vacchelli, E., Chaba, K., Enot, D. P., Adam, J., . . . Zitvogel, L. (2014). Cancer cell-autonomous contribution of type I interferon signaling to the efficacy of chemotherapy. *Nat Med, 20*(11), 1301-1309. doi:10.1038/nm.3708

Song, S., Peng, P., Tang, Z., Zhao, J., Wu, W., Li, H., . . . Gu, J. (2017). Decreased expression of STING predicts poor prognosis in patients with gastric cancer. *Sci Rep, 7*, 39858. doi:10.1038/srep39858

Stritzke, F., Poeck, H., & Heidegger, S. (2021). In Vivo Immunogenicity Screening of Tumor-Derived Extracellular Vesicles by Flow Cytometry of Splenic T Cells. *J Vis Exp*(175). doi:10.3791/62811

Such, L., Zhao, F., Liu, D., Thier, B., Le-Trilling, V. T. K., Sucker, A., . . . Paschen, A. (2020). Targeting the innate immunoreceptor RIG-I overcomes melanoma-intrinsic resistance to T cell immunotherapy. *J Clin Invest, 130*(8), 4266-4281. doi:10.1172/JCI131572

Szajnik, M., Czystowska, M., Szczepanski, M. J., Mandapathil, M., & Whiteside, T. L. (2010). Tumor-derived microvesicles induce, expand and up-regulate biological

activities of human regulatory T cells (Treg). *PLoS One, 5*(7), e11469. doi:10.1371/journal.pone.0011469

Tamai, K., Tanaka, N., Nakano, T., Kakazu, E., Kondo, Y., Inoue, J., . . . Sugamura, K. (2010). Exosome secretion of dendritic cells is regulated by Hrs, an ESCRT-0 protein. *Biochem Biophys Res Commun, 399*(3), 384-390. doi:10.1016/j.bbrc.2010.07.083

Teng, Y., Ren, Y., Hu, X., Mu, J., Samykutty, A., Zhuang, X., . . . Zhang, H. G. (2017). MVP-mediated exosomal sorting of miR-193a promotes colon cancer progression. *Nat Commun, 8*, 14448. doi:10.1038/ncomms14448

Thery, C., Witwer, K. W., Aikawa, E., Alcaraz, M. J., Anderson, J. D., Andriantsitohaina, R., . . . Zuba-Surma, E. K. (2018). Minimal information for studies of extracellular vesicles 2018 (MISEV2018): a position statement of the International Society for Extracellular Vesicles and update of the MISEV2014 guidelines. *J Extracell Vesicles, 7*(1), 1535750. doi:10.1080/20013078.2018.1535750

Thomas, L. (1982). On immunosurveillance in human cancer. *Yale J Biol Med, 55*(3-4), 329-333. doi:55(3-4):329-33

Van Allen, E. M., Miao, D., Schilling, B., Shukla, S. A., Blank, C., Zimmer, L., . . . Garraway, L. A. (2015). Genomic correlates of response to CTLA-4 blockade in metastatic melanoma. *Science, 350*(6257), 207-211. doi:10.1126/science.aad0095

van Niel, G., D'Angelo, G., & Raposo, G. (2018). Shedding light on the cell biology of extracellular vesicles. *Nat Rev Mol Cell Biol, 19*(4), 213-228. doi:10.1038/nrm.2017.125

Vanpouille-Box, C., Demaria, S., Formenti, S. C., & Galluzzi, L. (2018). Cytosolic DNA Sensing in Organismal Tumor Control. *Cancer Cell, 34*(3), 361-378. doi:10.1016/j.ccell.2018.05.013

Verdegaal, E. M., de Miranda, N. F., Visser, M., Harryvan, T., van Buuren, M. M., Andersen, R. S., . . . van der Burg, S. H. (2016). Neoantigen landscape dynamics during human melanoma-T cell interactions. *Nature, 536*(7614), 91-95. doi:10.1038/nature18945

Wang, R. F., & Wang, H. Y. (2017). Immune targets and neoantigens for cancer immunotherapy and precision medicine. *Cell Res, 27*(1), 11-37. doi:10.1038/cr.2016.155

Weichselbaum, R. R., Ishwaran, H., Yoon, T., Nuyten, D. S. A., Baker, S. W., Khodarev, N., . . . Minn, A. J. (2008). An interferon-related gene signature for DNA damage resistance is a predictive marker for chemotherapy and radiation for breast cancer. *Proceedings of the National Academy of Sciences, 105*(47), 18490-18495. doi:10.1073/pnas.0809242105

Wolfers, J., Lozier, A., Raposo, G., Regnault, A., Thery, C., Masurier, C., . . . Zitvogel, L. (2001). Tumor-derived exosomes are a source of shared tumor rejection antigens for CTL cross-priming. *Nat Med, 7*(3), 297-303. doi:10.1038/85438

Woo, S. R., Fuertes, M. B., Corrales, L., Spranger, S., Furdyna, M. J., Leung, M. Y., . . . Gajewski, T. F. (2014). STING-dependent cytosolic DNA sensing mediates innate

immune recognition of immunogenic tumors. *Immunity, 41*(5), 830-842. doi:10.1016/j.immuni.2014.10.017

Wu, J., & Chen, Z. J. (2014). Innate immune sensing and signaling of cytosolic nucleic acids. *Annu Rev Immunol, 32*, 461-488. doi:10.1146/annurev-immunol-032713-120156

Xia, T., Konno, H., Ahn, J., & Barber, G. N. (2016). Deregulation of STING Signaling in Colorectal Carcinoma Constrains DNA Damage Responses and Correlates With Tumorigenesis. *Cell Rep, 14*(2), 282-297. doi:10.1016/j.celrep.2015.12.029

Yatim, N., Cullen, S., & Albert, M. L. (2017). Dying cells actively regulate adaptive immune responses. *Nat Rev Immunol, 17*(4), 262-275. doi:10.1038/nri.2017.9

Yatim, N., Jusforgues-Saklani, H., Orozco, S., Schulz, O., Barreira da Silva, R., Reis e Sousa, C., . . . Albert, M. L. (2015). RIPK1 and NF-kappaB signaling in dying cells determines cross-priming of CD8(+) T cells. *Science, 350*(6258), 328-334. doi:10.1126/science.aad0395

Yoneyama, M., Kikuchi, M., Natsukawa, T., Shinobu, N., Imaizumi, T., Miyagishi, M., . . . Fujita, T. (2004). The RNA helicase RIG-I has an essential function in double-stranded RNA-induced innate antiviral responses. *Nat Immunol, 5*(7), 730-737. doi:10.1038/ni1087

Yost, K. E., Satpathy, A. T., Wells, D. K., Qi, Y., Wang, C., Kageyama, R., . . . Chang, H. Y. (2019). Clonal replacement of tumor-specific T cells following PD-1 blockade. *Nature Medicine, 25*(8), 1251-1259. doi:10.1038/s41591-019-0522-3

Zamarin, D., Holmgaard, R. B., Subudhi, S. K., Park, J. S., Mansour, M., Palese, P., . . . Allison, J. P. (2014). Localized oncolytic virotherapy overcomes systemic tumor resistance to immune checkpoint blockade immunotherapy. *Sci Transl Med, 6*(226), 226ra232. doi:10.1126/scitranslmed.3008095

Zappasodi, R., Merghoub, T., & Wolchok, J. D. (2018). Emerging Concepts for Immune Checkpoint Blockade-Based Combination Therapies. *Cancer Cell, 33*(4), 581-598. doi:10.1016/j.ccell.2018.03.005

Zeelenberg, I. S., Ostrowski, M., Krumeich, S., Bobrie, A., Jancic, C., Boissonnas, A., . . . Thery, C. (2008). Targeting tumor antigens to secreted membrane vesicles in vivo induces efficient antitumor immune responses. *Cancer Res, 68*(4), 1228-1235. doi:10.1158/0008-5472.CAN-07-3163

Zevini, A., Olagnier, D., & Hiscott, J. (2017). Crosstalk between Cytoplasmic RIG-I and STING Sensing Pathways. *Trends Immunol, 38*(3), 194-205. doi:10.1016/j.it.2016.12.004

Zimmerman, B., Kelly, B., McMillan, B. J., Seegar, T. C. M., Dror, R. O., Kruse, A. C., & Blacklow, S. C. (2016). Crystal Structure of a Full-Length Human Tetraspanin Reveals a Cholesterol-Binding Pocket. *Cell, 167*(4), 1041-1051.e1011. doi:10.1016/j.cell.2016.09.056

Zomer, A., & van Rheenen, J. (2016). Implications of Extracellular Vesicle Transfer on Cellular Heterogeneity in Cancer: What Are the Potential Clinical Ramifications? *Cancer Res, 76*(8), 2071-2075. doi:10.1158/0008-5472.CAN-15-2804

10. Attachments

10.1. Publication list

Bek, S., **Stritzke, F.**, Wintges, A., Nedelko, T., Bohmer, D. F. R., Fischer, J. C., . . . Heidegger, S. (2019). Targeting intrinsic RIG-I signaling turns melanoma cells into type I interferon-releasing cellular antitumor vaccines. *Oncoimmunology, 8*(4), e1570779. doi:10.1080/2162402X.2019.1570779

Heidegger, S., Kreppel, D., Bscheider, M., **Stritzke, F.**, Nedelko, T., Wintges, A., . . . Poeck, H. (2019). RIG-I activating immunostimulatory RNA boosts the efficacy of anticancer vaccines and synergizes with immune checkpoint blockade. *EBioMedicine, 41*, 146-155. doi:10.1016/j.ebiom.2019.02.056

Heidegger, S., Wintges, A., **Stritzke, F.**, Bek, S., Steiger, K., Koenig, P. A., . . . Poeck, H. (2019). RIG-I activation is critical for responsiveness to checkpoint blockade. *Sci Immunol, 4*(39), eaau8943. doi:10.1126/sciimmunol.aau8943

Stritzke, F., Poeck, H., & Heidegger, S. (2021). In Vivo Immunogenicity Screening of Tumor-Derived Extracellular Vesicles by Flow Cytometry of Splenic T Cells. *J Vis Exp*(175). doi:10.3791/62811

Heidegger, S., **Stritzke, F.**, Dahl, S., Daßler-Plenker, J., Joachim, L., Buschmann, D., Winter, C., Fan, K., Enssle, S., Li, S., Perl, M., Görgens, A., Haas, T., Thiele Orberg, E., Wölfel, C., Engleitner, T., Rad, R., Herr, W., Giebel, B., Ruland, J., Bassermann, F., Coch, C., Hartmann, G., and Poeck, H. Reprogramming biogenesis and immunomodulatory function of tumor-derived extracellular vesicles by targeting the RIG-I pathway

10.2. Included publications

Bek, S., **Stritzke, F.**, Wintges, A., Nedelko, T., Bohmer, D. F. R., Fischer, J. C., . . . Heidegger, S. (2019). Targeting intrinsic RIG-I signaling turns melanoma cells into type I interferon-releasing cellular antitumor vaccines. *Oncoimmunology, 8*(4), e1570779. doi:10.1080/2162402X.2019.1570779

Stritzke, F., Poeck, H., & Heidegger, S. (2021). In Vivo Immunogenicity Screening of Tumor-Derived Extracellular Vesicles by Flow Cytometry of Splenic T Cells. *J Vis Exp*(175). doi:10.3791/62811

Heidegger, S., **Stritzke, F.**, Dahl, S., Daßler-Plenker, J., Joachim, L., Buschmann, D., Winter, C., Fan, K., Enssle, S., Li, S., Perl, M., Görgens, A., Haas, T., Thiele Orberg, E., Wölfel, C., Engleitner, T., Rad, R., Herr, W., Giebel, B., Ruland, J., Bassermann, F., Coch, C., Hartmann, G., and Poeck, H. Reprogramming biogenesis and immunomodulatory function of tumor-derived extracellular vesicles by targeting the RIG-I pathway

ONCOIMMUNOLOGY
2019, VOL. 8, NO. 4, e1570779 (9 pages)
https://doi.org/10.1080/2162402X.2019.1570779

Taylor & Francis
Taylor & Francis Group

BRIEF REPORT

OPEN ACCESS Check for updates

Targeting intrinsic RIG-I signaling turns melanoma cells into type I interferon-releasing cellular antitumor vaccines

Sarah Bek[a*], Florian Stritzke[a*], Alexander Wintges[a], Tatiana Nedelko[a], Daniel F.R. Böhmer[b], Julius C. Fischer[a,c], Tobias Haas[a], Hendrik Poeck[a#], and Simon Heidegger [a#]

[a]Medizinische Klinik und Poliklinik 3, Klinikum rechts der Isar, Technische Universität, Munich, Germany; [b]Center of Integrated Protein Science Munich (CIPSM) and Division of Clinical Pharmacology, Medizinische Klinik und Poliklinik IV, Klinikum der Universität München, Munich, Germany; [c]Department of Radiation Oncology, Klinikum rechts der Isar, Technische Universität, Munich, Germany

ABSTRACT

Resistance to cell death and evasion of immunosurveillance are major causes of cancer persistence and progression. Tumor cell-intrinsic activation of the RNA receptor retinoic acid-inducible gene-I (RIG-I) can trigger an immunogenic form of programmed tumor cell death, but its impact on antitumor responses remains largely unexplored. We show that activation of intrinsic RIG-I signaling induces melanoma cell death that enforces cross-presentation of tumor-associated antigens by bystander dendritic cells. This results in systemic expansion and activation of tumor-antigen specific T cells *in vivo* with subsequent regression of pre-established melanoma. These processes were dependent on the signaling hub MAVS and type I interferon (IFN-I) signaling in the host cell. Using melanoma cells deficient for the transcription factors IRF3 and IRF7, we demonstrate that RIG-I-activated tumor cells used as a vaccine are a relevant source of IFN-I during T cell cross-priming *in vivo*. Thus, our findings may facilitate translational development of personalized anticancer vaccines.

ARTICLE HISTORY
Received 31 August 2018
Revised 11 December 2018
Accepted 7 January 2019

KEYWORDS
Immunogenic cell death; pattern recognition receptors; nucleic acid receptors; RIG-I; anticancer vaccine; dendritic cells; tumor immunotherapy; personalized medicine

Introduction

Next-generation sequencing and novel bioinformatic algorithms have led to the identification of somatic tumor mutations giving rise to tumor-specific neoantigens that can drive antitumor immunity. However, the development of spontaneous immune responses is often compromised by the immunosuppressive tumor milieu or insufficient levels of tumor antigen to reach the threshold for T cell recognition.[1] A prerequisite for tumor-specific adaptive immune responses is that specialized antigen presenting cells (APCs) – particularly dendritic cells (DCs) – take up, process and present tumor-associated antigens to cytotoxic T cells. Such cross-priming of tumor-specific T cells has been shown to be dependent on DC maturation mediated by type I IFN (IFN-I, that is IFN-α and IFN-β) signaling in DCs.[2,3] In contrast to microbial infections, the tumor microenvironment often lacks proinflammatory signals resulting in suboptimal DC activation.

Under certain circumstances, tumor cells can undergo a special form of programmed tumor cell death that favors recognition and elimination by the immune system. Such immunogenic cell death (ICD) has been shown in response to treatment with certain chemotherapeutic agents (oxaliplatin, doxorubicin) or radiation.[4] One of the characteristics of ICD seems to be the release of proinflammatory factors called danger-associated molecular patterns (DAMPs) that can lead to DC maturation via stimulation of innate pattern recognition receptors. In the context of immunogenic chemotherapy, the secretion of ATP and HMGB1 as well as exposure of calreticulin on the outer membrane leaflet have been suggested to contribute to the immunogenicity of ICD amongst others.[4] However, at this stage, it is unclear whether these mechanisms play a role in the treatment efficacy of chemotherapy used in human patients.

Increasing numbers of studies now harness different pathways to therapeutically induce ICD to improve the immunogenicity of cancer cells in order to use them as antigen source in the treatment of malignant disease.[5] The RNA receptor family of RIG-I-like helicases has recently been associated with ICD in pancreatic carcinoma.[6] Its eponymous member RIG-I is frequently expressed in the cytosol of most nucleated cells including malignant tumor cells.[7] Tumor-intrinsic RIG-I activation by the specific ligand 5′-triphosphorylated RNA (3pRNA) and subsequent signaling via the mitochondria-located adapter molecule MAVS has been found to trigger strong, cell autonomous apoptosis induction.[8,9] Hereby, RIG-I activation induces the pro-apoptotic BH3-only proteins Puma and Noxa, which results in programmed cell death by the executioner caspase-3. This pathway was found to be particularly active in malignant cells and to result in an immunogenic form of tumor cell death, associated with potent cross-priming of tumor-specific cytotoxic T cells *in vitro*.[6] Furthermore, RIG-I activation and downstream MAVS signaling in

CONTACT Simon Heidegger simon.heidegger@tum.de; Hendrik Poeck hendrik.poeck@tum.de
*These authors contributed equally.
#These authors share the senior authorship.

immune – and to a lesser extent in tumor cells – can induce NFκB-mediated pro-inflammatory cytokine production, ASC-containing inflammasome formation[10–12] and IFN-I release triggered by the transcription factors IRF3 and IRF7.[13–14] However, the *in vivo* relevance of RIG-I-mediated tumor cell death and the factors that mediate its immunogenicity remain to be determined.

We here demonstrate that targeting RIG-I within melanoma cells *in vitro* results in immunogenic cell death, turning melanoma cells into a cellular antitumor vaccine that activates host MAVS and IFN-I signaling in recipient animals.

Results and discussion

RIG-I signaling in melanoma cells triggers immunogenic cell death with potent CD8$^+$ T cell activation and subsequent antitumor immunity

To address the immunogenicity of tumor-intrinsic RIG-I signaling in melanoma, we used the B16 cell line expressing the model antigen ovalbumin (B16.OVA). Targeting the RIG-I pathway in melanoma cells by transfection of a specific ligand (*in vitro* transcribed and purified 5′-triphosphorylated-RNA, 3pRNA) induced rapid induction of apoptosis with surface expression of annexin-V on the plasma membrane and subsequent tumor cell death *in vitro* (Figure 1a). Cell death induction by 3pRNA but not the chemotherapeutic agent oxaliplatin was abolished in melanoma cells that are genetically deficient for *Ddx58* encoding RIG-I (RIG-I$^{-/-}$) (Figure 1b). Furthermore, RIG-I-mediated cell death but not oxaliplatin treatment induced potent cross-presentation of tumor-associated antigens by co-cultured bone marrow-derived dendritic cells *in vitro* (Figure 1c). Immunization of mice with B16.OVA cells undergoing RIG-I-mediated cell death following *in vitro* transfection with 3pRNA (termed "3p-B16") resulted in systemic expansion and activation of tumor-antigen specific cytotoxic T cells *in vivo* (Figure 1(d–e)).

To test whether tumor cell-intrinsic RIG-I signaling induces *bona fide* ICD, we injected such immunized mice with living B16.OVA melanoma cells. Indeed, immunization of mice with B16.OVA cells undergoing RIG-I-mediated cell death largely protected recipient animals from subsequent melanoma challenge (Figure 2a) with 7 out of 8 mice being tumor-free at data census. Consistent with this, tumor antigen-specific immunity induced by a RIG-I-activated 3p-B16 cellular vaccine also translated into strong regression of pre-established melanoma (Figure 2b). Depletion experiments showed that 3p-B16-induced antitumor immunity was mediated by both CD8$^+$ cytotoxic T cells and NK1.1$^+$ NK cells. The latter is in line with previous work demonstrating that therapeutic targeting of RIG-I can result in NK cell-mediated melanoma cell killing.[9] Importantly, we found that the immunogenicity of RIG-I-induced tumor cell death was not dependent on the presence of the model antigen OVA. Immunization of mice with poorly immunogenic B16-F10 melanoma cells undergoing RIG-I-induced cell death partially protected recipients from subsequent B16-F10 melanoma challenge, associated with strongly reduced tumor growth in this aggressive model and 33% of mice being tumor-free at data census (Figure 2c). Taken together, these data show that RIG-I signaling in melanoma cells induces ICD with potent cross-priming of tumor antigen-specific CD8$^+$ T cells and subsequent antitumor immunity.

Additionally, immunization with oxaliplatin-treated melanoma cells resulted in systemic anti-tumor immunity associated with delayed tumor progression (Figure 2c). However, this is not reflected by our *in vitro* data in which oxaliplatin-induced melanoma cell death failed to enhance tumor antigen cross-presentation by dendritic cells (Figure 1c). The latter findings are in line with previous studies in pancreatic carcinoma, in which the authors were able to detect enhanced maturation of DCs (as determined by upregulation of the co-stimulatory molecule CD86) and enhanced endosomal uptake of fluorescently labeled tumor antigen *in vitro* only in response to RIG-I-treated but not oxaliplatin-treated tumor cells.[6] Chemotherapy-induced ICD was initially described in the CT26 colon carcinoma and MCA205 fibrosarcoma cell lines. Whether the apparent lack of oxaliplatin-induced ICD in some of our assays is related to our experimental system or whether there are indeed differences in the susceptibility to oxaliplatin-induced ICD among different cancer cell lines and thus cancer entities, remains to be investigated.

Tumor-derived IFN-I contributes to the antitumor responses induced by a RIG-I-activated, cellular antitumor vaccine

We next addressed the molecular pathways that are involved in 3p-B16 cellular vaccine-induced immune responses. Generally, the importance of host IFN-I signaling – particularly within DCs – for the induction of T cell-based antitumor immunity has been widely acknowledged.[2,3] A contribution of tumor IFN-I has been suggested by an *in vitro* study showing that tumor cell-derived IFN-I can potentially mediate DC maturation following interaction with RIG-I-stimulated pancreatic tumor cells.[6] However, ultimate *in vivo* experimental evidence is lacking. To address this, we generated melanoma cell lines genetically deficient for the RIG-I downstream transcription factors IRF3 and IRF7 (IRF3/7$^{-/-}$ B16.OVA cells). We found that activation of the RIG-I pathway within melanoma cells (which eventually results in programmed cell death) triggers rapid production of tumor IFN-I via activation of IRF3 and IRF7 (Figure 3a). Following co-culture with B16.OVA melanoma cells undergoing RIG-I-induced programmed tumor cell death, maturation as well as cross-presentation of tumor-associated antigen was largely abolished in DCs deficient for IFN-I receptor signaling (Figure 3 (b–c)). Furthermore, tumor antigen-specific T-cell responses induced by a RIG-I-activated 3p-B16 cellular vaccine *in vivo* were strongly diminished in recipient mice with blocked IFN-I receptor signaling (Figure 3d).

From these data, we hypothesized that IRF3/7-mediated IFN-I release by melanoma cells during the initiation of RIG-I-induced programmed cell death contributes to its immunogenicity. In this, a 3p-B16 cellular vaccine of melanoma cells undergoing immunogenic cell death may be a relevant source of IFN-I for subsequent cross-priming of CD8$^+$ T cells, once transferred into tumor-bearing animals. Indeed, we found that B16.OVA cells undergoing RIG-I-mediated programmed cell death 48 h after *in vitro*

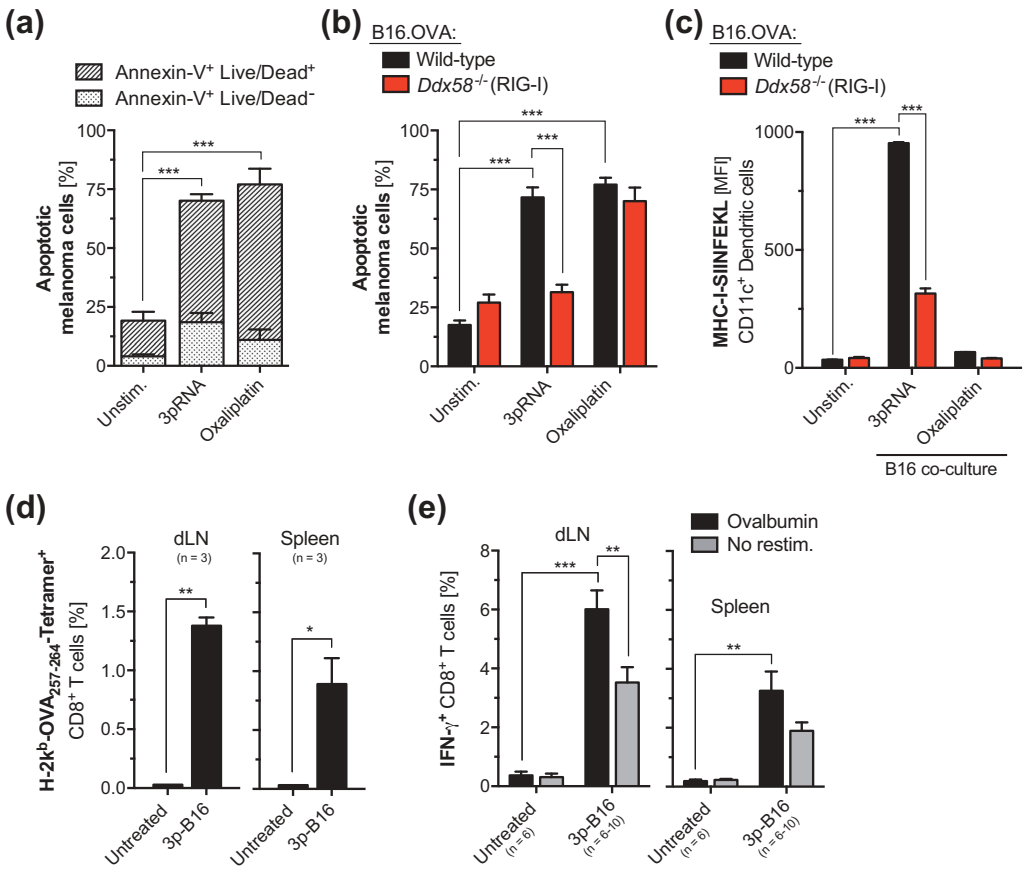

Figure 1. RIG-I signaling in melanoma cell death triggers immunogenic cell death with potent CD8$^+$ T cell cross-priming *in vivo*. (a) Wild-type B16.OVA melanoma cells were transfected with a specific RIG-I ligand (5′-triphosphorylated-RNA, 3pRNA) or were treated with the chemotherapeutic agent oxaliplatin for 48 h. Induction of melanoma cell death was assessed by Annexin-V and a Life/Dead marker (7-Aminoactinomycin D, 7-AAD) staining. Bars are divided in Annexin-V$^+$ Life/Dead$^-$ (early apoptotic) and Annexin-V$^+$ Life/Dead$^+$ (late apoptotic, secondary necrotic) cell fractions. (b) WT and RIG-I-deficient (*Ddx58*$^{-/-}$) B16.OVA cells were treated as described above. The frequency of apoptotic cells was determined as described above. (c) WT and RIG-I-deficient (*Ddx58*$^{-/-}$) B16.OVA cells were treated as described, were extensively washed and subsequently co-cultured with bone marrow-derived dendritic cells (BM-DCs). After 24 h exposure to tumor cells, cross-presentation of the processed OVA peptide-epitope SIINFEKL in the context of MHC-I by CD11c$^+$ conventional DCs was analyzed by flow cytometry. (d-e) WT B16.OVA cells were transfected with 3pRNA *in vitro* as described above. After 48 h, non-adherent cells (3p-B16) were harvested, washed and were repeatedly injected s.c. in WT recipient mice. 7 days after the second immunization, (d) the frequency of H-2K^b-SIINFEKL Tetramer$^+$ CD8$^+$ T cells in draining lymph nodes (dLNs) and spleen was determined. (e) Complete lymph node cells or splenocytes that were harvested from mice treated as described above were *ex vivo* restimulated with ovalbumin and IFN-γ release by CD8$^+$ T cells was analyzed by flow cytometry. Data give mean ± S.E.M. frequency of IFN-γ$^+$ cytotoxic T cells of n = 6–10 individual mice per group. All *in vitro* data show mean ± S.E.M. of at least triplicate samples. All data are pooled from or are representative of at least two independent experiments. MFI, mean fluorescence intensity. Unstim, Unstimulated. *, $P < 0.05$; **, $P < 0.01$; ***, $P < 0.001$.

transfection with 3pRNA, still produced significant levels of IFN-I when they were used as a cellular vaccine in recipient mice (Figure 3e). Importantly, apart from defective IFN-I production, IRF3/7$^{-/-}$ B16.OVA cells were still susceptible to RIG-I-mediated cell death (Figure 3f). Nevertheless, *in vivo* immunization with 3pRNA-pretreated IRF3/7$^{-/-}$ melanoma cells undergoing programmed cell death failed to induce CD8$^+$ T-cell activation in recipient mice (Figure 3g). In sum, these data show that IRF3/7-mediated IFN-I production within melanoma cells does not contribute to the induction of RIG-I-induced apoptosis. However, IFN-I release from tumor cells undergoing such *in vitro* induced programmed tumor cell death is critical for the immunogenicity of this process.

3p-cancer vaccines target host MAVS but not STING or NLRP3 inflammasome signaling

Different DAMPs can be involved in immunogenic cell death induced by chemotherapeutic agents. While IFN-I production

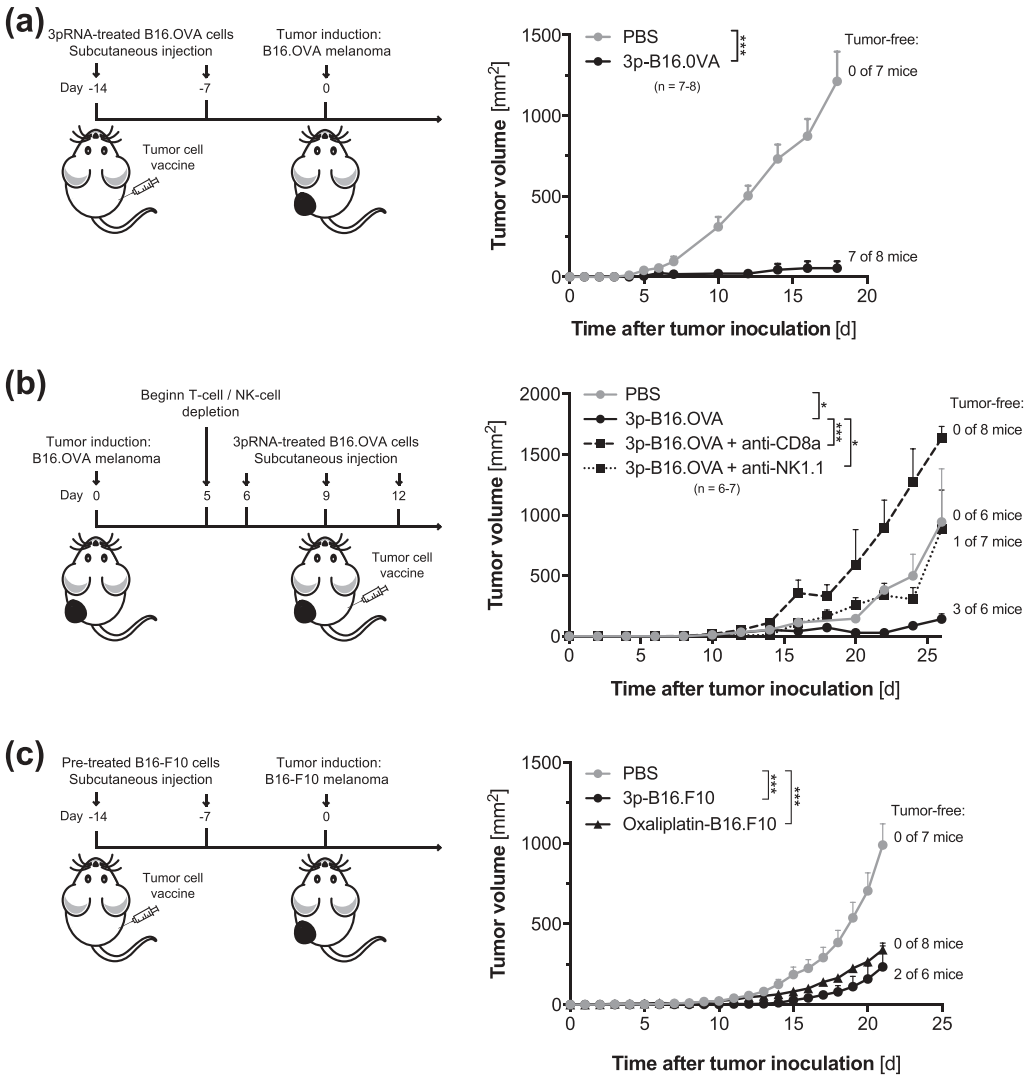

Figure 2. RIG-I-mediated ICD induces strong antitumor immunity. (a) B16.OVA cells were transfected with 3pRNA *in vitro*. After 48 h, non-adherent cells (3p-B16.OVA) were harvested washed and were repeatedly injected s.c. into recipient mice as described for Figure 1d. Seven days after the second immunization, mice were injected with 10^5 viable, untreated B16.OVA melanoma cells in the right flank. Data give mean tumor growth ± S.E.M. of n = 7–8 individual mice per group. (b) Mice were implanted with 1×10^5 viable, untreated B16.OVA cells in the right flank. When tumors were readily visible, recipient animals were s.c. injected on day 6, 9 and 12 with 3pRNA-pretreated B16 OVA cells (3p-B16.OVA, as described above). Some mice were additionally treated with T-cell (anti-CD8a) or NK-cell (anti-NK1.1) depleting antibodies. Data give mean tumor growth ± S.E.M. of n = 6–7 individual mice per group. (c) Poorly immunogenic B16-F10 melanoma cells were either transfected with 3pRNA or were treated with oxaliplatin *in vitro*. After 48 h, non-adherent cells (3p-B16.F10) were harvested washed and were repeatedly injected s.c. into the left flank of recipient mice as described for Figure 3a. Seven days after the second immunization, mice were injected with 10^5 viable untreated B16-F10 melanoma cells in the right flank. Data give mean tumor growth ± S.E.M. of n = 6–8 individual mice per group. All data are pooled from at least two independent experiments. *, $P < 0.05$; **, $P < 0.01$; ***, $P < 0.001$.

by tumor cells has been associated with the efficacy of the immunogenic anthracycline doxorubicin,[15] ATP release from dying tumors cells and subsequent activation of the NLRP3 inflammasome seems to be a critical factor for the immune system to perceive cell death as immunogenic in the context of oxaliplatin treatment.[16] We next addressed the latter pathways' role in RIG-I-induced immunogenic cell death. We hereby found, that – similar to oxaliplatin treatment – 3pRNA-mediated RIG-I

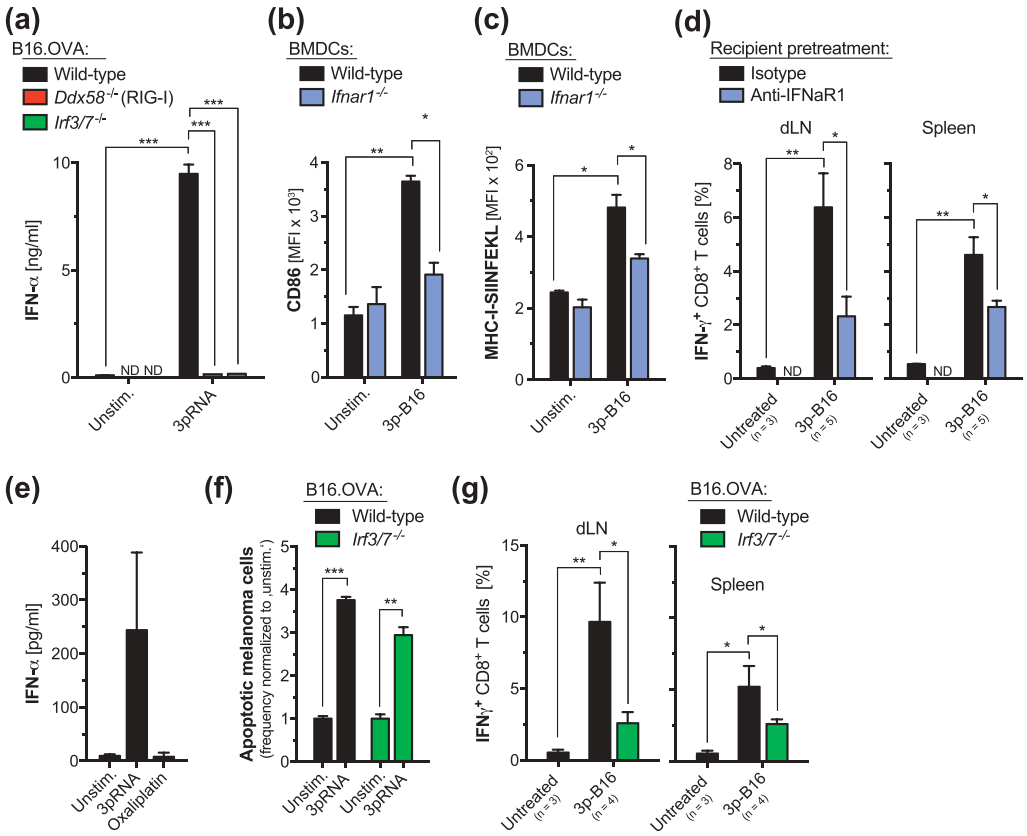

Figure 3. Tumor-derived IFN-I contributes to the antitumor responses induced by a RIG-I-activated, cellular antitumor vaccine. (a) Wild-type, RIG-I- (*Ddx58*$^{-/-}$) and IRF3/7-deficient (*Irf3/7*$^{-/-}$) B16.OVA cells were transfected with 3pRNA *in vitro* as described for Figure 1a. After 48 h, cumulated tumor cell-derived IFN-α was determined by ELISA. (b-c) 3pRNA-treated B16.OVA cells were extensively washed and were subsequently co-cultured with BM-DCs harvested from wild-type or IFNaR1-deficient (*Ifnar1*$^{-/-}$) donor mice. After 24 h exposure to tumor cells, (b) expression of the costimulatory molecule CD86 and (c) cross-presentation of the processed OVA peptide-epitope SIINFEKL in the context of MHC-I by CD11c^{+} conventional DCs was analyzed by flow cytometry. (d) WT B16.OVA cells were transfected with 3pRNA *in vitro* and were repeatedly injected s.c. in WT recipient mice as described for Figure 1d. Some mice were additionally treated with anti-IFNaR1 antibodies, beginning two days prior to the immunization. Complete draining lymph node (dLN) cells and splenocytes were harvested and the frequency of IFN-γ^{+} CD8^{+} T cells was analyzed by flow cytometry after *ex vivo* restimulation with ovalbumin. Data give the mean value ± S.E.M. of individual mice. (e) B16.OVA cells were transfected with 3pRNA *in vitro* as described. After 48 h, culture supernatant was discharged and cells were reseeded in fresh medium. Additional 24 h later, IFN-α levels were determined by ELISA. (f) Wild-type and IRF3/7-deficient (*Irf3/7*$^{-/-}$) B16.OVA cells were transfected with 3pRNA and induction of cell death was assessed by Annexin-V and Life/Dead marker staining. (g) WT and *Irf3/7*$^{-/-}$ B16.OVA cells were transfected with 3pRNA *in vitro* and were repeatedly injected s.c. in WT recipient mice as described for Figure 1d. Complete draining lymph node cells and splenocytes were harvested, and IFN-γ release by CD8^{+} T cells was analyzed by flow cytometry after *ex vivo* restimulation with ovalbumin. All results are representative of at least two independent experiments. Unstim, Unstimulated. ND, not determined. *, $P < 0.05$; **, $P < 0.01$; ***, $P < 0.001$.

activation of B16 melanoma cells resulted in i) the secretion of the DAMPs ATP and HMGB1 as well as ii) exposure of calreticulin on the outer membrane leaflet (Figure 4a). However, CD8^{+} T-cell activation following administration of a RIG-I-activated 3p-B16 cellular vaccine *in vivo* was independent of NLRP3 or its adapter molecule ASC in host cells (Figures 4(b–c)). This is in line with findings from a previous *in vitro* study in pancreatic carcinoma cells lines showing that RIG-I-induced ICD occurs independent of the interaction of ATP with the purinergic receptor P2X7 or NLRP3 as well as HMGB1 detection by TLR4 and RAGE, respectively.[6]

We also found that the induction of these ICD 'hallmark' DAMPs following oxaliplatin treatment was independent from tumor cell-intrinsic RIG-I signaling (Figure 4a). In this context, a recent study suggested that the release of immunostimulatory ATP and HMGB1 upon oxaliplatin treatment can be facilitated by RIPK3- and MLKL-mediated necroptotic signaling.[17] Hereby, it is important to mention that the immunogenicity of cell death is not only dictated by the form of cell death (apoptosis, necroptosis, pyroptosis, necrosis, etc.), but rather has been suggested to be dependent on specific (pro-inflammatory) signaling events triggered in dying cells.[18] Therefore, our data show

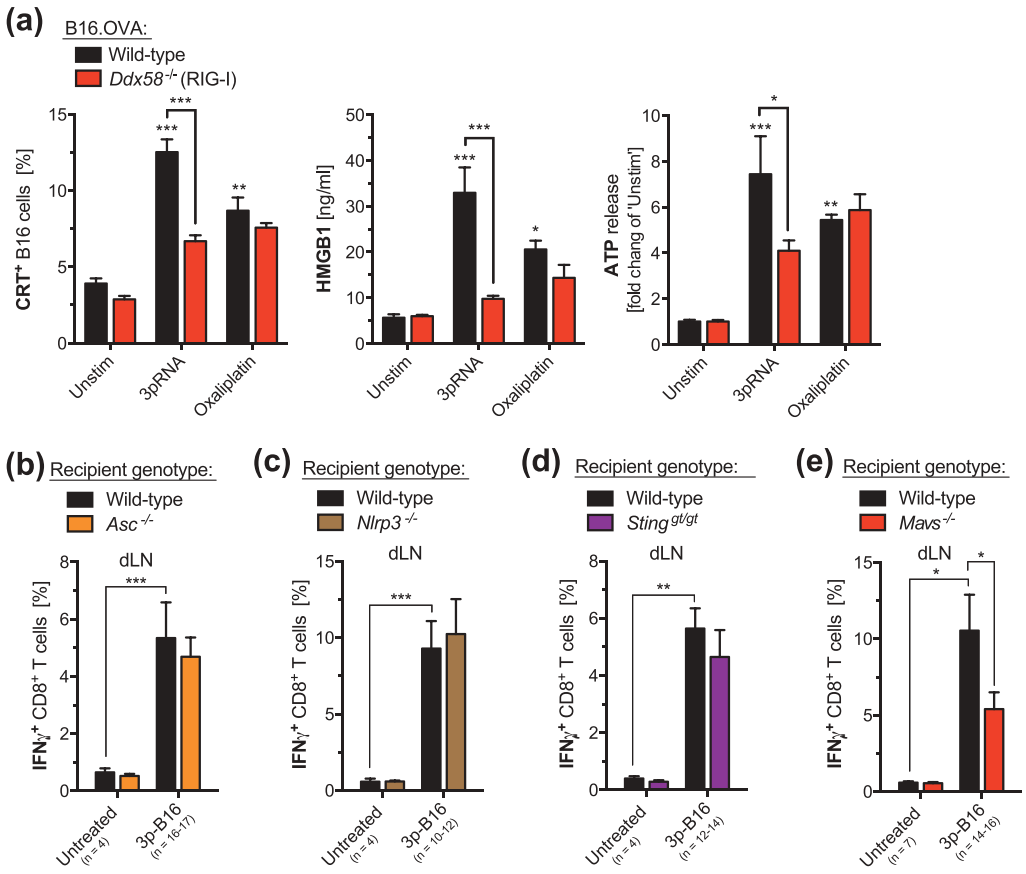

Figure 4. 3p-cancer vaccines target host MAVS but not STING or NLRP3 inflammasome signaling. (a) Wild-type (WT) and RIG-I-deficient (*Ddx58*$^{-/-}$) B16.OVA melanoma cells were transfected *in vitro* with 3pRNA or were treated with oxaliplatin as described for Figure 1. Cell culture supernatants were analyzed for the concentration of ATP and HMGB1 by ELISA. The frequency of B16 melanoma cells with calreticulin (CRT) exposed on the outer plasma membrane leaflet was determined by flow cytometry. Data show mean ± S.E.M. of at least n = 7 biological replicates pooled from two independent experiments. (b-e) Mice were immunized with 3pRNA-stimulated B16.OVA melanoma cells (3p-B16) as described for Figure 1d. Complete draining lymph node cells were harvested from immunized wild-type, (b) ASC-deficient (*Asc*$^{-/-}$), (c) NLRP3-deficient (*Nlrp3*$^{-/-}$), (d) STING-deficient (*Sting*$^{gt/gt}$) and (e) MAVS-deficient (*Mavs*$^{-/-}$) mice, and were *ex vivo* restimulated with ovalbumin. IFN-γ release by CD8$^+$ T cells was analyzed by flow cytometry. Data give mean ± S.E.M. of the indicated number of individual mice per group that were pooled from at least three independent experiments. Unstim, Unstimulated. *, $P < 0.05$; **, $P < 0.01$; ***, $P < 0.001$.

that RIG-I-induced and chemotherapy-induced ICD rely on different molecular mechanisms.

Host nucleic acid receptor systems have been associated with pro-inflammatory signaling and the development of antitumor T cell immunity. Detection of tumor-derived DNA via the cGAS/STING pathway within host DCs has been suggested to mediate spontaneous antitumor immunity in an immunogenic model of malignant melanoma.[19] We found that 3p-B16 cellular vaccine-mediated activation of tumor antigen-specific CD8$^+$ T cells was not compromised in STING-deficient animals (Figure 4d). In contrast, we found that 3p-B16 immunization efficacy was reduced in recipient animals deficient for the adaptor molecule MAVS and thus RIG-I downstream signaling in non-malignant host cells (Figure 4e). The latter is consistent with previous findings that RIG-I receptor activation has the potential to facilitate antigen-specific T-cell cross-priming in the context of antiviral immunity.[20] Yet, the identity of possible RIG-I ligands released *in vivo* by melanoma cells undergoing 3pRNA-induced cell death remain to be determined.

One limitation of our study is that the cellular vaccine may leak the *in vitro* transfected 3pRNA to – at least partly – facilitate host RIG-I/MAVS signaling *in vivo*. In addition, the finding that 3p-B16-mediated induction of antitumor immunity was independent of STING signaling in host cells is unexpected. Perhaps this could be explained by redundant activation of the RIG-I/MAVS and

cGAS/STING pathways in host DCs in this context. Likewise, i*n vivo* application of purified 3pRNA – as performed in a phase I/II clinical trial with intralesional 3pRNA administration in solid tumors and lymphomas (RGT100–001; ClinicalTrials.gov Identifier: NCT03065023) – may address different host pathways as compared to the *in vitro* generated "cellular 3p-B16 vaccine" described in our study.

Together, we here demonstrate that targeting RIG-I within melanoma cells *in vitro* results in immunogenic cell death, turning melanoma cells into an IFN-I releasing cellular vaccine. This approach may serve as the basis for the translational development of personalized anticancer vaccines from autologous tumor cells. However, new anticancer vaccines, when progressing from the preclinical phase to clinical testing, often fail to maintain immunogenicity when being produced in accordance with good manufacturing procedure (GMP) regulatory criteria. Thus, further studies will have to clarify whether RIG-I-induced cellular vaccines are still potent once they had been avitalized by physical cell death modalities to ensure complete cancer cell death prior to patient re-transplantation.

Material and methods

Mice

Female C57BL/6J mice were purchased from Janvier. *Nlrp3*$^{-/-}$ and *Asc*$^{-/-}$ mice were a gift from J. Tschopp. *Ifnar1*$^{-/-}$ and *Mavs*$^{-/-}$ mice were provided by U. Kalinke (Hannover, Germany). *Sting*-deficient mice (*Tmem173*$^{gt/gt}$) were from the Jackson Laboratory. All mouse strains have been described previously.[21–24] Mice were at least six weeks of age at the onset of experiments and were maintained in specific pathogen-free conditions. Animal studies were approved by the local regulatory agency (Regierung von Oberbayern, Munich, Germany).

Media and reagents

RPMI-1640 medium (Invitrogen) and DMEM (Invitrogen) were supplemented with 10% (v/v) FCS (Hyclone), 3 mM L-glutamine, 100 U/ml of penicillin and 100 µg/ml of streptomycin (all from Sigma-Aldrich). OptiMEM reduced serum medium was from Invitrogen. Double-stranded *in vitro*-transcribed 3pRNA (sense, 5′- UCA AAC AGU CCU CGC AUG CCU AUA GUG AGU CG –3′) was generated as described.[9]

Cell lines and CRISPR-cas9-mediated genome editing

The B16-F10 murine melanoma cell line expressing full-length chicken ovalbumin (here referred to as B16.OVA) was cultured in complete DMEM medium supplemented with 400 µg/ml G418 (from Sigma-Aldrich). Gene deficient B16.OVA cells were engineered using the CRISPR-Cas9 system as previously described.[25] In brief, B16.OVA cells were genetically edited using the *Streptococcus pyogenes* nuclease Cas9, together with different guide RNAs (Target sequences: *Ddx58* 5′-GGCTGATGAGGATGATGGAGCGG-3′, *Irf3* 5′-GCATGGAAACCCCGAAACCG-3′, *Irf7* 5′-CTACGACCGA AATGCTTCCA-3′). The guide RNAs were cloned into pSpCas9(BB)-2A-GFP (pX458, a gift from Feng Zhang; Addgene plasmid #48138), a bicistronic expression vector expressing Cas9 and a sgRNA. B16.OVA were transfected with Lipofectamin 2000, and GFP-expressing single cell clones were isolated by FACS 24 h after transfection. Gene deficient clones were identified by immunoblotting.

Cell culture experiments

In vitro, B16.OVA cells were transfected with 3pRNA (3 µg/ml) complexed in Lipofectamin 2000 (Life Technologies, Darmstadt, Germany) according to the manufacturer's protocol using Gibco® Opti-MEM. Alternatively, B16 cells were treated with 30 µg/ml oxaliplatin. 48 hours later, induction of cell death was assessed by staining with Annexin-V (BD Bioscience) and 7-AAD (BioLegend). ATP or HMBG1 release was determined using the ATP Assay Kit (Abcam) or a commercial ELISA (IBL) following the manufacturer's protocol, respectively. Levels of IFN-I were determined by self-established ELISAs as described earlier.[26] Bone marrow-derived dendritic cells (BMDCs) were generated by culturing bone marrow cells in complete RPMI medium supplemented with 20 ng/ml GM-CSF (from Immunotools, Friesoythe, Germany). For co-culture experiments, B16.OVA were treated as described above. After 48 h, B16.OVA cells were washed twice in PBS, and were then co-cultured with BM-DCs for 24 h.

Flow cytometry

Cell suspensions were stained in PBS with 3% FCS. Fluorochrome-coupled antibodies were purchased from eBioscience or BioLegend. Anti-calreticulin (ab2907) was purchased from Abcam. The anti-mouse $OVA_{257–264}$ (SIINFEKL) peptide bound to H-2K^{b}-antibody (clone 25-D1.16) was purchased from eBioscience. The iTAg MHC-I murine tetramers detecting SIINFEKL-specific CD8^{+} T cells were from MBL (Woburn, MA). For intracellular cytokine staining the Foxp3 Transcription Factor Fixation/Permeabilization Kit (eBioscience) was used. Data were acquired on a FACSCanto II (BD Biosciences) and analyzed using FlowJo software (TreeStar).

Immunization with 3pRNA-treated B16.OVA cells

For each mouse, 10^{6} B16.OVA cells were transfected *in vitro* with 3pRNA. After 48 h, all cells which were easily detached by rinsing the culture flask were extensively washed and were injected subcutaneously (s.c.) in the right hock. The therapy was repeated at day 7. At day 14 mice were sacrificed and draining lymph nodes and the spleen were removed. Single cell suspensions of these organs were cultured in the presence of 1 µg/ml OVA protein in complete RPMI medium for 72 h and IFN-γ levels of CD8^{+} T cells were analyzed by flow cytometry. In some experiments, mice were pre-treated intraperitoneally (i.p.) with 400 µg anti-murine IFNaR1 antibody (clone MAR1–5A3, BioXCell, West Lebanon, NH) one day prior to the above immunization.

Tumor challenge and treatment

For tumor challenge, mice were injected s.c. in the right flank with 10^5 untreated B16.OVA cells on day 0. When tumors were readily visible, 10^6 3pRNA-treated B16.OVA cells were injected s.c. in the right hock as described above. Treatment was repeated on day 3 and 6. Optional treatment with anti-CD8a (clone 2.43, BioXCell) or anti-NK1.1 (clone PK136) depleting antibodies was initiated one day prior to vaccination (100 µg i.p.) and was repeated twice weekly (50 µg i.p.). For the prophylactic models, mice were vaccinated twice with *in vitro* pre-treated B16 melanoma cells on days −14 and −7 as described above, before s.c. tumor induction with 10^5 B16.OVA or B16-F10 cells on day 0. Mice were euthanized when the maximum tumor diameter exceeded 15 mm according to standard legal procedure (responsible state office Regierung von Oberbayern).

Statistics

All data are presented as mean ± S.E.M. Statistical significance of single experimental findings was assessed with the independent two-tailed Student's t-test. For multiple statistical comparison of a data set the one-way ANOVA test with Bonferroni post-test was used. Significance was set at P values < 0.05, $p < 0.01$, and $p < 0.001$ and was then indicated with an asterisk (*, ** and ***). All statistical calculations were performed using Prism (GraphPad Software).

Acknowledgments

S.B., S.H., T.H., and H.P. designed the research, analyzed and interpreted the results. S.B., F.S., A.W., T.N., and D.F.R.B. did the experiments. J.C. F. provided substantial intellectual input. S.H. and H.P. prepared the manuscript and guided the study. H. P. is supported by the EMBO Young Investigator Program. This work is part of the doctoral thesis of S.B. and F.S. at the Technical University of Munich.

Disclosure of Potential Conflicts of Interest

No potential conflicts of interest were disclosed.

Funding

This work was supported by the Deutsche Forschungsgemeinschaft (DFG, German Research Foundation) [Project 360372040 - SFB 1335]; Deutsche Forschungsgemeinschaft [PO 1575/3-1]; Deutsche Krebshilfe [111620]; Else Kröner-Fresenius-Stiftung [2015_A06]; Else Kröner-Fresenius-Stiftung [2012_A61]; Else Kröner-Fresenius-Stiftung [Forschungskolleg TUM]; European Hematology Association; DKMS [Mechtild Harf Research Grant]; Carl Maximilian and Carl Manfred Bayer-Foundation.

ORCID

Simon Heidegger http://orcid.org/0000-0001-6394-5130

References

1. Hu Z, Ott PA, Wu CJ. Towards personalized, tumour-specific, therapeutic vaccines for cancer. Nat Rev Immunol. 2018;18:168–182. doi:10.1038/nri.2017.131.
2. Diamond MS, Kinder M, Matsushita H, Mashayekhi M, Dunn GP, Archambault JM, Lee H, Arthur CD, White JM, Kalinke U, et al. Type I interferon is selectively required by dendritic cells for immune rejection of tumors. J Exp Med. 2011;208:1989–2003. doi:10.1084/jem.20101158.
3. Fuertes MB, Kacha AK, Kline J, Woo SR, Kranz DM, Murphy KM, Gajewski TF. Host type I IFN signals are required for antitumor CD8 + T cell responses through CD8{alpha}+ dendritic cells. J Exp Med. 2011;208:2005–2016. doi:10.1084/jem.20101159.
4. Galluzzi L, Buque A, Kepp O, Zitvogel L, Kroemer G. Immunogenic cell death in cancer and infectious disease. Nat Rev Immunol. 2017;17:97–111. doi:10.1038/nri.2016.107.
5. Montico B, Nigro A, Casolaro V, Dal Col J. Immunogenic apoptosis as a novel tool for anticancer vaccine development. Int J Mol Sci. 2018;19:594. doi:10.3390/ijms19020594.
6. Duewell P, Steger A, Lohr H, Bourhis H, Hoelz H, Kirchleitner SV, Stieg MR, Grassmann S, Kobold S, Siveke JT, et al. RIG-I-like helicases induce immunogenic cell death of pancreatic cancer cells and sensitize tumors toward killing by CD8(+) T cells. Cell Death Differ. 2014;21:1825–1837. doi:10.1038/cdd.2014.96.
7. Barchet W, Wimmenauer V, Schlee M, Hartmann G. Accessing the therapeutic potential of immunostimulatory nucleic acids. Curr Opin Immunol. 2008;20:389–395. doi:10.1016/j.coi.2008.07.007.
8. Besch R, Poeck H, Hohenauer T, Senft D, Hacker G, Berking C, Hornung V, Endres S, Ruzicka T, Rothenfusser S, et al. Proapoptotic signaling induced by RIG-I and MDA-5 results in type I interferon-independent apoptosis in human melanoma cells. J Clin Invest. 2009;119:2399–2411. doi:10.1172/JCI37155.
9. Poeck H, Besch R, Maihoefer C, Renn M, Tormo D, Morskaya SS, Kirschnek S, Gaffal E, Landsberg J, Hellmuth J, et al. 5′-Triphosphate-siRNA: turning gene silencing and Rig-I activation against melanoma. Nat Med. 2008;14:1256–1263. doi:10.1038/nm.1887.
10. Poeck H, Bscheider M, Gross O, Finger K, Roth S, Rebsamen M, Hannesschläger N, Schlee M, Rothenfusser S, Barchet W, et al. Recognition of RNA virus by RIG-I results in activation of CARD9 and inflammasome signaling for interleukin 1 beta production. Nat Immunol. 2010;11:63–69. doi:10.1038/ni.1824.
11. Franchi L, Eigenbrod T, Munoz-Planillo R, Ozkurede U, Kim YG, Chakrabarti A, Gale M, Silverman RH, Colonna M, Akira S, et al. Cytosolic double-stranded RNA activates the NLRP3 inflammasome via MAVS-induced membrane permeabilization and K+ efflux. J Immunol. 2014;193:4214–4222. doi:10.4049/jimmunol.1400582.
12. Pothlichet J, Meunier I, Davis BK, Ting JP, Skamene E, von Messling V, Vidal SM, Pekosz A. Type I IFN triggers RIG-I/TLR3/NLRP3-dependent inflammasome activation in influenza A virus infected cells. PLoS Pathog. 2013;9:e1003256. doi:10.1371/journal.ppat.1003256.
13. Goubau D, Schlee M, Deddouche S, Pruijssers AJ, Zillinger T, Goldeck M, Schuberth C, Van der Veen AG, Fujimura T, Rehwinkel J, et al. Antiviral immunity via RIG-I-mediated recognition of RNA bearing 5′-diphosphates. Nature. 2014;514:372–375. doi:10.1038/nature13590.
14. Hornung V, Ellegast J, Kim S, Brzozka K, Jung A, Kato H, Poeck H, Akira S, Conzelmann -K-K, Schlee M, et al. 5′-Triphosphate RNA is the ligand for RIG-I. Sci. 2006;314:994–997. doi:10.1126/science.1132505.
15. Sistigu A, Yamazaki T, Vacchelli E, Chaba K, Enot DP, Adam J, Vitale I, Goubar A, Baracco EE, Remédios C, et al. Cancer cell-autonomous contribution of type I interferon signaling to the efficacy of chemotherapy. Nat Med. 2014;20:1301–1309. doi:10.1038/nm.3708.
16. Ghiringhelli F, Apetoh L, Tesniere A, Aymeric L, Ma Y, Ortiz C, Vermaelen K, Panaretakis T, Mignot G, Ullrich E, et al. Activation of the NLRP3 inflammasome in dendritic cells induces IL-1beta-dependent adaptive immunity against tumors. Nat Med. 2009;15:1170–1178. doi:10.1038/nm.2028.

17. Yang H, Ma Y, Chen G, Zhou H, Yamazaki T, Klein C, Pietrocola F, Vacchelli E, Souquere S, Sauvat A, et al. Contribution of RIP3 and MLKL to immunogenic cell death signaling in cancer chemotherapy. Oncoimmunol. 2016;5: e1149673. doi:10.1080/2162402X.2016.1149673.
18. Yatim N, Jusforgues-Saklani H, Orozco S, Schulz O, Barreira da Silva R, Reis E Sousa C, Green DR, Oberst A, Albert ML. RIPK1 and NF-κB signaling in dying cells determines cross-priming of CD8⁺ T cells. Sci. 2015;350:328–334. doi:10.1126/science.aad0395.
19. Woo SR, Fuertes MB, Corrales L, Spranger S, Furdyna MJ, Leung MY, Duggan R, Wang Y, Barber GN, Fitzgerald KA, et al. STING-dependent cytosolic DNA sensing mediates innate immune recognition of immunogenic tumors. Immunity. 2014;41:830–842. doi:10.1016/j.immuni.2014.10.017.
20. Hochheiser K, Klein M, Gottschalk C, Hoss F, Scheu S, Coch C, Hartmann G, Kurts C. Cutting edge: the RIG-I ligand 3pRNA potently improves CTL cross-priming and facilitates antiviral vaccination. J Immunol. 2016;196:2439–2443. doi:10.4049/jimmunol.1501958.
21. Mariathasan S, Newton K, Monack DM, Vucic D, French DM, Lee WP, Roose-Girma M, Erickson S, Dixit VM. Differential activation of the inflammasome by caspase-1 adaptors ASC and Ipaf. Nature. 2004;430:213–218. doi:10.1038/nature02664.
22. Muller U, Steinhoff U, Reis LF, Hemmi S, Pavlovic J, Zinkernagel RM, Aguet M. Functional role of type I and type II interferons in antiviral defense. Sci. 1994;264:1918–1921.
23. Sauer JD, Sotelo-Troha K, von Moltke J, Monroe KM, Rae CS, Brubaker SW, Hyodo M, Hayakawa Y, Woodward JJ, Portnoy DA, et al. The N-ethyl-N-nitrosourea-induced Goldenticket mouse mutant reveals an essential function of Sting in the in vivo interferon response to Listeria monocytogenes and cyclic dinucleotides. Infect Immun. 2011;79:688–694. doi:10.1128/IAI.00999-10.
24. Seth RB, Sun L, Ea CK, Chen ZJ. Identification and characterization of MAVS, a mitochondrial antiviral signaling protein that activates NF-kappaB and IRF 3. Cell. 2005;122:669–682. doi:10.1016/j.cell.2005.08.012.
25. Ran FA, Hsu PD, Wright J, Agarwala V, Scott DA, Zhang F. Genome engineering using the CRISPR-Cas9 system. Nat Protocols. 2013;8:2281–2308. doi:10.1038/nprot.2013.143.
26. Bourquin C, Hotz C, Noerenberg D, Voelkl A, Heidegger S, Roetzer LC, Storch B, Sandholzer N, Wurzenberger C, Anz D, et al. Systemic cancer therapy with a small molecule agonist of toll-like receptor 7 can be improved by circumventing TLR tolerance. Cancer Res. 2011;71:5123–5133. doi:10.1158/0008-5472.CAN-10-3903.

jove

In Vivo Immunogenicity Screening of Tumor-Derived Extracellular Vesicles by Flow Cytometry of Splenic T Cells

Florian Stritzke[1,2], **Hendrik Poeck**[1,2,3,4], **Simon Heidegger**[1,2]

[1] Department of Medicine III, School of Medicine, Technical University of Munich [2] Center for Translational Cancer Research (TranslaTUM), School of Medicine, Technical University of Munich [3] Department of Internal Medicine III, University Hospital Regensburg [4] National Centre for Tumor Diseases WERA

Corresponding Authors

Florian Stritzke
f.stritzke@tum.de

Simon Heidegger
simon.heidegger@tum.de

Citation

Stritzke, F., Poeck, H., Heidegger, S. *In Vivo* Immunogenicity Screening of Tumor-Derived Extracellular Vesicles by Flow Cytometry of Splenic T Cells. *J. Vis. Exp.* (175), e62811, doi:10.3791/62811 (2021).

Date Published

September 23, 2021

DOI

10.3791/62811

URL

jove.com/video/62811

Abstract

Immunogenic cell death of tumors, caused by chemotherapy or irradiation, can trigger tumor-specific T cell responses by releasing danger-associated molecular patterns and inducing the production of type I interferon. Immunotherapies, including checkpoint inhibition, primarily rely on preexisting tumor-specific T cells to unfold a therapeutic effect. Thus, synergistic therapeutic approaches that exploit immunogenic cell death as an intrinsic anti-cancer vaccine may improve their responsiveness. However, the spectrum of immunogenic factors released by cells under therapy-induced stress remains incompletely characterized, especially regarding extracellular vesicles (EVs). EVs, nano-scale membranous particles emitted from virtually all cells, are considered to facilitate intercellular communication and, in cancer, have been shown to mediate cross-priming against tumor antigens. To assess the immunogenic effect of EVs derived from tumors under various conditions, adaptable, scalable, and valid methods are sought-for. Therefore, herein a relatively easy and robust approach is presented to assess EVs' *in vivo* immunogenicity. The protocol is based on flow cytometry analysis of splenic T cells after *in vivo* immunization of mice with EVs, isolated by precipitation-based assays from tumor cell cultures under therapy or steady-state conditions. For example, this work shows that oxaliplatin exposure of B16-OVA murine melanoma cells resulted in the release of immunogenic EVs that can mediate the activation of tumor-reactive cytotoxic T cells. Hence, screening of EVs *via in vivo* immunization and flow cytometry identifies conditions under which immunogenic EVs can emerge. Identifying conditions of immunogenic EV release provides an essential prerequisite to testing EVs' therapeutic efficacy against cancer

and exploring the underlying molecular mechanisms to ultimately unveil new insights into EVs' role in cancer immunology.

Introduction

The immune system plays a pivotal role in the fight against cancer, both when incited by immune checkpoint inhibition and for the efficacy of conventional cancer therapies. Tumor cells succumbing to genotoxic therapies such as the chemotherapeutic agents oxaliplatin and doxorubicin, or ionizing radiation treatment can release antigens and danger-associated molecular patterns (DAMPs) that potentially initiate an adaptive anti-tumor immune response[1]. The most prominent DAMPs, in the context of immunogenic cell death, include find-me signals such as chemotactic ATP, eat-me signals such as the exposure of calreticulin, that promotes tumor cell uptake by antigen-presenting cells, and the release of HMGB1, that activates pattern recognition receptors, thereby enhancing the cross-presentation of tumor antigens[2]. Furthermore, type I interferons (IFN-I), induced *via* tumor-derived immunogenic nucleic acids or other stimuli, are sensed by dendritic cells, enabling them to effectively prime tumor-specific cytotoxic T cells[3,4]. Clinically, activated and proliferating $CD8^+$ T cells infiltrating the tumor provide an independent prognostic factor for prolonged survival in many cancer patients. Released from such activated T cells, IFN-γ mediates direct antiproliferative effects on cancer cells and drives Th1 polarization and cytotoxic T cell differentiation, thereby contributing to effective immunosurveillance against cancer[5,6]. Oxaliplatin is a bona fide immunogenic cell death inducer, mediating such adaptive immune response against cancer[7]. However, the plethora of initial immunogenic signals released by tumor cells under therapy-induced stress remains to be fully unveiled. Despite significant advances in cancer immunotherapy, expanding its benefits to a larger portion of patients remains a challenge. A more detailed understanding of immunogenic signals that initiate T cell activation may guide the development of novel therapies.

A heterogeneous group of membrane-enclosed structures, known as extracellular vesicles (EVs), seem to serve as intercellular communication devices. Emitted by virtually all cell types, EVs carry functional proteins, RNA, DNA, and other molecules to a recipient cell or may alter a cell's functional state just by binding to receptors on the cell surface. Their biologically active cargo varies significantly by the type and functional state of the generating cell[8]. In cancer immunology, EVs released from tumor cells have been predominantly regarded as adversarial to immunotherapy because they eventually promote invasive growth, preform metastatic niches[9], and suppress the immune response[10]. In contrast, some studies have shown that EVs can transfer tumor antigens to dendritic cells for effective cross-presentation[11,12]. EVs may provide immunostimulatory nucleic acids if they emerge under therapy-induced stress, facilitating an anti-tumor immune response[13,14]. Sensing of such RNA and DNA innate immune ligands in the tumor microenvironment has recently been shown to modulate responsiveness to checkpoint blockade significantly[15,16,17]. Hence, the immunogenic role of EVs released by tumor cells under different therapy-induced stress needs to be further elucidated. Since EVs constitute a young yet growing field of research, standardization of methods is still ongoing. Therefore, sharing knowledge is essential to improve the research reproducibility on interactions between EVs and

cancer immunology. With this in mind, this manuscript describes a simple protocol to assess the immunogenic effect of tumor-derived EVs *in vivo*.

This assessment is performed by generating tumor-derived EVs, immunizing recipient mice with those EVs, and analyzing splenic T cells *via* flow cytometry. EV generation is ideally performed by seeding murine tumor cells in an EV-free cell culture medium for a high degree of purity. Cells are treated with a specific cell stress stimulus, such as chemotherapy, to compare the effect of therapy-induced EVs against baseline immunogenicity of respective tumor-derived EVs. The isolation of EVs may well be performed by various techniques that should be selected according to *in vivo* applicability and local availability. The following protocol describes a precipitation-based assay with a commercial kit for EV purification. Mice are immunized twice with those EVs. Fourteen days after the first injection, T cells are extracted from the spleen and analyzed for IFN-γ production *via* flow cytometry to evaluate a systemic immune response. With this, the potential of tumor-derived EVs, emerging under different therapeutic regimens, to induce anti-tumor T cell responses is assessed relatively easily, quickly, and with high validity[13]. Therefore, this method is suitable for an immunological screening of EVs derived from cancer cells under various conditions.

Protocol

At the onset of experiments, mice were at least 6 weeks of age and were maintained under specific pathogen-free conditions. The present protocol complies with the Institutional ethical standards and prevailing local regulations. Animal studies were approved by the local regulatory agency (Regierung von Oberbayern, Munich, Germany). Possible sex-related biases were not investigated in these studies.

1. Generation and isolation of EVs derived from tumor cells after chemotherapy exposure

1. Culture murine B16 melanoma cells expressing ovalbumin (B16-OVA) in DMEM (containing 4 mM L-glutamine and 4.5 g/L D-glucose) supplemented with FCS (10% v/v), penicillin (100 Units/mL), and streptomycin (100 µg/mL) at 37 °C, until cells grow steadily and are approximately 90% confluent.
   NOTE: Perform this section of the protocol entirely under sterile conditions using a cell culture hood. For analysis of other cancer entities, cell lines expressing a potent antigen are preferable to assess antigen-specific T cell responses, as they allow for specific *ex vivo* antigen restimulation.
2. To prepare the cell culture media required for EV generation, deplete bovine EVs within FCS by ultracentrifugation at 100,000 x *g* for 24 h at 4 °C, and then discard the pellet. Alternatively, choose a commercial preparation low in animal EVs beforehand.
3. Harvest B16-OVA cells and wash them twice in PBS, and then seed at a concentration of 400,000 cells/mL in EV-depleted media.
   NOTE: Adapt the cell concentration to the growth dynamic of the cell line under investigation so that cells do not overgrow.
4. Treat B16-OVA cells by adding 30 µg of oxaliplatin per mL and incubate for 24 h at 37 °C. Leave control conditions untreated. At the first use of a genotoxic substance, titrate the desired cytotoxic efficacy using cell-viability assays such as trypan blue exclusion[18].

NOTE: This assay may also evaluate EVs generated in cell cultures treated with other immune-modulating substances or ionizing irradiation besides chemotherapeutics.

CAUTION: Oxaliplatin causes skin and severe eye irritation and may cause an allergic skin reaction and respiratory irritation. Oxaliplatin is suspected of causing cancer. As a precaution, use personal protective equipment, including adequate gloves, goggles, masks, and clothing, cleaned before reuse. Avoid inhalation and wash hands thoroughly after handling. Avoid release into the environment and dispose oxaliplatin according to prevailing regulations. Obtain detailed information from the safety data sheet.

5. Collect cell culture supernatant. Centrifuge first at 400 x *g* for 5 min at 4 °C, and then at 2,000 x *g* for 30 min at 4 °C, each time discarding the pellet. Finally, filter through a 220 nm PVDF membrane. Use a fresh tube for each step to remove any cell debris.

   NOTE: At this stage, the EV-containing supernatant may be stored at 4 °C for a day before resuming the protocol. However, it is strongly recommended to adhere to the described schedule with immediate EV purification.

6. Mix 1 mL of supernatant with 0.5 mL of a specific commercially available exosome isolation reagent (see **Table of Materials**) in a V-shaped 1.5 mL tube. Thoroughly pipette up and down or vortex to create a homogenous solution. Incubate overnight at 4 °C.

7. Centrifuge at 10,000 x *g* for 60 min at 4 °C. Carefully discard the supernatant. Remove the remaining drops by tapping the 1.5 mL tube upside down on a paper towel and by aspiration through a pipette with a fine tip without touching the EV-pellet at the bottom.

   1. Thoroughly remove all fluids to prevent uncontrolled dilution of the EV-pellet. Also, execute these tasks quickly to prevent the pellet from drying out.

8. Resuspend the EVs in cold PBS by pipetting up and down without scratching the pellet from the tube's wall with the tip. Now, transfer the suspension step by step from the first to the last tube to pool the EVs.

   NOTE: Use a volume of PBS that equals 5 µL multiplied by the number of tubes. 5 µL of the final suspension contains the isolated EVs released from 400,000 cells under chemotherapy or at a steady state.

9. Preferably, use EVs directly. If this is not possible, store EV suspensions at -80 °C in siliconized vessels for up to 28 days until application.

   NOTE: The EVs described here and in several other publications do not lose their respective biological function when stored at -80 °C for that time period[19].

10. Quantify and characterize EV isolates according to the MISEV2018 guidelines[20].

    NOTE: Possible methods for quantification include nanoparticle tracking analysis (NTA)[21] and the detection of EV's membrane-bound proteins[22]. Possible approaches to further characterize EVs include electron microscopy[23] and western blot[20].

2. Immunization of mice with EVs

1. Plan the *in vivo* experiment with C57BL/6 mice (or other syngeneic mice corresponding to the tumor cell line), including treatment groups receiving EVs derived from treated cells, untreated cells, and PBS (vehicle), respectively.

NOTE: Preferably, use mice at the age of 6-8 weeks to prevent physiological senescence from diminishing the immune response[24].

2. Mix 5 µL of EV-suspension with 55 µL cold PBS for each mouse within the respective treatment group to immunize it with EVs isolated from 4.0 x 10^5 B16-OVA cells.
   NOTE: This amount of EVs corresponds to approximately 2 x 10^9 particles measured by nanoparticle tracking analysis (data not shown). OVA protein mixed with an adjuvant (e.g., LPS) can be applied as a potent vaccine positive control.
   1. Fill syringes (needle size 26-30 G) with 60 µL of the diluted EVs or PBS, respectively and put immediately on ice.
      NOTE: In the protocol, the amount of injected EVs is normalized to the number of EV-releasing tumor cells to experimentally consider both qualitative and quantitative effects of oxaliplatin on tumor cell EV biogenesis. For some readers, normalization to a specific concentration of produced EVs may better fit their experimental setup depending on their scientific question.
3. Inoculate EVs or PBS subcutaneously into the medial aspect of the mice's thigh and repeat the immunization after 7 days. Fourteen days after the first treatment, sacrifice mice, e.g., by cervical dislocation to analyze the immune response.
   NOTE: Alternative subcutaneous injection routes may be used, according to the local standards.

3. Flow cytometry analysis of splenic T cells

1. Prepare and cool complete RPMI (cRPMI), supplementing RPMI-1640 with FCS (10% v/v), penicillin (100 Units/mL), streptomycin (100 µg/mL), L-glutamine (2 mM), and β-mercaptoethanol (50 µM).
2. Resect the spleen from the opened abdominal cavity. Mash the spleen with a moistened 100 µm cell strainer and the plastic plunger of a syringe and flush the splenic cells into a 50 mL tube with 5-10 mL of cRPMI. Centrifuge at 400 x *g* for 5 min at 4 °C and discard the supernatant.
   NOTE: Keep cells on ice whenever possible. To analyze the local rather than the splenic immune response, resect the draining popliteal and inguinal lymph nodes, following the same protocol. In this case, skip the next step for the lysis of erythrocytes.
3. To remove erythrocytes from the cell suspension, resuspend the pellet with 2 mL of red blood cell lysis buffer (see **Table of Materials**) and incubate for 5 min at room temperature. Then, stop the reaction by adding cRPMI. Centrifuge at 400 x *g* for 5 min at 4 °C and discard the supernatant.
4. For seeding, resuspend the cell pellet in cRPMI and count the cells to place triplicates of 200,000 cells with 200 µL cRPMI into each well, using a 96-well plate with a U-shaped bottom. Incubate for 48 h at 37 °C.
   NOTE: To address the antigen-specificity of activated T cells, add 1 µg/mL soluble ovalbumin (or another tumor antigen corresponding to cell line under investigation) or leave without additional stimulus, respectively. Adding the immune-dominant peptide epitope SIINFEKL, instead of full-length ovalbumin, allows for a shorter incubation period. Besides flow cytometry, the mice's serum and the cell culture supernatant after 48 h of incubation can be analyzed for various cytokines.
5. After 48 h, to enhance intracellular IFN-γ staining by, inter alia, blocking the Golgi-mediated secretion of proteins,

add Brefeldin A (5 ng/mL), PMA (20 ng/mL), and Ionomycin (1 µg/mL) to the cell culture. Incubate for 4 h at 37 °C.

6. Before staining surface biomarkers, transfer splenocytes to a 96-well plate with a V-shaped bottom and wash twice with PBS. Then, add fluorescent antibodies, compatible with the locally available flow cytometer, directed against surface biomarkers, CD3, CD8, and CD4 (see **Table of Materials**), diluted 1:400, plus a fixable viability dye, diluted 1:1,000 in PBS. Resuspend pelleted splenocytes in the staining solution and incubate for 30 min at 4 °C, protected from light.

7. For fixation and permeabilization of splenocytes, wash twice in FACS-buffer (PBS plus 3% v/v FCS), and then resuspend in 100 µL of fixation/permeabilization buffer (see **Table of Materials**) per well. Incubate for 30 min at 4 °C, protected from light.

8. For staining of intracellular IFN-γ, wash splenocytes in fixation/permeabilization buffer and resuspend with fluorescent antibodies against IFN-γ, diluted 1:200 in the buffer. Incubate for at least 1 h (up to a maximum of 12 h) at 4 °C, protected from light.

9. Before measuring the samples by flow cytometry, wash splenocytes twice in fixation/permeabilization buffer and resuspend in FACS-buffer. Analyze the activation of cytotoxic T cells according to the gating strategy displayed in **Figure 2**.

    1. First, to detect single cells, blot FSC-H against FSC-A. Then, to detect lymphoid cells, blot SSC against FSC-A. Subsequently, select living $CD3^+$, $CD4^-$, $CD8^+$ cells and determine their IFN-γ-producing subset to quantify the activation of cytotoxic T cells in the spleen.

NOTE: Include a Fluorescence-minus-one (FMO) stain with all fluorochromes except the fluorochrome targeted against IFN-γ as negative technical control.

Representative Results

This protocol is intended to facilitate the straightforward and easily reproducible assessment of the immunogenicity of tumor-derived EVs. Hereby, mice are inoculated with EVs derived from *in vitro* cultures of tumor cells expressing the model antigen chicken ovalbumin (OVA). The subsequent immune response is analyzed in splenic T cells *via* flow cytometry.

Figure 1 gives an overview of the practical steps of the entire protocol. Since the work focuses on immunogenic cell death, cross-presentation, and EV-induced anti-tumor immunity, this protocol is restricted to the function of CD8+ cytotoxic T cells. As displayed in **Figure 2**, cells were gated as single cells, lymphocyte subset (by size and granularity), viable cells (excluding a life/dead marker), and $CD3^+$ $CD4^-$ $CD8^+$ cytotoxic T cells. Intracellular accumulation of IFN-γ was assessed as a surrogate marker for activation. Possible additional markers regarding T cell differentiation and exhaustion are discussed below.

Using the method described here, mice were immunized with EVs derived from OVA-expressing tumor cells cultured either under steady-state (untreated) or genotoxic stress conditions (oxaliplatin-treated). Only mice injected with EVs derived from tumor cells under genotoxic stress conditions induced potent activation of splenic cytotoxic T cells in recipient animals (**Figure 3A**). Injection of EVs derived from tumors under steady-state conditions resulted in some T cell activation, but that was not significantly different from T cell activation in mice injected with the PBS vehicle. These

data show that under genotoxic stress, tumor cells can release potently immunogenic EVs. The production of IFN-γ was particularly increased when splenocytes of tumor EV-treated animals were *ex vivo* restimulated with the model tumor antigen OVA before analysis (**Figure 3B**). These data suggest that tumor-derived EVs can induce tumor antigen-specific immune responses. Interestingly, IFN-γ-production - even though to a much lesser extent - is also detected in the absence of antigen-specific restimulation. Possibly, other melanoma-associated antigens, such as the differentiation antigen TRP2[25], may be targeted by some part of the EV-induced T cell response.

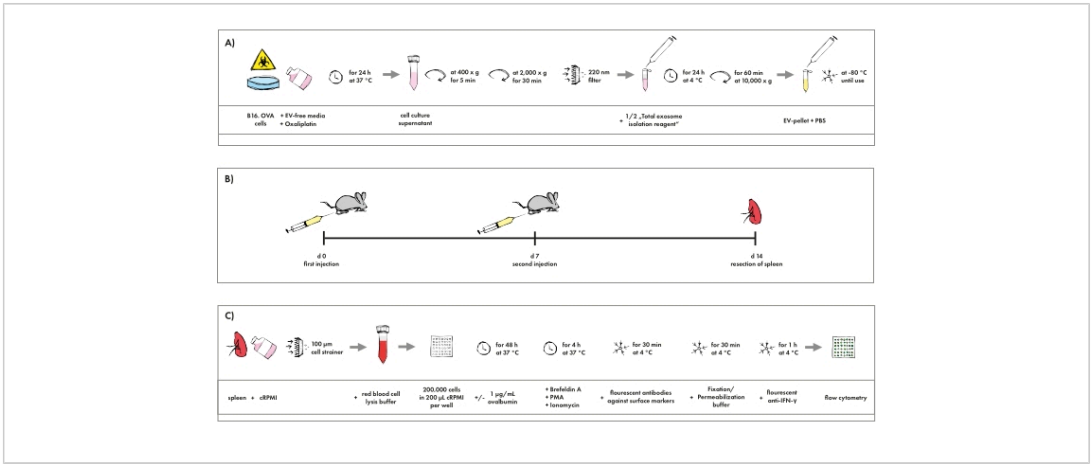

Figure 1: Pictographic overview of the protocol. (**A**) Isolation procedure of EVs generated in tumor cell cultures resembling chemotherapy. (**B**) Schedule for the immunization of mice with EVs. (**C**) Staining protocol for flow cytometry analysis of cytotoxic T cells. Please click here to view a larger version of this figure.

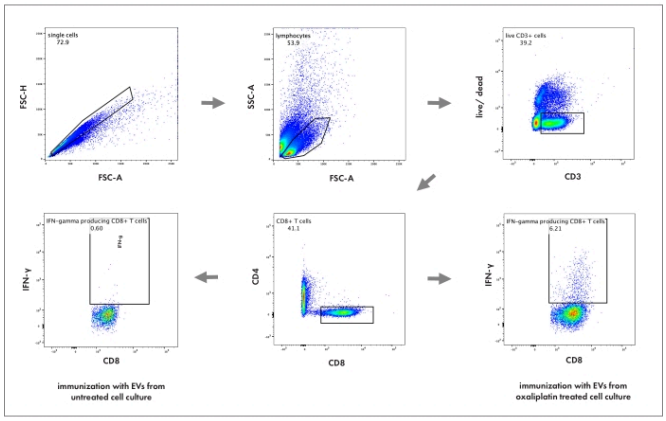

Figure 2: Flow cytometry gating strategy to analyze cytotoxic T cell activation in the spleen. The numbers represent the percentage of its respective parent population. FSC-A: forward scatter area; FSC-H: forward scatter height; SSC: sideward scatter; live/dead: cell death marker. Please click here to view a larger version of this figure.

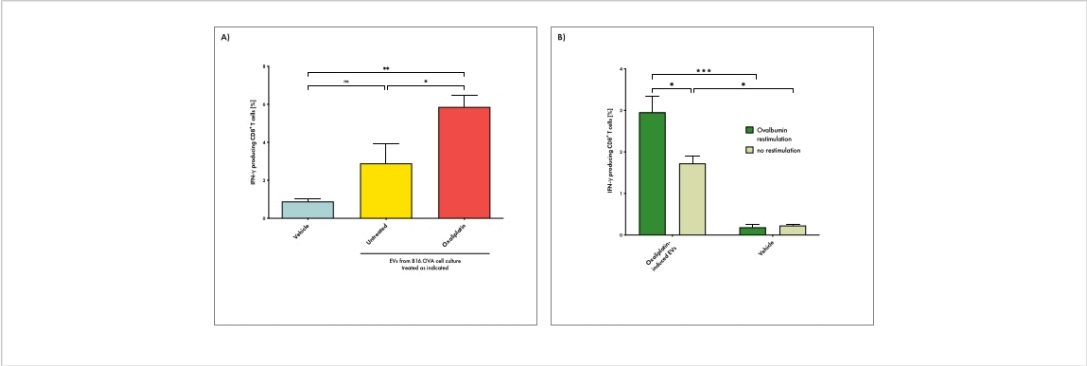

Figure 3: EVs derived from tumor cells under genotoxic stress can induce antigen-specific T cell responses in recipient animals. (**A**) Mice were immunized with EVs derived from tumor cells cultured either under steady-state (untreated) or genotoxic stress conditions (oxaliplatin-treated). Vehicle (PBS) injections were used as a negative control. IFN-γ production by cytotoxic T cells in the spleen upon EV immunization was determined. With this, splenic cell suspensions were restimulated with ovalbumin *ex vivo* before analysis. (**B**) Mice were treated with EVs derived from tumor cells under genotoxic stress conditions as described above. Splenic T cell activation was determined after *ex vivo* restimulation either in the presence or absence of ovalbumin. Bars depict the mean per group and whiskers its standard error. The one-way analysis of variance (ANOVA) test with Bonferroni posttest was used for multiple statistical comparisons of a dataset. The significance level was set at $P < 0.05$, $P < 0.01$, and $P < 0.001$ and is indicated here with asterisks (*, **, and ***). Please click here to view a larger version of this figure.

Discussion

This protocol provides an immunological *in vivo* assessment of EVs derived from melanoma cells under chemotherapy-induced stress while adapting to EVs emitted from various cancers under various treatments. Immunizing mice with EVs derived from oxaliplatin-treated B16-OVA cells, for instance, expands IFN-γ-producing $CD8^+$ T cells in the spleen, which are further stimulated by *ex vivo* incubation with ovalbumin, indicating a tumor-specific immune response. Thus, detection of immunogenic EVs by screening through this protocol facilitates a more comprehensive understanding of conventional cancer therapies and enables a focused investigation into the role of EVs in cancer immunology.

Of note, experiments with EVs require some special considerations. In this protocol, EVs are semi-quantitatively normalized to the number of tumor cells released within 24 h. This approach reflects the aim to identify enhanced immunogenicity, regardless of whether it emerges from alterations in quality or quantity of released EVs. Therefore, reproducible *in vivo* results rely on the constant isolation efficacy of EVs. To this end, ensuring that EV pellets are

resuspended entirely and promptly to avoid desiccation is a critical step.

Additionally, EVs must be quantified and characterized, e.g., by nanoparticle tracking analysis and western blot of canonical transmembrane, luminal, and at least one negative EV-marker[20]. Quantifying and characterizing EVs controls for inconstant isolation and addresses quantitative differences in EVs or EV subsets. This type of EV characterization constitutes a part of the minimum information that needs to be reported in studies about extracellular vesicles, according to the International Society of Extracellular Vesicles (ISEV) guidelines. However, various characterization methods are equally legitimate and should be selected concerning local availability and the individual research question. Notably, defining dosage of a substance of interest or ionizing irradiation constitutes another critical step of the protocol, which may require experimental validation to achieve an adequate level of cell death.

In general, potential contamination of isolated EVs with the treatment substance, soluble proteins, and lipoproteins must be considered. One strategy in this regard consists in reproducing the experiment with complementary EV-isolation techniques that the same type of contamination[20] may not compromise. Immunoaffinity, for instance, isolates EVs with a lower yield but higher specificity than purely precipitation-based methods and may provide an appropriate control in this regard[26]. An alternative approach is to compare wild-type cell-derived EVs with isolations from genetically engineered cells with a specific deletion of genes involved in EV biogenesis or deploy substances that reduce EVs emission[20].

Results obtained from this protocol should be complemented by a more comprehensive characterization of the EV-mediated immune response. Especially the classification of $CD8^+$ T cells into effector and effector memory cells, through CD44[27], as well as antigen-naïve and central memory cells, through CD62L[28], may convey deeper insight. Furthermore, the analysis of T helper cells, regulatory T cells, and NK cells may be of interest. For testing the anti-tumor efficacy of EVs, mice may be challenged with the corresponding cancer cells after receiving EV immunization or treated with EVs against a preestablished cancer, thereby adapting the guidelines for detection of immunogenic cell death[2,29] to this cell-free tumor derivate. However, conclusions from all these experimental setups are limited by the fact that cancer cells in a Petri dish potentially generate functionally different EVs than cancer cells embedded in a dynamic tumor microenvironment[30] that often suppresses anti-cancer immunity. Thus, assessing EVs derived from tumor/fibroblast cocultures or *ex vivo* tumor tissue may better reflect the actual situation. In a next translational step toward clinical reality, EVs from patient material may be analyzed for immunogenicity before and during therapy to assess their usability as biomarkers.

As cancer-derived EVs were recently found to - under certain circumstances - modulate the immune system, the journey of exploring their clinical potential has only just begun[31]. For an in-depth analysis of the immune mechanisms co-opted by immunogenic EVs, useful tools comprise fluorescence microscopy visualizing the EV uptake by specific cells, the deployment of mice with genetic deficiencies for specific immune pathways, and screening methods for molecular alterations in the EV content. Ultimately, identifying immunogenic tumor-derived EVs, with screening methods described herein, will enable a better understanding of the underlying mechanisms behind EV-mediated immunity and

therefore constitutes a crucial step toward harnessing their potential against cancer.

Disclosures

The authors declare that there is no conflict of interest.

Acknowledgments

This study was supported by the Deutsche Forschungsgemeinschaft (DFG, German Research Foundation) - Projektnummer 360372040 - SFB 1335 and Projektnummer 395357507 - SFB 1371 (to H.P.), a Mechtild Harf Research Grant from the DKMS Foundation for Giving Life (to H.P.) a Young Investigator Award by the Melanoma Research Alliance (to S.H.), a scholarship by the Else-Kröner-Fresenius-Stiftung (to F.S.), a Seed Fund by the Technical University Munich (to S.H.) and a research grant by the Wilhelm Sander Foundation (2021.041.1, to S.H.). H. P. is supported by the EMBO Young Investigator Program.

AUTHOR CONTRIBUTIONS:

F.S., H.P., and S.H. designed the research, analyzed, and interpreted the results. F.S. and S.H. wrote the manuscript. H.P. and S.H. guided the study.

References

1. Kroemer, G., Galluzzi, L., Kepp, O., Zitvogel, L. Immunogenic cell death in cancer therapy. *Annual Review of Immunology.* **31**, 51-72 (2013).
2. Kepp, O. et al. Consensus guidelines for the detection of immunogenic cell death. *Oncoimmunology.* **3** (9), e955691 (2014).
3. Fuertes, M. B. et al. Host type I IFN signals are required for antitumor CD8+ T cell responses through CD8{alpha}+ dendritic cells. *The Journal of Experimental Medicine.* **208** (10), 2005-2016 (2011).
4. Sistigu, A. et al. Cancer cell-autonomous contribution of type I interferon signaling to the efficacy of chemotherapy. *Nature Medicine.* **20** (11), 1301-1309 (2014).
5. Fridman, W. H., Pages, F., Sautes-Fridman, C., Galon, J. The immune contexture in human tumours: impact on clinical outcome. *Nature reviews. Cancer.* **12** (4), 298-306 (2012).
6. Shankaran, V. et al. IFNgamma and lymphocytes prevent primary tumour development and shape tumour immunogenicity. *Nature.* **410** (6832), 1107-1111 (2001).
7. Tesniere, A. et al. Immunogenic death of colon cancer cells treated with oxaliplatin. *Oncogene.* **29** (4), 482-491 (2010).
8. van Niel, G., D'Angelo, G., Raposo, G. Shedding light on the cell biology of extracellular vesicles. *Nature reviews. Molecular Cell Biology.* **19** (4), 213-228 (2018).
9. Zomer, A., van Rheenen, J. Implications of extracellular vesicle transfer on cellular heterogeneity in cancer: What are the potential clinical ramifications? *Cancer Research.* **76** (8), 2071-2075 (2016).
10. Whiteside, T. L. Exosomes and tumor-mediated immune suppression. *The Journal of Clinical Investigation.* **126** (4), 1216-1223 (2016).
11. Wolfers, J. et al. Tumor-derived exosomes are a source of shared tumor rejection antigens for CTL cross-priming. *Nature Medicine.* **7** (3), 297-303 (2001).
12. Zeelenberg, I. S. et al. Targeting tumor antigens to secreted membrane vesicles in vivo induces efficient

antitumor immune responses. *Cancer Research.* **68** (4), 1228-1235 (2008).

13. Diamond, J. M. et al. Exosomes Shuttle TREX1-Sensitive IFN-Stimulatory dsDNA from Irradiated Cancer Cells to DCs. *Cancer Immunology Research.* **6** (8), 910-920 (2018).
14. Kitai, Y. et al. DNA-containing exosomes derived from cancer cells treated with topotecan activate a STING-dependent pathway and reinforce antitumor immunity. *Journal of Immunology.* **198** (4), 1649-1659 (2017).
15. Heidegger, S. et al. RIG-I activation is critical for responsiveness to checkpoint blockade. *Science Immunology.* **4** (39), eaau8943 (2019).
16. Schadt, L. et al. Cancer-cell-intrinsic cGAS expression mediates tumor immunogenicity. *Cell Reports.* **29** (5), 1236-1248 e1237 (2019).
17. Cheng, Y. et al. In situ immunization of a TLR9 agonist virus-like particle enhances anti-PD1 therapy. *Journal for Immunotherapy of Cancer.* **8** (2) (2020).
18. Strober, W. Trypan blue exclusion test of cell viability. *Current Protocols in Immunology.* **111**, A3 B 1-A3 B 3 (2015).
19. Jeyaram, A., Jay, S. M. Preservation and storage stability of extracellular vesicles for therapeutic applications. *The AAPS Journal.* **20** (1), 1 (2017).
20. Thery, C. et al. Minimal information for studies of extracellular vesicles 2018 (MISEV2018): a position statement of the International Society for Extracellular Vesicles and update of the MISEV2014 guidelines. *Journal of Extracellular Vesicles.* **7** (1), 1535750 (2018).
21. Vestad, B. et al. Size and concentration analyses of extracellular vesicles by nanoparticle tracking analysis: a variation study. *Journal of Extracellular Vesicles.* **6** (1), 1344087 (2017).
22. Suarez, H. et al. A bead-assisted flow cytometry method for the semi-quantitative analysis of Extracellular Vesicles. *Scientific Reports.* **7** (1), 11271 (2017).
23. Yuana, Y. et al. Cryo-electron microscopy of extracellular vesicles in fresh plasma. *Journal of Extracellular Vesicles.* **2** (2013).
24. Kapasi, Z. F., Murali-Krishna, K., McRae, M. L., Ahmed, R. Defective generation but normal maintenance of memory T cells in old mice. *European Journal of Immunology.* **32** (6), 1567-1573 (2002).
25. Bloom, M. B. et al. Identification of tyrosinase-related protein 2 as a tumor rejection antigen for the B16 melanoma. *The Journal of Experimental Medicine.* **185** (3), 453-459 (1997).
26. Patel, G. K. et al. Comparative analysis of exosome isolation methods using culture supernatant for optimum yield, purity and downstream applications. *Scientific Reports.* **9** (1), 5335 (2019).
27. DeGrendele, H. C., Kosfiszer, M., Estess, P., Siegelman, M. H. CD44 activation and associated primary adhesion is inducible via T cell receptor stimulation. *The Journal of Immunology.* **159** (6), 2549-2553 (1997).
28. Yang, S., Liu, F., Wang, Q. J., Rosenberg, S. A., Morgan, R. A. The shedding of CD62L (L-selectin) regulates the acquisition of lytic activity in human tumor reactive T lymphocytes. *PLoS One.* **6** (7), e22560 (2011).
29. Bek, S. et al. Targeting intrinsic RIG-I signaling turns melanoma cells into type I interferon-releasing cellular antitumor vaccines. *Oncoimmunology.* **8** (4), e1570779 (2019).

30. Nabet, B. Y. et al. Exosome RNA unshielding couples stromal activation to pattern recognition receptor signaling in cancer. *Cell.* **170** (2), 352-366 e313 (2017).

31. Pitt, J. M., Kroemer, G., Zitvogel, L. Extracellular vesicles: masters of intercellular communication and potential clinical interventions. *The Journal of Clinical Investigation.* **126** (4), 1139-1143 (2016).

jove

Materials List for

In Vivo Immunogenicity Screening of Tumor-Derived Extracellular Vesicles by Flow Cytometry of Splenic T Cells

Florian Stritzke[1,2], **Hendrik Poeck**[1,2,3,4], **Simon Heidegger**[1,2]

[1]Department of Medicine III, School of Medicine, Technical University of Munich [2]Center for Translational Cancer Research (TranslaTUM), School of Medicine, Technical University of Munich [3]Department of Internal Medicine III, University Hospital Regensburg [4]National Centre for Tumor Diseases WERA

Corresponding Authors

Florian Stritzke
f.stritzke@tum.de

Simon Heidegger
simon.heidegger@tum.de

Citation

Stritzke, F., Poeck, H., Heidegger, S. *In Vivo* Immunogenicity Screening of Tumor-Derived Extracellular Vesicles by Flow Cytometry of Splenic T Cells. *J. Vis. Exp.* (175), e62811, doi:10.3791/62811 (2021).

Date Published

September 23, 2021

DOI

10.3791/62811

URL

jove.com/video/62811

Materials

Name	Company	Catalog Number	Comments
Anti-CD3 FITC	Biolegend	100204	Clone 17A2
Anti-CD4 PacBlue	Biolegend	100428	Clone GK1.5
Anti-CD8 APC	Biolegend	100712	Clone 53-6.7
Anti-IFNγ PE	eBioscience	RM90022	Clone XMG1.2
Brefeldin A	Biolegend	420601	Brefeldin A Solution (1,000x)
Cell Strainer, 100 µm	Greiner	542000	EASYstrainer 100 µm
DMEM	Sigma-Aldrich	D6429	Dulbecco's Modified Eagle's Medium with D-glucose (4.5 g/L) and L-glutamine (4 mM)
FBS Good Forte	PAN BIOTECH	P40-47500	Fetal Calf Serum (FCS)
Fixable Viability Dye eFluor 506	eBioscience, division of Thermo Fischer Scientific	65-0866-14	
Fixation/Permeabilization Concentrate	eBioscience	00-5123-43	Fixation/Permeabilization Concentrate (10x)
Fixation/Permeabilization Diluent	eBioscience	00-5223-56	
Ionomycin	Sigma-Aldrich	407952	From Streptomyces conglobatus - CAS 56092-82-1, ≥ 97% (HPLC)
L-Glutamine	Gibco	25030-032	L-Glutamine (200 mM)
Ovalbumin	InvivoGen	vac-pova	Ovalbumine with < 1 EU/mg endotoxin - CAS 9006-59-1
Oxaliplatin	Pharmacy of MRI hospital		
PBS	Sigma-Aldrich	D8537	Phosphate Buffered Saline without calcium chloride and magnesium chloride
Penicillin-Streptomycin	Gibco	1514-122	Mixture of penicillin (10,000 U/mL) and streptomycin (10,000 ug/mL)
PMA	Sigma-Aldrich	P1585	Phorbol 12-myristate 13-acetate, ≥ 99% (HPLC)

PVDF filter, 0,22 µm, for syringes	Merck Millipore	SLGV033RS	Millex-GV Filter Unit 0.22 µm Durapore PVDF Membrane
Red Blood Cell Lysis Buffer	Invitrogen	00-4333-57	
RPMI 1640	Thermo Fischer Scientific	11875	Roswell Park Memorial Institute 1640 Medium with D-glucose (2.00 g/L) and L-glutamine (300 mg/L), without HEPES
Syringe, 26 G	BD Biosciences	305501	1 mL Sub-Q Syringes with needle (0.45 mm x 12.7 mm)
Total Exosome Isolation Reagent	Invitrogen	4478359	For isolation from cell culture media
β-Mercaptoethanol	Thermo Fischer Scientific	31350	β-Mercaptoethanol (50 mM)

Target	Isotype	Clone	Distributor	Identifier
CD3	Rat IgG2b, κ	17A2	Biolegend	Cat#100203; RRID: AB_312660
CD4	Rat / IgG2b, κ	GK1.5	eBioscience	Cat#48-0041-82; RRID: AB_10718983
CD11b	Rat IgG2b, κ	M1/70	Biolegend	Cat#101212
CD11c	Armenian Hamster IgG	N418	Biolegend	Cat#117322
CD8a	Rat / IgG2a, κ	53-6.7	Biolegend	Cat#100711; RRID: AB_312750
CD45	Rat IgG2b, κ	30-F11	Biolegend	Cat#109924
CD86 (B7-2)	Rat / IgG2a, κ	GL1	eBioscience	Cat#25-0862-82; RRID: AB_2573372
CD103	Armenian Hamster IgG	2E7	Biolegend	Cat#121415
IFN-γ	Rat / IgG1a, κ	XMG1.2	Biolegend	Cat#505807; RRID: AB_315401
MHC II (I-A/I-E)	Rat IgG2b, κ	M5/114.15.2	Biolegend	Cat#107606
NK1.1	Mouse IgG2a, κ	PK136	Biolegend	Cat#108710

Table S6. Fluorochrome-coupled antibodies used for flow cytometry analysis of murine cells. Related to STAR Methods.

Cell Reports
Medicine

Article

Targeting nucleic acid sensors in tumor cells to reprogram biogenesis and RNA cargo of extracellular vesicles for T cell-mediated cancer immunotherapy

Graphical abstract

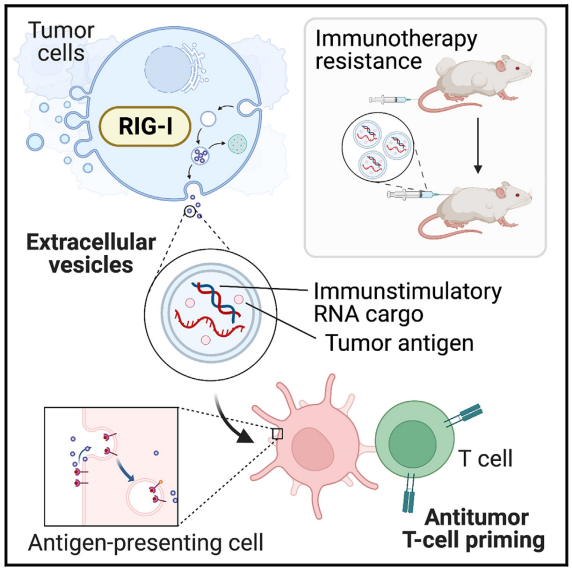

Highlights

- RIG-I activity regulates biogenesis and function of tumor cell-derived EVs
- Cancer-intrinsic RIG-I signaling governs the composition of the EV RNA cargo
- Immunostimulatory EVs trigger T cell-based antitumor immunity in mice and humans
- EV and RIG-I gene signatures in melanomas correlate with response to immunotherapy

Authors

Simon Heidegger, Florian Stritzke, Sarah Dahl, ..., Christoph Coch, Gunther Hartmann, Hendrik Poeck

Correspondence

simon.heidegger@tum.de (S.H.), hendrik.poeck@ukr.de (H.P.)

In brief

Extracellular vesicles harbor extraordinary potential for cancer therapy, but one limitation is an inadequate understanding of signaling pathways that regulate their biogenesis and function. Heidegger et al. define a tumor-intrinsic molecular pathway that can be targeted to modulate tumor EV cargo constituents and thus their immunomodulatory potential on T cell immunity.

Heidegger et al., 2023, Cell Reports Medicine *4*, 101171
September 19, 2023
https://doi.org/10.1016/j.xcrm.2023.101171

CellPress

Cell Reports Medicine

CellPress
OPEN ACCESS

Article

Targeting nucleic acid sensors in tumor cells to reprogram biogenesis and RNA cargo of extracellular vesicles for T cell-mediated cancer immunotherapy

Simon Heidegger,[1,2,20,21,*] Florian Stritzke,[1,2,3,20] Sarah Dahl,[1] Juliane Daßler-Plenker,[4,5] Laura Joachim,[1,2] Dominik Buschmann,[6] Kaiji Fan,[7] Carolin M. Sauer,[8] Nils Ludwig,[9] Christof Winter,[2,10,11] Stefan Enssle,[1,2] Suqi Li,[7] Markus Perl,[7] André Görgens,[12,13] Tobias Haas,[1] Erik Thiele Orberg,[1,2,10] Sascha Göttert,[7] Catherine Wölfel,[14] Thomas Engleitner,[2,15] Isidro Cortés-Ciriano,[8] Roland Rad,[2,10,15,16] Wolfgang Herr,[7] Bernd Giebel,[13] Jürgen Ruland,[2,10,11] Florian Bassermann,[1,2,10] Christoph Coch,[4,17] Gunther Hartmann,[4] and Hendrik Poeck[7,18,19,22,23,*]

[1]Department of Medicine III, School of Medicine, Technical University of Munich, Munich, Germany
[2]Center for Translational Cancer Research (TranslaTUM), School of Medicine, Technical University of Munich, Munich, Germany
[3]Department of Radiation Oncology, Heidelberg University Hospital, Heidelberg, Germany
[4]Institute of Clinical Chemistry and Clinical Pharmacology, University Hospital Bonn, Bonn, Germany
[5]Cold Spring Harbor Laboratory, Cold Spring Harbor, NY, USA
[6]Division of Animal Physiology and Immunology, TUM School of Life Sciences Weihenstephan, Technical University Munich, Freising, Germany
[7]Department of Internal Medicine III, University Hospital Regensburg, Regensburg, Germany
[8]European Molecular Biology Laboratory, European Bioinformatics Institute, Hinxton, Cambridge, UK
[9]Department of Oral and Maxillofacial Surgery, University Hospital Regensburg, Regensburg, Germany
[10]German Cancer Consortium (DKTK), Partner Site Munich and German Cancer Research Center (DKFZ), Heidelberg, Germany
[11]Institute of Clinical Chemistry and Pathobiochemistry, School of Medicine, Technical University of Munich, Munich, Germany
[12]Clinical Research Center, Department of Laboratory Medicine, Karolinska Institute, Stockholm, Sweden
[13]Institute for Transfusion Medicine, University Hospital Essen, University of Duisburg-Essen, Essen, Germany
[14]Internal Medicine III, University Cancer Center and Research Center for Immunotherapy, University Medical Center Johannes Gutenberg University and German Cancer Consortium (DKTK), Partner Site Frankfurt/Mainz, Mainz, Germany
[15]Institute of Molecular Oncology and Functional Genomics, School of Medicine, Technical University of Munich, Munich, Germany
[16]Department of Medicine II, School of Medicine, Technical University of Munich, Munich, Germany
[17]Department of Neurosurgery, University Hospital Leipzig, Leipzig, Germany
[18]Leibniz Institute for Immunotherapy (LIT), Regensburg, Germany
[19]Center for Immunomedicine in Transplantation and Oncology (CITO), Regensburg, Germany
[20]These authors contributed equally
[21]Twitter: @HeideggerS_MD
[22]Twitter: @HendrikPoeck
[23]Lead contact
*Correspondence: simon.heidegger@tum.de (S.H.), hendrik.poeck@ukr.de (H.P.)
https://doi.org/10.1016/j.xcrm.2023.101171

SUMMARY

Tumor-derived extracellular vesicles (EVs) have been associated with immune evasion and tumor progression. We show that the RNA-sensing receptor RIG-I within tumor cells governs biogenesis and immunomodulatory function of EVs. Cancer-intrinsic RIG-I activation releases EVs, which mediate dendritic cell maturation and T cell antitumor immunity, synergizing with immune checkpoint blockade. Intact RIG-I, autocrine interferon signaling, and the GTPase Rab27a in tumor cells are required for biogenesis of immunostimulatory EVs. Active intrinsic RIG-I signaling governs composition of the tumor EV RNA cargo including small non-coding stimulatory RNAs. High transcriptional activity of EV pathway genes and RIG-I in melanoma samples associate with prolonged patient survival and beneficial response to immunotherapy. EVs generated from human melanoma after RIG-I stimulation induce potent antigen-specific T cell responses. We thus define a molecular pathway that can be targeted in tumors to favorably alter EV immunomodulatory function. We propose "reprogramming" of tumor EVs as a personalized strategy for T cell-mediated cancer immunotherapy.

INTRODUCTION

Cancer immunotherapy by immune checkpoint blockade (ICB) has shown great clinical efficacy for solid and hematologic malignancies, yet response heterogeneity to ICB remains a clinical challenge. Therefore, it is important to better understand the mechanisms driving ICB-induced antitumor responses and therapy resistance. Engagement of type I interferon (IFN-I)-inducing

CellPress
OPEN ACCESS

Cell Reports Medicine
Article

cytosolic nucleic acid sensing pathways—particularly the cGAS/STING and RIG-I/MAVS pathways—is critical in generating antigen-specific antitumor immune responses.[1–4] The DNA sensor cGAS and the downstream effector STING constitute a cytosolic pattern recognition receptor system that recognizes cytosolic DNA derivates from exogenous (microbial pathogens, dead cells) and endogenous (e.g., mitochondrial damage) sources to trigger innate immune gene transcription and IFN-I production.[5,6] The success of ICB with anti-CTLA-4 and anti-PD-1 are both dependent on cGAS/STING signaling in the tumor microenvironment (TME).[1,4,7,8] The cytosolic RNA receptor RIG-I (encoded by *DDX58*) detects double-stranded 5′-triphosphate RNA (3pRNA) from exogenous and endogenous sources (e.g., viruses, bacteria, non-coding RNAs [ncRNAs]).[6,9,10] Downstream signaling via the adapter molecule MAVS and transcription factors IRF3/IRF7 can induce potent IFN-I production. Therapeutic targeting of cGAS/STING and RIG-I in the TME has demonstrated strong antitumor effects mediated via IFN-I production by host immune cells and simultaneous induction of regulated cell death in malignant cells.[3,11] We recently demonstrated that immunotherapy with anti-CTLA-4 and its combination with anti-PD-1 or radiation therapy rely on tumor cell-intrinsic activation of RIG-I but not STING signaling.[12,13] However, the mechanisms of tumor-host communication following activation of these nucleic acid receptor pathways within tumor cells remain elusive.

As a new paradigm in intercellular communication, information exchange via extracellular vesicles (EVs) has become the focus of intense research.[14,15] EVs are a heterogeneous group of membrane-encapsuled vesicles that are released from virtually all cells, including cancer cells. Depending on the mechanism of EV biogenesis, distinct groups can be distinguished: microvesicles/ectosomes are formed by direct outward budding of the plasma membrane, while exosomes originate from the endosomal system.[14] EVs carry a vast bioactive cargo consisting of proteins, lipids, metabolites, and nucleic acids, which vary greatly by type and functional state of their cellular source.[16] Intrinsic properties of EVs in regulating complex intracellular pathways in target cells have sparked widespread interest in their potential utility in the therapeutic control of cancer. EVs released within the TME have been predominantly regarded as immunosuppressive and adversarial to immunotherapy,[17] yet the role of EVs in cancer is likely dynamic and specific to cancer type, genetics, and stage. EVs were also found to elicit potent immune reactions in a context-dependent manner. Tumor-derived EVs can induce activation of dendritic cells (DCs) via transfer of tumor-associated antigens (TAAs) and subsequent cross-priming of specific T cells.[18,19] However, conditions under which cancer cells release such immunostimulatory EVs, the involved signaling pathways, and their impact on T cell-based antitumor immunity and, thus, interaction with clinically established immunotherapies remain unclear. We here systematically dissect key molecules governing the biogenesis, cargo, and immunomodulatory function of tumor EVs. We show that cancer-intrinsic cytosolic RIG-I/IFN-I signaling can be harnessed for the generation of immunogenic tumor EVs that trigger potent antitumor T cell responses and synergize with ICB cancer immunotherapy.

RESULTS

RIG-I signaling does not influence quantitative EV release from tumor cells

To determine the role of tumor cell-intrinsic RIG-I signaling on EV content and release, murine B16 melanoma cells expressing the model antigen ovalbumin (B16.OVA) were transfected with a well-established RIG-I ligand (*in vitro* transcribed 5′-triphosphorylated RNA, 3pRNA). Twenty-four hours later, melanoma-cell-derived EVs were enriched from the culture supernatant (SN) using mainly a precipitation-based assay. EV preparations were termed by their cellular origin: RIG-I-EVs for EVs from SN of B16.OVA cells with active RIG-I receptor signaling (induced by 3pRNA), and control EVs (Ctrl-EVs) from SN of untreated cells under steady-state conditions. The enriched EV preparations were analyzed by electron microscopy and quantified by nanoparticle tracking analysis (NTA). Particles were found to be homogenously sized with a median diameter of 130–140 nm and showed a uniform distribution of number and concentration in different samples (Figures S1A–S1D). Presence of EV marker proteins that are generally associated with exosomes (Alix, Flotillin 1, HSP70, CD81, CD63), and strong under-representation of negative quality control markers (cytochrome *c*, calnexin) were confirmed by western blot (Figures S1E and S1F), following the MISEV2018 consensus guidelines by the International Society for Extracellular Vesicles.[20] Active tumor cell-intrinsic RIG-I signaling did not impact on size, protein load, or the number of released particles. By contrast, genetic loss of RIG-I activity did not impact on the abundance of EV protein markers (Figure S1G).

Tumor cell-intrinsic RIG-I signaling mediates the release of immunogenic EVs

To assess the immunomodulatory capacity of tumor EVs released during active RIG-I signaling, bone marrow-derived DCs were exposed to B16.OVA melanoma-derived tumor EV preparations. If not stated otherwise, the amount of EVs was normalized to the amount of tumor cells that generated these EVs and not the absolute particle numbers. Tumor cell-derived EVs released under steady-state conditions (Ctrl-EVs) did not result in detectable levels of IFN-I in DC cultures (Figure 1A). In contrast, EVs released by tumor cells undergoing RIG-I signaling induced maturation and strong IFN-I production in DCs (Figures 1A and S2A). EVs released by melanoma cells that were transfected with a sequence-identical non-triphosphate, synthetic RNA (synRNA) did not induce IFN-I production in DCs. By similar precipitation of medium supplemented with 3pRNA complexed in liposomes in the absence of tumor cells (mock-EVs), we excluded that 3pRNA-liposomes (used to activate RIG-I signaling in tumor cells) were co-purified within tumor EV preparations. Activation of the cGAS/STING pathway resulted in the release of poorly immunostimulatory cGAS-EVs from melanoma cells with low-level IFN-I-inducing capacity in DCs. The immunostimulatory potential of RIG-I-induced EV preparations in DCs showed clear dose dependency (Figure S2B). Cationic lipids such as lipofectamine have previously been applied to increase cellular uptake and, thus, bioactivity of EVs.[21] For *in vitro* experiments, we found that lipofectamine could increase the bioactivity of low-dose EVs, while IFN-I

Cell Reports Medicine
Article

CellPress
OPEN ACCESS

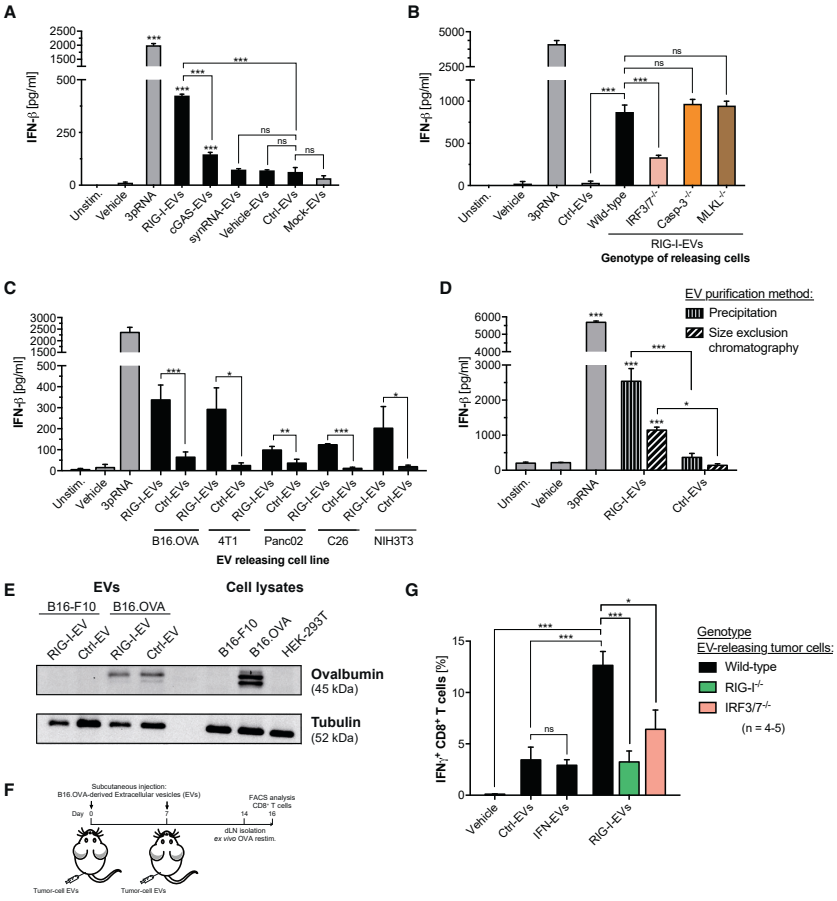

Figure 1. Tumor cell-intrinsic RIG-I signaling mediates the release of immunogenic EVs

B16.OVA melanoma cells were transfected with a RIG-I ligand (3p-RNA, RIG-I-EVs), interferon-stimulating DNA (cGAS-EVs), or synthetic RNA (synRNA-EVs). Extracellular vesicles (EVs) were enriched from the culture supernatant of treated and untreated (ctrl-EVs) cells. Precipitation of 3pRNA-liposomes in the absence of tumor cells was performed as negative control (mock-EVs).

(A) IFN-β release (ELISA) by dendritic cells (DCs) exposed to tumor cell-derived EV samples. Some DCs were directly transfected with *in vitro* transcribed 3pRNA as positive control.

(B–D) IFN-β release from DCs exposed to RIG-I-EV preparations: (B) prepared from different melanoma clones that lack specific downstream signaling components of nucleic acid receptor pathways; (C) enriched from various murine tumor cell lines: mammary (4T1), pancreatic (Panc02), colon (C26) carcinoma; and (D) enriched by precipitation or size-exclusion chromatography. All data are presented as mean values ± SEM of at least quadruplicate technical replicates per group and are representative of two independent experiments. Asterisks without brackets indicate statistical comparison with Ctrl-EV-treated cells.

(E) Presence of the antigen OVA (by western blot) in melanoma cell EV samples.

(F) Treatment model. C57BL6/j mice were repeatedly injected subcutaneously with tumor EV samples prepared from cultures of wild-type, RIG-I-deficient (RIG-I$^{-/-}$), or IRF3/7-deficient (IRF3/7$^{-/-}$) B16.OVA melanoma cells.

(G) IFN-γ release by CD8$^+$ T cells from draining lymph nodes after *ex vivo* OVA restimulation (flow cytometry).

Data are presented as mean values ± SEM of n = 4–5 individual mice per group and were pooled from two independent experiments. Unstim, unstimulated. See also Figures S1–S3.

CellPress
OPEN ACCESS

Cell Reports Medicine
Article

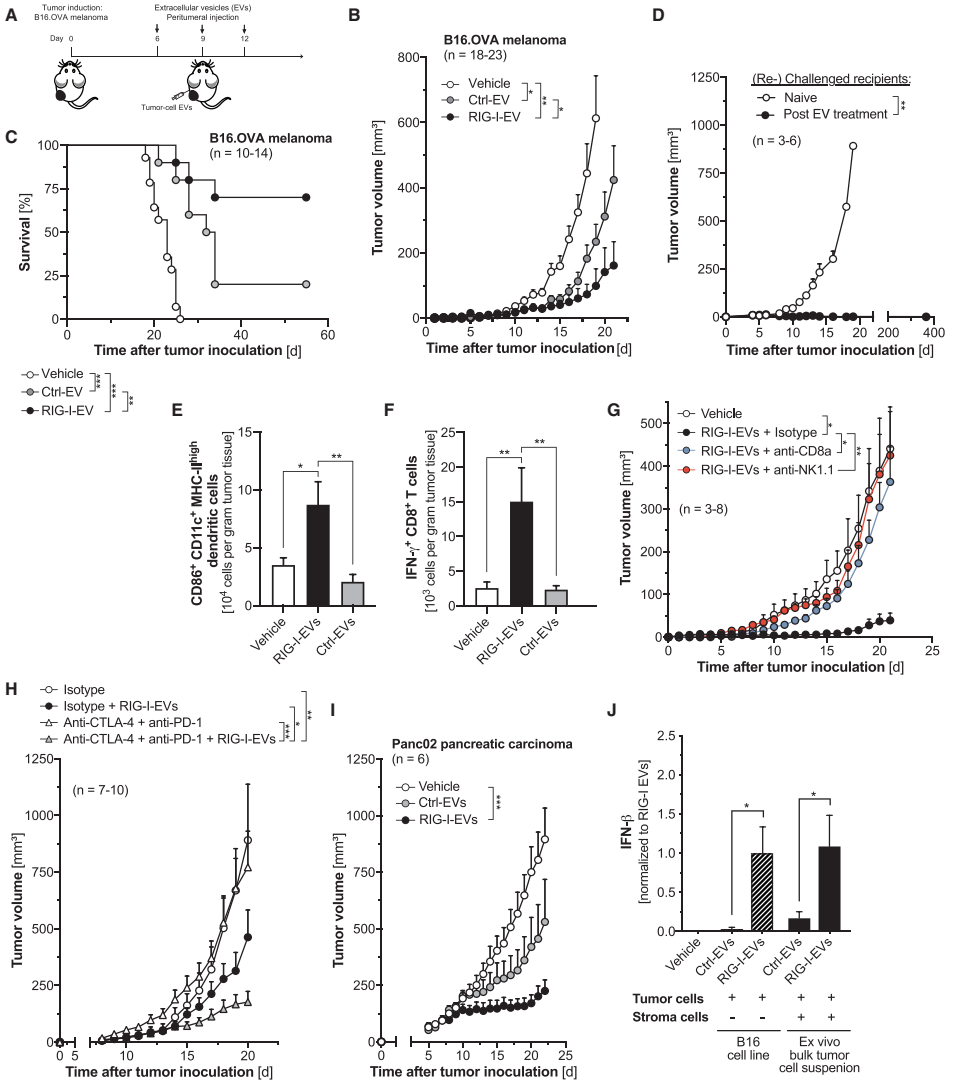

Figure 2. EVs released from RIG-I-activated tumor cells induce potent cytotoxic antitumor immunity and synergize with checkpoint inhibitors

(A) B16.OVA-bearing mice were injected peritumorally with melanoma-cell-derived EV samples.

(B and C) (B) Tumor growth and (C) overall survival.

(D) Tumor growth after rechallenge with a second, contralateral injection of viable B16.OVA cells in mice with initially complete tumor regression in response to EV treatment.

(E and F) Abundance of activated tumor-infiltrating (E) DCs and (F) $CD8^+$ T cells (n = 8–12 mice per group).

(legend continued on next page)

Cell Reports Medicine
Article

CellPress
OPEN ACCESS

induction in DCs by exposure to high concentrations of EV preparations could not be further enhanced by application of lipofectamine (Figure S2B). If not stated otherwise, we used lipofectamine for *in vitro* experiments to increase the efficiency of low-dose EV treatment.

Next, we analyzed the molecular mechanisms downstream of RIG-I in the induction of immunostimulatory EV (isEV) release. The immunostimulatory capacity of tumor EVs released upon RIG-I activation was abrogated in tumor cells deficient for IRF3/7, two transcription factors central to the production of IFN-I (Figure 1B). We did not observe transfer of tumor cell-derived IFN-I in enriched tumor EV preparations (Figure S2C), yet activation of the RIG-I pathway within tumor cells can also induce an immunogenic form of programmed cell death[3,22,23] (Figure S2D). However, tumor-intrinsic genetic deficiency for the central executioner proteins of apoptosis (caspase-3) or necroptosis (MLKL), which prevents tumor cells from undergoing programmed cell death in response to RIG-I activation,[12] did not impact on the release of isEVs (Figure 1B). Furthermore, the immunostimulatory effect of RIG-I-induced EV preparations was observed in various murine tumor cell lines including mammary, pancreatic, and colorectal carcinomas, but also in non-transformed fibroblasts (Figure 1C). These data suggest that biogenesis and release of isEVs is a conserved cellular response pattern that requires coupling of cancer-intrinsic active RIG-I signaling to downstream IFN-I production via IRF3/7, but it occurs independent of regulated cell death.

Most methods used for EV enrichment co-isolate different EV populations of diverse biogenic origin.[14] Utilizing size-exclusion chromatography (SEC) or differential ultracentrifugation, we found that the immunostimulatory nature of RIG-I-induced EVs did not depend on the method used to enrich tumor EV preparations (Figures 1D and S2E–S2H). These very similar and overlapping findings for different enrichment assays imply that the RIG-I-induced immunostimulatory function is indeed mediated by isEVs and not by products of specific particle preparation methods.

Tumor-derived EVs have been attributed with the potential to induce efficient activation of DCs via transfer of TAAs and subsequent cross-priming of tumor-reactive T cells *in vivo*.[19] We found that B16.OVA melanoma-derived EVs indeed contained OVA antigen (Figure 1E). Shuttling of such TAA was not influenced by active RIG-I signaling in the EV-releasing cells. To better characterize the role of tumor cell-intrinsic RIG-I receptor pathway activity on the immunogenicity of tumor cell-released EVs *in vivo*, mice were immunized with B16.OVA-derived EV preparations, and T cell activation in draining lymph nodes was analyzed (Figure 1F). We found that immunization with isEVs released from melanoma cells during active RIG-I signaling showed strong immunogenic potential with potent activation of $CD8^+$ T cells *in vivo* (Figures 1G and S3A). Application of tumor EVs in mice was not associated with any clinically apparent signs of adverse events or systemic organ toxicity (Figure S3B). In line with our *in vitro* findings, the *in vivo* immunogenicity of RIG-I-induced isEVs was critically dependent on active RIG-I as well as IRF3/7 signaling in the EV-releasing tumor cells (Figure 1G). Without active simultaneous RIG-I signaling, *in vitro* treatment of tumor cells with recombinant IFN-I (IFN-EVs) was not sufficient to trigger the release of T cell-activating isEVs. Defective signaling of the RIG-I/IRF3/7 axis in tumor cells did not impact on quantitative EV release (Figure S3C). The potential of tumor cell-derived isEV preparations to induce T cell responses *in vivo* could be reproduced with complementary *ex vivo* EV enrichment methods such as SEC (Figure S3D). Tumor cell EVs also shuttled endogenous melanoma TAAs such as gp100 (Figures S3E and S3F). RIG-I-induced isEV preparations from otherwise poorly immunogenic B16-F10 melanoma were able to induce T cell immunity in the absence of artificial OVA antigen.

EVs released from RIG-I-activated tumor cells induce potent cytotoxic antitumor immunity and synergize with checkpoint inhibitors

Therapeutic application of isEVs enriched from *in vitro* RIG-I-activated B16.OVA cells showed strong antitumor effects accompanied by growth delay of melanomas *in vivo* with prolonged survival of tumor-bearing mice (Figures 2A–2C). Intriguingly, animals with stable tumor control after isEV treatment were protected against a second challenge with viable melanoma cells, indicating the formation of antitumor immunological memory (Figure 2D). Treatment with RIG-I-induced isEV preparations was associated with increased abundance of mature DCs as well as activated $CD4^+$ and $CD8^+$ T cells in the TME (Figures 2E, 2F, and S3G). The potent antitumor activity of isEVs was completely abrogated following antibody-mediated depletion of $CD8^+$ cytotoxic T cells (Figure 2G). Depletion of $NK1.1^+$ natural killer (NK) cells reduced the therapeutic efficacy of isEVs to a similar extent. In a melanoma model of suboptimal-dosed anti-PD-1/-CTLA-4, treatment with RIG-I-induced isEVs rendered tumors susceptible to ICB under conditions otherwise associated with tumor resistance to immunotherapy (Figure 2H). isEV preparations from syngeneic pancreatic tumor cells also showed high antitumor potency in a murine model of pancreatic carcinoma (Figure 2I). In possible translational use of tumor-derived isEVs as personalized tumor treatment, short-term culture of resected tumors may serve as a potential source of autologous isEV preparations. However, the composition of such *ex vivo* tumor cell cultures would be much more complex than the monoclonal murine tumor cell lines used here. At the same time, stromal-cell-derived EVs from cancer-associated fibroblasts have been postulated to harbor pro-tumorigenic function in the TME.[24] To account for the diversity of EVs within the TME, we generated EV preparations from short-term cultures of freshly isolated bulk tumor tissue. Similar to isEVs derived from homogeneous tumor cell lines, RIG-I stimulation resulted in the enrichment of isEV preparations from these heterogeneous cell cultures and subsequent induction of IFN-I in exposed DCs (Figure 2J).

(G and H) Tumor growth in mice additionally injected with (G) anti-CD8a- or anti-NK1.1-depleting antibodies, or (H) anti-PD-1/CTLA-4 checkpoint inhibitors.
(I) Panc02 pancreatic carcinoma growth in mice injected peritumorally with Panc02-cell-derived EV samples.
(J) IFN-β release from DCs exposed to RIG-I-induced EVs from either culture of B16.OVA melanoma cells or *ex vivo* cell suspensions of freshly isolated bulk tumors (mean ± SEM of n = 8 biological replicates pooled from at least three independent experiments).
All data are presented as mean tumor growth ± SEM and are pooled from or representative of at least two independent experiments. See also Figures S3 and S4.

As the basis for an alternative approach to harness the therapeutic potential of isEVs, we have previously shown that *in situ* vaccination with intra-tumoral injection of a RIG-I ligand has potent antitumor activity.[12,25] By analyzing a set of genes whose products were previously associated with vesicle secretion in tumor cell lines,[26] we found that targeted activation of RIG-I signaling in bulk tumors *in vivo* resulted in high transcriptional activity of vesiculation-associated genes (Figure 3A). The small guanosine triphosphatase Rab27a has been shown to be critically involved in the secretion of EVs of the endocytic biogenesis pathway.[27] Indeed, Rab27a deficiency in melanoma cells resulted in overall reduced numbers of released particles (Figures 3B–3D). In accordance with the dose dependency of isEV effects (Figure S2A), we found that reduced numbers of particles released by a fixed number of Rab27a$^{-/-}$ melanoma cells induced only low-level IFN-I production in DCs (Figure 3E). Mice bearing bilateral melanomas were *in situ* vaccinated by unilateral intratumoral injection of a RIG-I agonist (Figure 3F). The previously described[12] expansion of circulating tumor-antigen-specific T cells and systemic regression of tumors in response to RIG-I activation in the TME was largely diminished in mice bearing Rab27a$^{-/-}$ tumors (Figures 3G and 3H). These data suggest that (1) antitumor effects of *in situ* vaccination via tumor-intrinsic RIG-I activation rely in part on the production of EVs, and (2) the release of RIG-I-induced isEVs (but also Ctrl-EVs) depends on Rab27a-mediated EV biogenesis pathways.

Tumor cell-derived EVs are actively taken up by dendritic cells via endocytic pathways

Different mechanisms of EV uptake in recipient cells can have direct consequences for the distinct intracellular localization, degradation, and functional outcomes of EV constituents.[28] Tumor EV particles labeled with a fluorescent membrane marker showed rapid uptake by DCs, with an intracellular distribution pattern of the dye that suggested cytosolic delivery (Figures S4A and S4B). Blocking clathrin- and caveolin-dependent endocytosis (dynasore) or macropinocytosis (amiloride) with chemical inhibitors abrogated internalization of labeled particles by DCs (Figures S4C and S4D). Only inhibition of particle uptake via macropinocytosis prevented subsequent IFN-I induction in recipient DCs (Figure S4E). These data suggest that (1) tumor-derived EVs are actively ingested by DCs via endocytic pathways, and (2) the immunostimulatory effect of RIG-I-induced isEV preparations requires uptake via macropinocytosis in recipient cells. In fact, macropinocytosis of EVs has been associated with cytosolic delivery of cargo nucleic acids,[29] where they could in principle be detected by RIG-I/MAVS and/or cGAS/STING.

Immunogenicity of RIG-I-induced tumor isEVs is mediated via host nucleic acid receptor signaling and IFN-I activity in myeloid cells

Next, we aimed to identify the molecular pathways within host cells that are targeted by RIG-I-induced isEVs and their constituents. The importance of IFN-I signaling within host antigen-presenting cells (APCs) for the induction of antitumor T cell immunity has been widely acknowledged.[30,31] Using antibodies to block the common interferon-α receptor subunit 1 (IFNaR1), we found that T cell activation *in vivo* in response to RIG-I-induced EV preparations was critically dependent on host IFN-I signaling (Figure 4A). Furthermore, we applied isEV preparations in mice with conditional genetic deficiency that specifically lack IFNaR1 in either CD11c$^+$ DCs or LysM$^+$ macrophages. Hereby, we found that T cell activation by RIG-I-induced tumor isEVs depends on IFN-I receptor activity in both APC types (Figure 4B).

Activation of nucleic acid receptor signaling within host immune cells is a very potent stimulus for IFN-I release and has been found to be critical in the induction of antitumor immunity.[4] We treated mice that genetically lacked either the RIG-I adapter MAVS (*Mavs*$^{-/-}$) or the cGAS adapter STING (*Sting*$^{gt/gt}$) with tumor EVs, and found that isEV-induced T cell activation was largely abrogated in the absence of functional MAVS signaling within host cells (Figure 4C). Host cell deficiency for STING partially reduced T cell immunity in response to RIG-I-induced isEVs *in vivo*. To further characterize the role of host nucleic acid receptors in the detection of isEVs and their cargo, DCs derived from *Mavs*$^{-/-}$ or *Sting*$^{gt/gt}$ donor mice were exposed to melanoma-cell-derived EV samples *in vitro*. *Mavs*$^{-/-}$ DCs showed drastically reduced IFN-I production in response to RIG-I-induced isEVs (Figure 4D), while STING-deficient DCs only showed a partial defect in isEV detection *in vitro*. In contrast, genetic deficiency for Toll-like receptor 3 (TLR-3) or MyD88 (the adapter protein for the nucleic acid sensing TLRs 7–9) did not impact on the ability of DCs to release IFN-I upon interaction with RIG-I-induced isEVs (Figure 4E). These data suggest that RIG-I activity within tumor cells fosters the release of particularly immunogenic EVs that initiate IFN-I signaling within host APCs. This presumably happens via the transfer of RIG-I/MAVS-activating (and to a lesser extent cGAS/STING-activating) ligands, and subsequent activation of T cells.

Tumor-intrinsic RIG-I pathway activity mediates shuttling of immunostimulatory RNA within EVs

To address the possible transfer of immunostimulatory tumor RNA via EVs, we fluorescently labeled the bulk RNA cargo of tumor EV samples prior to their exposure to DCs. We observed concentration-dependent transfer of labeled EV RNA cargo to DCs (Figure 5A). Next, we extracted nucleic acids from tumor cell-derived EV samples and transfected DCs with liposome-bound EV RNA *in vitro*. We found that only RNA purified from RIG-I-induced isEV preparations induced potent IFN-I production in DCs (Figure 5B). Treatment of isEV-derived RNA with alkaline phosphatase to cleave 5′-triphosphate groups and, thus, the RIG-I-activating moiety significantly reduced its immunostimulatory capacity. However, despite alkaline phosphatase treatment, EV-extracted RNA still showed significant IFN-I induction in DCs, suggesting that immunostimulatory isEV-RNA is heterogeneous and is composed of both RIG-I-activating 3pRNAs and other non-RIG-I-targeting stimulatory RNAs. Exposure of tumor EV preparations to RNAse A, an endoribonuclease digesting single- and double-stranded RNA, did not impact on IFN-I production of recipient DCs (Figure S5A), suggesting that RNA in these samples was indeed shuttled inside membranous particles, protecting it from enzymatic degradation. Next, tumor cells were transfected with fluorescently labeled 3pRNA, and subsequently released isEVs were analyzed by imaging flow cytometry. We detected labeled, *in vitro* transcribed 3pRNA only within a very small fraction of tumor

Cell Reports Medicine
Article

CellPress
OPEN ACCESS

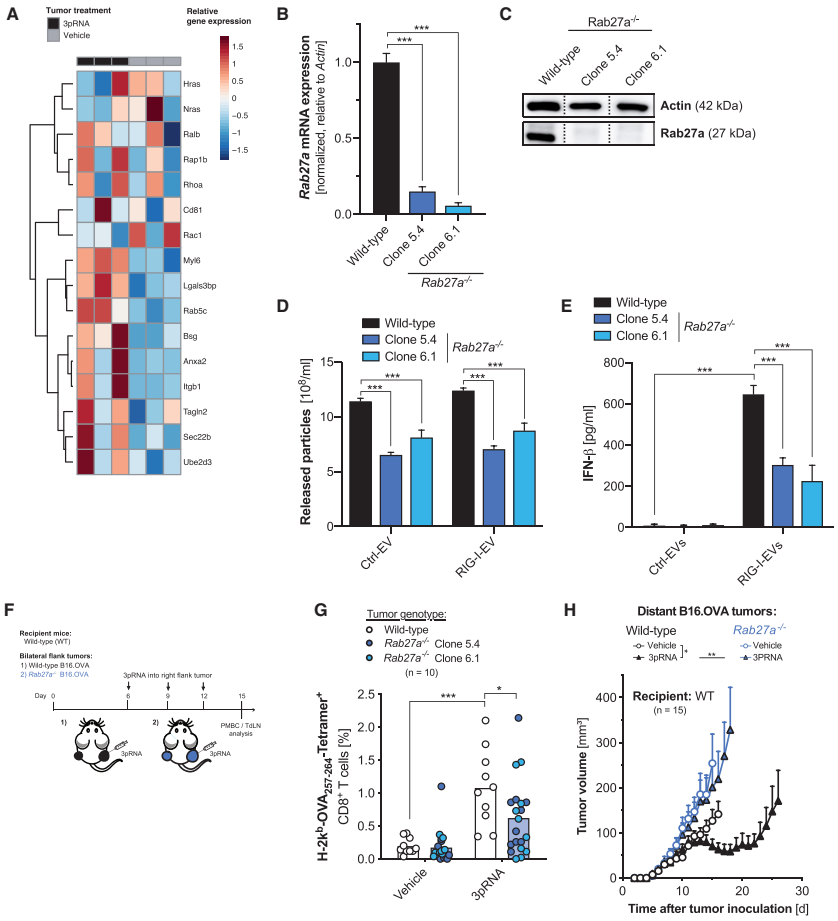

Figure 3. Therapeutic *in situ* activation of the RIG-I pathway modulates tumor EV generation for systemic antitumor immunity

(A) RNA-seq of bulk tumor after a single intratumoral injection of 3pRNA in B16.OVA melanoma-bearing mice. Heatmap shows *Z*-transformed expression of genes associated with tumor EV biogenesis and cargo loading.

(B and C) (B) Rab27a mRNA copy numbers of two different Rab27a-deficient (Rab27a$^{-/-}$) clones and (C) corresponding protein expression (western blot).

(D and E) EVs were enriched from Rab27a$^{-/-}$ B16 cell cultures. (D) Particle quantification within EV preparations by NTA. (E) IFN-I induction in DCs exposed to EVs from Rab27a$^{-/-}$ B16.OVA cells.

(F) Mice bilaterally bearing either wild-type or Rab27a$^{-/-}$ melanomas were injected with 3pRNA into right-sided tumors.

(G) Mean and individual frequency of H-2Kb-SIINFEKL tetramer^{+} CD8^{+} T cells in peripheral blood of n = 10 mice per group pooled from two independent experiments.

(H) Mean volume of left-sided tumors ± SEM of n = 15 individual mice per group pooled from three independent experiments.

All *in vitro* data show mean ± SEM of at least quadruplicate technical replicates, representative of at least two independent experiments.

cell-derived EVs (Figures S5B and S5C). After EV lysis with a detergent the fluorescence signal was no longer detectable, indicating that the RNA-bound fluorescent dye indeed accumulated within membranous EVs rather than unspecific protein aggregates (Figure S5D). Together with our findings that the generation of immunostimulatory EVs is dependent on active RIG-I signaling

CellPress
OPEN ACCESS

Cell Reports Medicine
Article

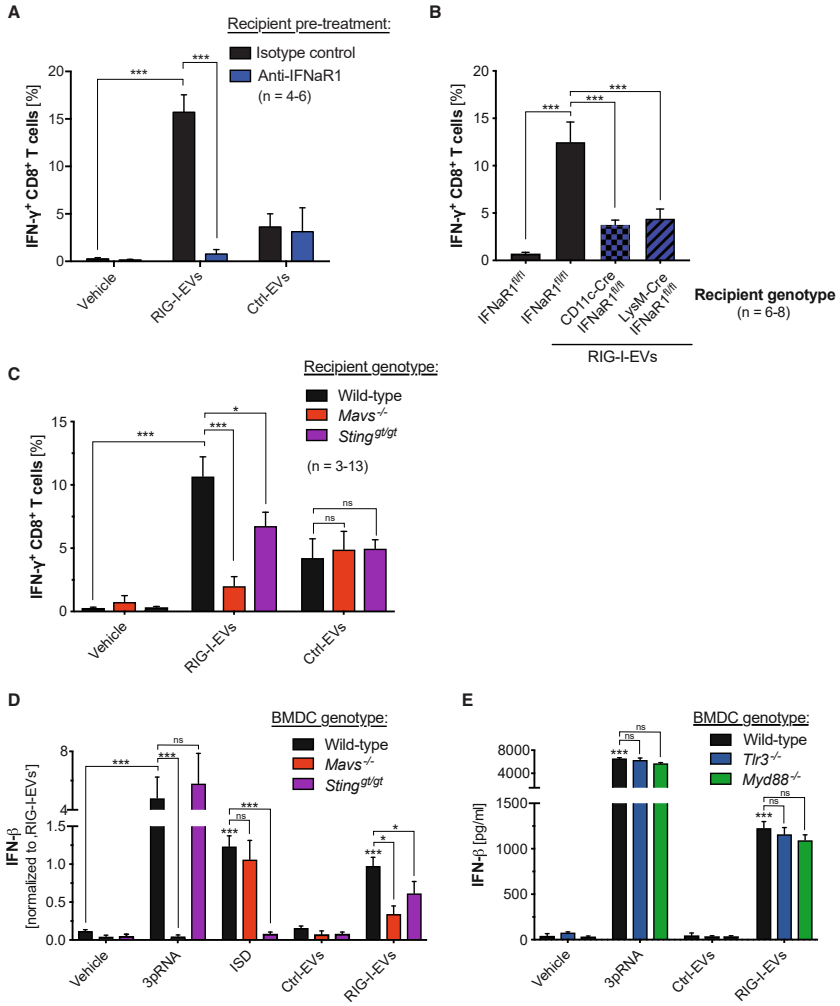

Figure 4. Immunogenicity of RIG-I-induced isEVs is mediated via host cytosolic nucleic acid receptor signaling and IFN-I activity in myeloid antigen-presenting cells

(A) Mice were treated with anti-IFNaR1 antibodies prior to immunization with B16.OVA melanoma cell EV samples. IFN-γ release by $CD8^+$ T cells (flow cytometry).

(B and C) IFN-γ release by $CD8^+$ T cells upon tumor EV immunization in mice with genetic deficiency (B) for IFNaR1 in DCs (*CD11c-Cre Ifnar*$^{fl/fl}$) or macrophages (*LysM-Cre Ifnar*$^{fl/fl}$), and (C) globally for MAVS (*Mavs*$^{-/-}$) or STING (*Sting*$^{gt/gt}$). Data represent the mean value ± SEM of individual mice per group pooled from at least two independent experiments.

(D and E) IFN-I production in (D) *Mavs*$^{-/-}$ or *Sting*$^{gt/gt}$ DCs and (E) TLR-3-deficient (*Tlr3*$^{-/-}$) or Myd88-deficient (*Myd88*$^{-/-}$) DCs exposed *in vitro* to melanoma EV samples.

All *in vitro* data show mean ± SEM of at least triplicate technical replicates, representative of at least two independent experiments. Asterisks without brackets indicate statistical comparison to vehicle-treated control cells. See also Figure S4.

Cell Reports Medicine
Article

CellPress
OPEN ACCESS

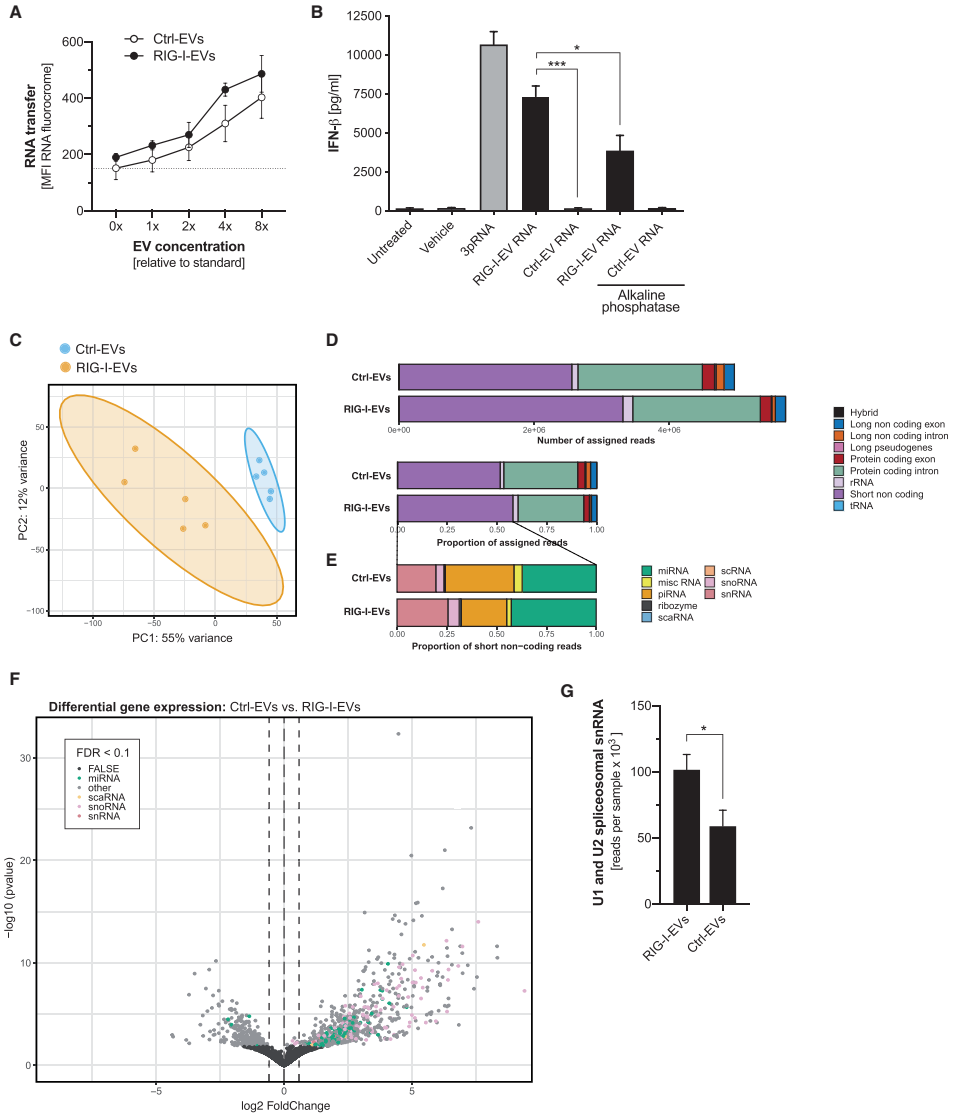

Figure 5. Tumor-intrinsic RIG-I pathway activity mediates shuttling of immunostimulatory RNA within EVs

(A) Transfer of EV RNA to DCs after exposure to B16 melanoma EVs with fluorescently labeled RNA cargo (flow cytometry).

(B) IFN-β release by DCs upon transfection with tumor EV extracted RNA or *in vitro* transcribed 3pRNA. Some EV RNA was treated with alkaline phosphatase prior to DC transfection (ELISA, mean value ± SEM of at least triplicate technical replicates, representative of at least two independent experiments).

(legend continued on next page)

CellPress
OPEN ACCESS

Cell Reports Medicine
Article

in EV-releasing tumor cells (Figure 1G), these data speak against passive transfer of *in vitro* transcribed 3pRNA used for melanoma RIG-I activation into tumor isEVs in biologically relevant abundance.

The amount of DNA that we were able to extract from tumor cell EV preparations was drastically lower than for RNA (Figure S5E). We pooled the extracted DNA from very large numbers of tumor EV samples and transfected DCs with liposome-bound EV DNA. EV DNA induced IFN-I production in DCs via activation of the STING pathway (Figure S5F). However, its immunostimulatory potential was independent of active RIG-I signaling in EV-releasing tumor cells. Reduced IFN-I induction by EV preparations that were treated with DNase I prior to EV lysis for DNA extraction suggested that some EV DNA was surface-bound and not internal EV cargo. From this we concluded that RIG-I signaling in tumor cells results in the shuttling of different endogenous immunostimulatory RNAs within EVs. The biological role of tumor EV DNA is less clear. If anything, not qualitative but quantitative changes in EV DNA cargo might alter EV immunostimulatory function; but these changes seem independent of tumor cell-intrinsic RIG-I activity.

Cargo RNAs of EV include various biotypes that represent a selected portion of the RNA content of the source cell, with a strong bias toward small ncRNAs.[32] We performed next-generation sequencing of the endogenous RNA cargo extracted from tumor EV preparations. Given the proposed role of small nuclear RNA (snRNA) and small nucleolar RNA (snoRNA) as endogenous RIG-I ligands and their accumulation in the cytosol in tumor cells during cellular stress situations,[33] we performed library preparation and RNA sequencing (RNA-seq) optimized for the analysis of small RNAs. Hereby, we found that RIG-I signaling in tumor cells indeed actively shaped the global EV RNA composition (Figure 5C). Short ncRNAs were abundant in all tumor EVs (Figure 5D). However, active RIG-I signaling within the EV-releasing melanoma cells altered subsequent EV cargo composition with a general enrichment of snRNAs (Figures 5E and S6A) and a shift in the abundance of particular ncRNAs including snoRNAs (Figure 5F and Table S1). Some of the snRNA transcripts that were found to be particularly enriched in RIG-I-induced isEV preparations, such as the U1 and U2 spliceosomal RNAs (Figure 5G), have been implicated as endogenous ligands for cytosolic RIG-I-like helicases in tumor cells.[33] The RIG-I-activating endogenous ncRNA RN7SL1, which was previously described to promote tumor growth, metastasis, and therapy resistance in breast cancer cells after EV-mediated transfer,[24] was significantly less abundant in RIG-I-EVs (Figure S6B).

EVs can shuttle functional microRNA (miRNA) to regulate gene activity in distant target cells. However, to the best of our knowledge, none of the top hits among the 60 miRNAs we found to be differentially regulated in the EV cargo of RIG-I-activated tumor cells (Figure 5F and Table S2) have previously been linked to RIG-I-like receptor activity and/or EV function in the context of cancer. Additionally, ncRNAs arising from repetitive elements that are typically silenced yet often highly expressed in cancers have been implicated in the activation of innate immunity.[34] These ncRNAs were not found to be enriched in RIG-I-EVs (Figure S6C). Finally, even though our analysis was not designed to analyze long RNA, we identified mRNA fragments within the tumor EV cargo, the vast majority of which mapped to intronic regions (Figure 5D). For the mRNA exonic sequences, our data cannot evaluate whether they contain any full-length protein-encoding sequences or only mRNA fragments. Nevertheless, we performed gene set enrichment analysis (GSEA) and found that significantly enriched RNAs in the RIG-I-EV cargo mainly clustered in immune-related pathways (Figure S6D). Hereby, we found large overlap with the cellular transcriptome of RIG-I-activated melanoma cells, derived from a previously published GSEA of *ex vivo* bulk tumor RNA-seq.[12] These data confirm that the tumor EV RNA cargo reflects the cellular RNA content and show that RIG-I signaling activity in tumor cells results in the preferred shuttling of specific RNAs of different biotypes within tumor cell-derived EVs, thereby contributing to their immunostimulatory potential.

RIG-I signaling dictates the immunogenicity of EVs released by human melanoma cells

To assess translational relevance of our findings, we enriched EVs from culture supernatants of the human melanoma cell line D04mel under steady-state conditions (Ctrl-EVs) or active RIG-I signaling induced by 3pRNA (RIG-I-EVs). Peripheral blood mononuclear cells (PBMCs) from healthy donors were exposed to tumor EV preparations in *ex vivo* cultures. Uptake of carboxyfluorescein succinimidyl ester-labeled particles was largely restricted to monocytes but could also be observed in NK cells (Figure S7A). RIG-I-induced human tumor isEV samples stimulated potent release of IFN-I and the IFN-I-induced chemokine CXCL10 by the monocyte subpopulation within PBMCs (Figure 6A) but not of pro-inflammatory cytokines (Figures S7B and S7C). RNA extracted from tumor isEV preparations enriched from different RIG-I-activated human melanoma or non-malignant human primary fibroblast cultures showed immunostimulatory potential in PBMCs, which was largely abrogated when EV-extracted RNA was pretreated with 3pRNA-inactivating alkaline phosphatase (Figures 6B and S7D). Human DCs also potently produced IFN-I after exposure to RIG-I-induced melanoma isEV samples (Figure S7E). The immunostimulatory potential of EVs released from 3pRNA-treated human tumor cells was critically dependent on active RIG-I and autocrine IFN-I signaling but not cGAS/STING signaling (Figure 6C). Hereby, the level of tumor cell-intrinsic RIG-I expression correlated with the immunostimulatory capacity of released isEVs (Figure S7F). Tumor-derived EVs released during active cGAS or STING signaling in human tumor cells did not induce IFN-I in monocytic THP-1 cells

(C–G) RNA-seq of small RNA content extracted from B16.OVA melanoma cell EVs (n = 3 biological replicates per group). (C) Principal component analysis of the RNA content of Ctrl-EVs vs. RIG-I-EVs. (D) Absolute (upper panel) and relative abundance (lower panel) of the indicated RNA biotypes. (E) Relative abundance of the indicated short non-coding RNA. (F) Differential gene expression volcano plot of RNA content in RIG-I- vs. Ctrl-EVs. Significantly differentially expressed small non-coding RNAs are color-coded by their respective biotypes. (G) Cumulative abundance of U1 and U2 splicesosomal RNA reads in the RNA content of EVs, normalized to the overall library size.
See also Figures S5 and S6; Tables S1 and S2.

Cell Reports Medicine
Article

CellPress
OPEN ACCESS

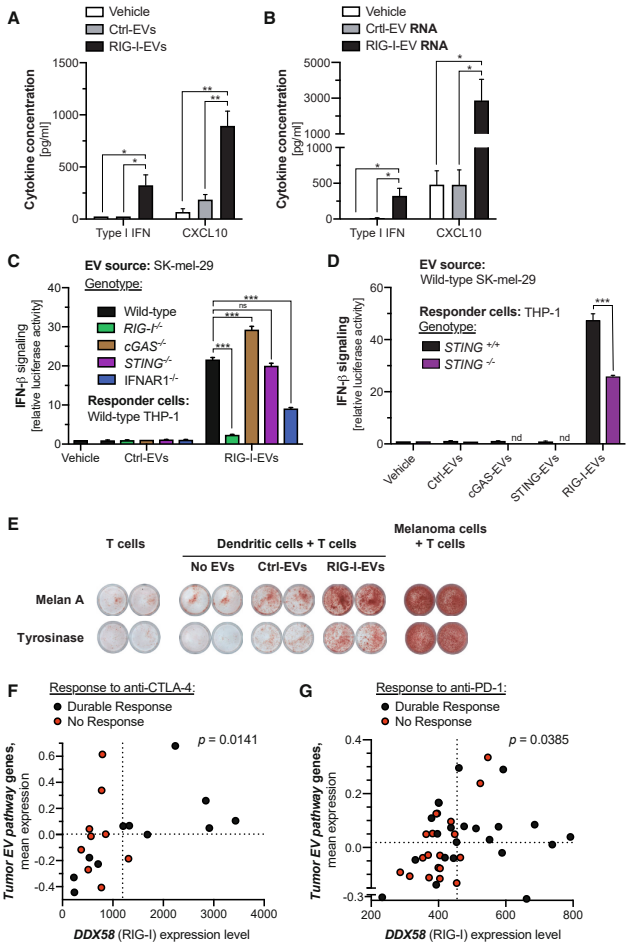

Figure 6. Tumor-intrinsic RIG-I activation in human melanoma mediates shuttling of immunostimulatory RNA within EVs and associates with beneficial clinical response

(A and B) Production of CXCL10 and IFN-I in human peripheral blood mononuclear cells (PBMCs) upon exposure to (A) human melanoma cell (D04mel)-derived RIG-I-EVs vs. Ctrl-EVs or (B) RNA purified from melanoma EV samples.

(C) IFN-I response in monocytic THP-1 reporter cells after exposure to EV samples derived from human melanoma cell lines with deficiency in RIG-I, cGAS, STING, or IFNAR1.

(D) IFN-I response in THP-1 cells with overexpression (*STING*$^{+/+}$) or gene-deficiency for *STING* (*STING*$^{-/-}$) upon exposure to different human melanoma EV preparations.

(E) Melanoma antigen-specific T cell response against Melan A (upper panel) or tyrosinase (lower panel) induced by melanoma EV samples in co-culture with autologous HLA-matched DCs (IFN-γ ELISpot, n = 2 technical replicates per group).

(F–G) Transcriptional activity of RIG-I-encoding *DDX58* and the *Tumor EV pathway* gene set in tumor samples from individual patients undergoing immune checkpoint inhibition. The dotted lines give mean transcriptional activity of the indicated genes. Gene expression and treatment response in (F) 20 melanoma patients treated with anti-CTLA-4 and (G) 41 melanoma patients treated with anti-PD-1.

All bar graphs show mean ± SEM of at least triplicate technical replicates, representative of at least two independent experiments. nd, not determined. See also Figures S7 and S8; Table S3.

We analyzed genome-wide transcriptional programs in 456 primary melanoma patient samples from The Cancer Genome Atlas (TCGA) determined by RNA-seq. Unfortunately, gene sets that are associated with specific EV release patterns are poorly defined. However, by screening 60 tumor cell lines, a recent study identified 25 commonly expressed genes whose expression level correlated with the total number of vesicles secreted specifically by tumor cells.[26] Indeed, we found for human melanoma samples in the TCGA that

(Figure 6D). However, IFN-I release induced by RIG-I-activated tumor EV samples was partly reduced in STING-deficient THP-1 cells (Figure 6D), suggesting that human tumor isEV preparations also contain immunostimulatory DNA. Similar to our findings in murine EVs, human melanoma EVs can shuttle TAAs such as Melan A, which was independent of RIG-I signaling in tumor cells (Figures S7G and S7H). Exposure of HLA-matched immature DCs to RIG-I-induced isEV samples from D05mel melanoma cells and subsequent co-culture with autologous T cell clones with receptor specificity for the melanoma antigens Melan A or tyrosinase resulted in cross-priming of tumor-antigen-specific T cells with potent IFN-γ release (Figure 6E).

24 genes of this predefined gene set were much more highly expressed in comparison to the remaining genome, and tended to be more transcriptionally active in tumor cells than in healthy tissue (Figures S8A and S8B). They were thus integrated as the *Tumor EV pathway* gene set for further analysis. In line with the current understanding of often pro-tumorigenic EV functions in the TME,[17] we found that high expression of the *Tumor EV pathway* gene set was associated with reduced overall survival in patients with malignant melanoma (Figure S8C). Patients with high *Tumor EV pathway* gene set expression were additionally stratified by median *DDX58* (the gene encoding for RIG-I) expression within the tumor samples. Within this unfavorable patient cohort with poor

overall survival, concomitantly high *DDX58* expression in melanoma samples was associated with a significantly prolonged survival (Figure S8D). In line with our previous findings on tumor-intrinsic *DDX58* transcript numbers,[12] multivariable Cox regression identified both high *Tumor EV pathway* gene set expression and low *DDX58* expression in melanoma samples as independent risk factors for death (Table S3A).

Based on the aforementioned challenges in the analysis of transcriptional programs in the context of EV biogenesis with no consensus on a universally defined ''EV pathway'' associated gene set, we validated this data analysis with a second, recently published, more broadly defined EV gene signature.[35] While the *Tumor EV pathway* signature adapted from Hurwitz et al.[26] only contains genes associated with EV production by tumor cells, the signature by Fathi et al.[35] represents multiple genes generally linked to EV production in a variety of different malignant and non-malignant cell types and is therefore hereafter referred to as the *Common EV pathway* gene set. The two signatures only overlap by two genes (*RAB7A* and *RALB*) and can thus be considered independent gene sets. The *Common EV pathway* gene set was not specifically active in human melanomas (Figures S8E and S8F). In line with our data in murine tumor samples (Figure 3A), we found that both EV pathway gene signatures' transcriptional activity in human melanoma samples strongly correlated with *DDX58* expression (Figure S8G), indicating a close relationship of EV biogenesis and activity of the RIG-I pathway. However, in contrast to the *Tumor EV pathway*, high expression levels of the *Common EV pathway* in human melanoma samples were not associated with reduced overall survival (Figure S8H). When analyzing the *Common EV pathway* and concomitant transcriptional activity of RIG-I-encoding *DDX58*, multivariable Cox regression did not identify high *Common EV pathway* gene set expression in melanoma samples as independent risk factor for death (Table S2B). These data suggest that transcriptional activity of genes modulating EV biogenesis seems to strongly differ between tumors and healthy tissue. In two independent cohorts of melanoma patients, simultaneously high transcriptional activity of both the *Tumor EV pathway* gene set and RIG-I-encoding *DDX58* was retrospectively associated with durable clinical response to ICB immunotherapy (Figures 6F and 6G). However, high *Tumor EV pathway* genetic activity was not an absolute predictive marker for treatment response, which is in line with the known existence of multiple other factors that co-drive treatment response.

DISCUSSION

The role of EVs in cancer progression is likely dynamic and specific to cancer type, genetics, and stage. Conditions under which cancer cells release immunostimulatory T cell-activating EVs remain unclear, but seem be dependent on external ''triggers'' such as genotoxic stress by chemotherapy or radiation therapy.[36,37] We here advance this concept and show that targeted activation of cancer-cell-intrinsic RIG-I signaling induces the generation of isEVs. These conditions of isEV release may be linked to each other, as genotoxic stress has been shown to result in intrinsic RIG-I activation by endogenous U1 and U2 RNA ligands in tumor cells.[33] In addition, tumor cell-intrinsic activation of the DNA receptor cGAS and, possibly, downstream signaling via STING have been implicated in tumor immunosurveillance and immunotherapy.[7,38] However, targeted activation of cGAS/STING in melanoma cells only induced poorly immunostimulatory EVs. This might be explained by the pathway's generally low activity in melanoma cells,[12] as the magnitude of effective cGAS/STING signaling in cancer cells has been shown to dictate effector responses.[39] As we found that release of isEVs in response to strong innate immune activation via RIG-I is a conserved cellular response pattern of various human and murine tumor cells types, cGAS/STING signaling may very well shape EV biogenesis and cargo in tumors with more active DNA sensing. To what extent such innate immune-regulated tumor EV release contributes to immunosurveillance during spontaneous tumor development (in the absence of strong external stimuli) remains to be determined.

At this time, it is unclear whether packaging of nucleic acids into EVs in response to active RIG-I signaling is a directed process or a mere stochastic event dependent on the abundance of certain nucleic acid sequences in the cytosol and/or endosome of tumor cells. Translocation of endogenous RIG-I ligands from the nucleus to the cytosol, as described for tumor cell stress situations,[33] may account for their preferred packing into RIG-I-EVs, as high abundance and cytoplasmic (vs. nuclear) location favor EV incorporation of specific RNAs.[32] The finding that active RIG-I signaling in tumor cells favors the shuttling of immunostimulatory RNAs within tumor EVs that subsequently engage the same pathway in recipient (immune) cells may suggest that the RIG-I protein or alternative RNA-binding proteins are actively involved in transporting RNA motifs to the intracellular vesiculation machinery.[32] Indeed, we did find RIG-I protein within murine B16 cell-derived EVs, but its abundance was independent of its activation status in EV-releasing tumor cells, arguing against a decisive RNA transporting function in regard to EV immunostimulatory capacity. Furthermore, we found different immunostimulatory RNA types within RIG-I-activated tumor-derived EVs that likely do not bind to RIG-I. The importance of the downstream transcription factors IRF3/7 further implicate an important role of active RIG-I and autocrine/paracrine IFN-I signaling for the generation of isEVs. Several components of the RIG-I pathway, including the receptor itself, are IFN-stimulated genes. Feedback loops via the IFN-I receptor have been shown to prime tumor cells for RIG-I-mediated effects.[40] Together, our data suggest that the RIG-I-IFN-I pathway in cancer cells regulates biogenesis and content packaging of exosomal EVs, which are subsequently released in a Rab27a-dependent manner.

Ctrl-EVs enriched from steady-state tumor cells had some antitumor activity but failed to induce long-term tumor control. This might suggest initiation of innate but not adaptive antitumor immune responses, independent of the IFN-I/DC/T cell axis. The involvement of NK cells in RIG-I-induced EV-mediated antitumor immunity falls in line with our recent study demonstrating that activation of RIG-I in melanoma cells results in the release of EVs with an increased expression of the NKp30 ligand on their surface, thus triggering NK-cell-mediated lysis of melanoma cells.[41] For RIG-I-induced isEVs, we observed potent antitumor synergism with anti-CTLA4/-PD1. We have previously shown that immunotherapy with ICB relies on both tumor and host immune cell-intrinsic RIG-I signaling.[12] Our current findings

suggest that RIG-I-induced EVs may shuttle immunostimulatory tumor-derived endogenous and exogenous RNAs to be detected in host immune cells to boost ICB efficacy. Accordingly, we found that high transcriptional activity of both RIG-I-encoding *DDX58* and a gene pattern associated with EV biogenesis in tumor samples were associated with improved overall survival of melanoma patients and beneficial clinical response to ICB with either anti-CTLA-4 or anti-PD-1. For this analysis, we used a predefined gene set whose gene products were identified to be associated with high EV production by screening 60 tumor cell lines.[26] However, our approach remains restricted by current limitations in the general understanding of EV biogenesis and its regulation. Intersections of the EV biogenesis pathway with other molecular pathways associated with the trafficking of intracellular vesicles (e.g., endocytosis) will inherently confound the interpretation of our gene expression studies, which will need to be verified by alternative methods. Furthermore, the ligands that activate RIG-I within tumor cells remain unclear and may comprise endogenous tumor RNA leaked into the cytosol under stress conditions, endogenous retroviral elements, or foreign bacterial RNAs. Also, under which conditions these RNAs are present in the cytosol and can activate RIG-I within tumor cells (for downstream isEV biogenesis) remains to be determined.

Our data also highlight the context-dependent, contrasting roles of EVs in the TME regarding immune activation and evasion. Numerous previous reports highlighted adversary effects of tumor EVs, which can inhibit immune cell function. In our study, generation of immunostimulatory EVs from various cancers strictly required previous RIG-I stimulation. Interestingly, tumor EVs enriched during steady-state conditions of untreated cancer cells did not actively promote tumor growth in our study. For future translational application of isEVs it will be essential to understand to which degree RIG-I signaling in tumor cells actively suppresses these immune-inhibitory functions of EVs or whether they are counterbalanced by strong immunostimulatory signals. Furthermore, endogenous ncRNAs in EVs also have the potential to activate cell-intrinsic pattern recognition receptors with detrimental outcome and progressive tumor growth. EV-mediated transfer of ncRNAs such as unshielded RN7SL1 RNA from stromal to breast cancer cells can activate both the RIG-I and NOTCH3 pathways, resulting in tumor growth and therapy resistance.[24,42] These data suggest that despite activation of the same pathway, the cellular source of EVs and also the conditions under which these EVs are generated can contribute to either immune evasion or antitumor efficacy. Nonetheless, using bulk tumor cell cultures isolated from freshly isolated melanoma tumor tissue, we confirm that production of RIG-I-induced isEVs is robust and not principally impaired by the inclusion of stromal cells in the TME known to potentially release inhibitory EVs.[26].

In sum, our findings uncover a hitherto unknown function of cytosolic nucleic acid sensors in cancer cells for the production and immunoregulatory function of tumor-derived EVs in both mice and humans. We identify the tumor cell-intrinsic RIG-I signaling pathway as a crucial mechanism to alter the composition of endogenous RNA within EVs and, thus, the immunostimulatory capacity of these vesicles. Given the availability of clinical-grade RIG-I agonists which are currently undergoing early phase 1/2 clinical testing (NCT03065023, NCT03739138, NCT02828098, NCT03203005, NCT03291002), targeting the RIG-I pathway in tumor cells may be a promising approach to beneficially "reprogram" the functionality of tumor cell-derived EVs.

Limitations of the study

Several questions remain to be addressed before a possible translational move of such "defined" cancer EV therapeutics into the clinic can be considered. (1) A precise analysis of the molecular mechanisms in the TME that determine the secretion of immunostimulatory vs. immunoinhibitory EVs upon stimulation with defined RIG-I agonists is required. (2) More data on isEVs in human subjects is needed to strengthen the translational relevance of our findings (e.g., by using patient-derived tumor organoid-immune cell co-cultures and/or xenograft models). (3) We followed an exploratory approach to gather sufficient functional information of murine and human tumor EVs in various different scenarios. Therefore, both EV cellular source and target cells differed for cell culture as well as *in vivo* systems to test tumor cell EVs for cancer treatment. Thus, we had to carefully titrate the amount of EVs for each experimental setting, even though the differences between EV concentrations in similar experimental scenarios were minimal. As effects of EV interactions with recipient cells could be concentration- and time-dependent, isEV dosages should be standardized for prospective use in advanced preclinical model systems. (4) The general efforts on standardizing the isolation and purification methods of EVs in the overall field have not brought us to a point that can match the potential of EVs for clinical use. At first, current challenges of good manufacturing practice-compliant manufacturing of cancer EVs, including insufficient large-scale manufacturing technologies and low yield, will need to be solved.

STAR★METHODS

Detailed methods are provided in the online version of this paper and include the following:

- KEY RESOURCES TABLE
- RESOURCE AVAILABILITY
  - Lead contact
  - Materials availability
  - Data and code availability
- EXPERIMENTAL MODEL AND STUDY PARTICIPANT DETAILS
  - Mice
  - Cell lines
- METHOD DETAILS
  - Generation of Rab27a deficient murine melanoma cells
  - Generation of gene deficient SK-mel-29 human melanoma cells
  - Reagents
  - Preparation of EVs and nucleic acid extraction
  - Murine bone marrow-derived dendritic cell culture
  - Quantification of cytokines
  - Western blot
  - Flow cytometry
  - Immunization with EVs
  - Tumor challenge and treatment

- Sequencing of murine EV-RNA
- Human PBMC EV stimulation
- ELISpot
- RNA-seq analysis of human melanoma samples
- Nanoparticle tracking analysis (NTA)
- Transmission electron microscopy
- Protein quantification with BCA assay
- Quantifying gene expression by real-time PCR
- Bulk murine melanoma RNA-sequencing
- Imaging flow cytometry

● QUANTIFICATION AND STATISTICAL ANALYSIS

SUPPLEMENTAL INFORMATION

Supplemental information can be found online at https://doi.org/10.1016/j.xcrm.2023.101171.

ACKNOWLEDGMENTS

This study was supported by Deutsche Forschungsgemeinschaft – Projektnummer 360372040 – SFB 1335 (to H.P. and F.B.), Projektnummer 395357507 – SFB 1371 (to H.P.), Projektnummer 324392634 – TRR 221 (to H.P.) and BA 2851/6-1 (to F.B.), German Cancer Aid (70114547 to H.P.), BZKF (TLG/05/R and SG AML to H.P.), the Wilhelm Sander Foundation (2021.041.1 to S.H., 2021.040.1 to H.P.), the European Hematology Association (to H.P.), the Bavarian State Ministry for Science and Art (to H.P.), DKMS Foundation for Giving Life (to H.P.), a Young Investigator award (Melanoma Research Alliance to S.H.), and the Germany José Carreras Foundation (DJCLS 07 R/2020 to S.H.). H.P. is supported by the EMBO Young Investigator Program.

AUTHOR CONTRIBUTIONS

S.H., F.S., and H.P. designed the research, and analyzed and interpreted the results. F.S., S.D., L.J., and S.E. conducted murine EV cell-culture and animal experiments. D.B. performed RNA-seq. A.G. performed imaging flow cytometry. C.W., C.M.S., N.L., and T.E. analyzed human and murine melanoma RNA-seq datasets. J.D.-P., K.F., S.L., and M.P. conducted experiments with human EVs. S.H. and H.P. prepared the manuscript. E.T.O., S.G., C.W., T.H., R.R., I.C.-C., W.H., B.G., J.R., F.B., C.C., and G.H. gave methodological support and conceptual advice. S.H. and H.P. guided the study.

DECLARATION OF INTERESTS

S.H. has been a consultant for Bristol Myers-Squibb (BMS), Novartis, Merck, Abbvie, and Roche, has received research funding from BMS and Novartis, and is an employee of and holds equity interest in Roche/Genentech. A.G. is a consultant for and has equity interest in Evox Therapeutics Ltd. and is inventor on several patent applications related to extracellular vesicles. B.G. is a scientific advisory board member of Innovex Therapeutics SL, PL BioScience, and Mursla Ltd, consultant for FUJIFILM Wako Chemicals, and a founding director of Exosla Ltd. G.H. is inventor on a patent covering synthetic RIG-I ligand, and co-founder of Rigontec GmbH. H.P. is a consultant for Gilead, Abbvie, Pfizer, Novartis, Servier, and BMS, and has received research funding from BMS.

Received: August 31, 2022
Revised: May 4, 2023
Accepted: August 3, 2023
Published: August 31, 2023

REFERENCES

1. Deng, L., Liang, H., Xu, M., Yang, X., Burnette, B., Arina, A., Li, X.D., Mauceri, H., Beckett, M., Darga, T., et al. (2014). STING-Dependent Cytosolic DNA Sensing Promotes Radiation-Induced Type I Interferon-Dependent Antitumor Immunity in Immunogenic Tumors. Immunity *41*, 843–852. https://doi.org/10.1016/j.immuni.2014.10.019.
2. Fischer, J.C., Bscheider, M., Eisenkolb, G., Lin, C.C., Wintges, A., Otten, V., Lindemans, C.A., Heidegger, S., Rudelius, M., Monette, S., et al. (2017). RIG-I/MAVS and STING signaling promote gut integrity during irradiation- and immune-mediated tissue injury. Sci. Transl. Med. *9*, eaag2513. https://doi.org/10.1126/scitranslmed.aag2513.
3. Poeck, H., Besch, R., Maihoefer, C., Renn, M., Tormo, D., Morskaya, S.S., Kirschnek, S., Gaffal, E., Landsberg, J., Hellmuth, J., et al. (2008). 5′-Triphosphate-siRNA: turning gene silencing and Rig-I activation against melanoma. Nat. Med. *14*, 1256–1263. https://doi.org/10.1038/nm.1887.
4. Woo, S.R., Fuertes, M.B., Corrales, L., Spranger, S., Furdyna, M.J., Leung, M.Y.K., Duggan, R., Wang, Y., Barber, G.N., Fitzgerald, K.A., et al. (2014). STING-Dependent Cytosolic DNA Sensing Mediates Innate Immune Recognition of Immunogenic Tumors. Immunity *41*, 830–842. https://doi.org/10.1016/j.immuni.2014.10.017.
5. Ablasser, A., and Hur, S. (2020). Regulation of cGAS- and RLR-mediated immunity to nucleic acids. Nat. Immunol. *21*, 17–29. https://doi.org/10.1038/s41590-019-0556-1.
6. Bartok, E., and Hartmann, G. (2020). Immune Sensing Mechanisms that Discriminate Self from Altered Self and Foreign Nucleic Acids. Immunity *53*, 54–77. https://doi.org/10.1016/j.immuni.2020.06.014.
7. Marcus, A., Mao, A.J., Lensink-Vasan, M., Wang, L., Vance, R.E., and Raulet, D.H. (2018). Tumor-Derived cGAMP Triggers a STING-Mediated Interferon Response in Non-tumor Cells to Activate the NK Cell Response. Immunity *49*, 754–763.e4. https://doi.org/10.1016/j.immuni.2018.09.016.
8. Schadt, L., Sparano, C., Schweiger, N.A., Silina, K., Cecconi, V., Lucchiari, G., Yagita, H., Guggisberg, E., Saba, S., Nascakova, Z., et al. (2019). Cancer-Cell-Intrinsic cGAS Expression Mediates Tumor Immunogenicity. Cell Rep. *29*, 1236–1248.e7. https://doi.org/10.1016/j.celrep.2019.09.065.
9. Hartmann, G. (2017). Nucleic Acid Immunity. Adv. Immunol. *133*, 121–169. https://doi.org/10.1016/bs.ai.2016.11.001.
10. Hornung, V., Ellegast, J., Kim, S., Brzózka, K., Jung, A., Kato, H., Poeck, H., Akira, S., Conzelmann, K.K., Schlee, M., et al. (2006). 5′-Triphosphate RNA is the ligand for RIG-I. Science *314*, 994–997. https://doi.org/10.1126/science.1132505.
11. Corrales, L., Glickman, L.H., McWhirter, S.M., Kanne, D.B., Sivick, K.E., Katibah, G.E., Woo, S.R., Lemmens, E., Banda, T., Leong, J.J., et al. (2015). Direct Activation of STING in the Tumor Microenvironment Leads to Potent and Systemic Tumor Regression and Immunity. Cell Rep. *11*, 1018–1030. https://doi.org/10.1016/j.celrep.2015.04.031.
12. Heidegger, S., Wintges, A., Stritzke, F., Bek, S., Steiger, K., Koenig, P.A., Göttert, S., Engleitner, T., Öllinger, R., Nedelko, T., et al. (2019). RIG-I activation is critical for responsiveness to checkpoint blockade. Sci. Immunol. *4*, eaau8943. https://doi.org/10.1126/sciimmunol.aau8943.
13. Poeck, H., Wintges, A., Dahl, S., Bassermann, F., Haas, T., and Heidegger, S. (2021). Tumor cell-intrinsic RIG-I signaling governs synergistic effects of immunogenic cancer therapies and checkpoint inhibitors in mice. Eur. J. Immunol. *51*, 1531–1534. https://doi.org/10.1002/eji.202049158.
14. Möller, A., and Lobb, R.J. (2020). The evolving translational potential of small extracellular vesicles in cancer. Nat. Rev. Cancer *20*, 697–709. https://doi.org/10.1038/s41568-020-00299-w.
15. van den Boorn, J.G., Dassler, J., Coch, C., Schlee, M., and Hartmann, G. (2013). Exosomes as nucleic acid nanocarriers. Adv. Drug Deliv. Rev. *65*, 331–335. https://doi.org/10.1016/j.addr.2012.06.011.
16. Pitt, J.M., Kroemer, G., and Zitvogel, L. (2016). Extracellular vesicles: masters of intercellular communication and potential clinical interventions. J. Clin. Invest. *126*, 1139–1143. https://doi.org/10.1172/jci87316.
17. Kosaka, N., Yoshioka, Y., Fujita, Y., and Ochiya, T. (2016). Versatile roles of extracellular vesicles in cancer. J. Clin. Invest. *126*, 1163–1172. https://doi.org/10.1172/jci81130.

18. Andre, F., Schartz, N.E.C., Movassagh, M., Flament, C., Pautier, P., Morice, P., Pomel, C., Lhomme, C., Escudier, B., Le Chevalier, T., et al. (2002). Malignant effusions and immunogenic tumour-derived exosomes. Lancet *360*, 295–305. https://doi.org/10.1016/s0140-6736(02)09552-1.

19. Wolfers, J., Lozier, A., Raposo, G., Regnault, A., Théry, C., Masurier, C., Flament, C., Pouzieux, S., Faure, F., Tursz, T., et al. (2001). Tumor-derived exosomes are a source of shared tumor rejection antigens for CTL cross-priming. Nat. Med. *7*, 297–303. https://doi.org/10.1038/85438.

20. Théry, C., Witwer, K.W., Aikawa, E., Alcaraz, M.J., Anderson, J.D., Andriantsitohaina, R., Antoniou, A., Arab, T., Archer, F., Atkin-Smith, G.K., et al. (2018). Minimal information for studies of extracellular vesicles 2018 (MISEV2018): a position statement of the International Society for Extracellular Vesicles and update of the MISEV2014 guidelines. J. Extracell. Vesicles *7*, 1535750. https://doi.org/10.1080/20013078.2018.1535750.

21. Nakase, I., and Futaki, S. (2015). Combined treatment with a pH-sensitive fusogenic peptide and cationic lipids achieves enhanced cytosolic delivery of exosomes. Sci. Rep. *5*, 10112. https://doi.org/10.1038/srep10112.

22. Besch, R., Poeck, H., Hohenauer, T., Senft, D., Häcker, G., Berking, C., Hornung, V., Endres, S., Ruzicka, T., Rothenfusser, S., and Hartmann, G. (2009). Proapoptotic signaling induced by RIG-I and MDA-5 results in type I interferon-independent apoptosis in human melanoma cells. J. Clin. Invest. *119*, 2399–2411. https://doi.org/10.1172/jci37155.

23. Duewell, P., Steger, A., Lohr, H., Bourhis, H., Hoelz, H., Kirchleitner, S.V., Stieg, M.R., Grassmann, S., Kobold, S., Siveke, J.T., et al. (2014). RIG-I-like helicases induce immunogenic cell death of pancreatic cancer cells and sensitize tumors toward killing by CD8(+) T cells. Cell Death Differ. *21*, 1825–1837. https://doi.org/10.1038/cdd.2014.96.

24. Nabet, B.Y., Qiu, Y., Shabason, J.E., Wu, T.J., Yoon, T., Kim, B.C., Benci, J.L., DeMichele, A.M., Tchou, J., Marcotrigiano, J., and Minn, A.J. (2017). Exosome RNA Unshielding Couples Stromal Activation to Pattern Recognition Receptor Signaling in Cancer. Cell *170*, 352–366.e13. https://doi.org/10.1016/j.cell.2017.06.031.

25. Poeck, H., Bscheider, M., Gross, O., Finger, K., Roth, S., Rebsamen, M., Hannesschläger, N., Schlee, M., Rothenfusser, S., Barchet, W., et al. (2010). Recognition of RNA virus by RIG-I results in activation of CARD9 and inflammasome signaling for interleukin 1 beta production. Nat. Immunol. *11*, 63–69. https://doi.org/10.1038/ni.1824.

26. Hurwitz, S.N., Rider, M.A., Bundy, J.L., Liu, X., Singh, R.K., and Meckes, D.G., Jr. (2016). Proteomic profiling of NCI-60 extracellular vesicles uncovers common protein cargo and cancer type-specific biomarkers. Oncotarget *7*, 86999–87015. https://doi.org/10.18632/oncotarget.13569.

27. Ostrowski, M., Carmo, N.B., Krumeich, S., Fanget, I., Raposo, G., Savina, A., Moita, C.F., Schauer, K., Hume, A.N., Freitas, R.P., et al. (2010). Rab27a and Rab27b control different steps of the exosome secretion pathway. Nat. Cell Biol. *12*, 19–30. https://doi.org/10.1038/ncb2000.

28. Mulcahy, L.A., Pink, R.C., and Carter, D.R.F. (2014). Routes and mechanisms of extracellular vesicle uptake. J. Extracell. Vesicles *3*, 24641. https://doi.org/10.3402/jev.v3.24641.

29. Desai, A.S., Hunter, M.R., and Kapustin, A.N. (2019). Using macropinocytosis for intracellular delivery of therapeutic nucleic acids to tumour cells. Philos. Trans. R. Soc. Lond. B Biol. Sci. *374*, 20180156. https://doi.org/10.1098/rstb.2018.0156.

30. Diamond, M.S., Kinder, M., Matsushita, H., Mashayekhi, M., Dunn, G.P., Archambault, J.M., Lee, H., Arthur, C.D., White, J.M., Kalinke, U., et al. (2011). Type I interferon is selectively required by dendritic cells for immune rejection of tumors. J. Exp. Med. *208*, 1989–2003. https://doi.org/10.1084/jem.20101158.

31. Fuertes, M.B., Kacha, A.K., Kline, J., Woo, S.R., Kranz, D.M., Murphy, K.M., and Gajewski, T.F. (2011). Host type I IFN signals are required for antitumor CD8+ T cell responses through CD8{alpha}+ dendritic cells. J. Exp. Med. *208*, 2005–2016. https://doi.org/10.1084/jem.20101159.

32. O'Brien, K., Breyne, K., Ughetto, S., Laurent, L.C., and Breakefield, X.O. (2020). RNA delivery by extracellular vesicles in mammalian cells and its applications. Nat. Rev. Mol. Cell Biol. *21*, 585–606. https://doi.org/10.1038/s41580-020-0251-y.

33. Ranoa, D.R.E., Parekh, A.D., Pitroda, S.P., Huang, X., Darga, T., Wong, A.C., Huang, L., Andrade, J., Staley, J.P., Satoh, T., et al. (2016). Cancer therapies activate RIG-I-like receptor pathway through endogenous non-coding RNAs. Oncotarget *7*, 26496–26515. https://doi.org/10.18632/oncotarget.8420.

34. Tanne, A., Muniz, L.R., Puzio-Kuter, A., Leonova, K.I., Gudkov, A.V., Ting, D.T., Monasson, R., Cocco, S., Levine, A.J., Bhardwaj, N., and Greenbaum, B.D. (2015). Distinguishing the immunostimulatory properties of noncoding RNAs expressed in cancer cells. Proc. Natl. Acad. Sci. USA *112*, 15154–15159. https://doi.org/10.1073/pnas.1517584112.

35. Fathi, M., Joseph, R., Adolacion, J.R.T., Martinez-Paniagua, M., An, X., Gabrusiewicz, K., Mani, S.A., and Varadarajan, N. (2021). Single-Cell Cloning of Breast Cancer Cells Secreting Specific Subsets of Extracellular Vesicles. Cancers *13*, 4397. https://doi.org/10.3390/cancers13174397.

36. Diamond, J.M., Vanpouille-Box, C., Spada, S., Rudqvist, N.P., Chapman, J.R., Ueberheide, B.M., Pilones, K.A., Sarfraz, Y., Formenti, S.C., and Demaria, S. (2018). Exosomes Shuttle TREX1-Sensitive IFN-Stimulatory dsDNA from Irradiated Cancer Cells to DCs. Cancer Immunol. Res. *6*, 910–920. https://doi.org/10.1158/2326-6066.Cir-17-0581.

37. Kitai, Y., Kawasaki, T., Sueyoshi, T., Kobiyama, K., Ishii, K.J., Zou, J., Akira, S., Matsuda, T., and Kawai, T. (2017). DNA-Containing Exosomes Derived from Cancer Cells Treated with Topotecan Activate a STING-Dependent Pathway and Reinforce Antitumor Immunity. J. Immunol. *198*, 1649–1659. https://doi.org/10.4049/jimmunol.1601694.

38. Harding, S.M., Benci, J.L., Irianto, J., Discher, D.E., Minn, A.J., and Greenberg, R.A. (2017). Mitotic progression following DNA damage enables pattern recognition within micronuclei. Nature *548*, 466–470. https://doi.org/10.1038/nature23470.

39. Gulen, M.F., Koch, U., Haag, S.M., Schuler, F., Apetoh, L., Villunger, A., Radtke, F., and Ablasser, A. (2017). Signalling strength determines proapoptotic functions of STING. Nat. Commun. *8*, 427. https://doi.org/10.1038/s41467-017-00573-w.

40. Boehmer, D.F.R., Formisano, S., de Oliveira Mann, C.C., Mueller, S.A., Kluge, M., Metzger, P., Rohlfs, M., Hörth, C., Kocheise, L., Lichtenthaler, S.F., et al. (2021). OAS1/RNase L executes RIG-I ligand-dependent tumor cell apoptosis. Sci. Immunol. *6*, eabe2550. https://doi.org/10.1126/sciimmunol.abe2550.

41. Daßler-Plenker, J., Reiners, K.S., van den Boorn, J.G., Hansen, H.P., Putschli, B., Barnert, S., Schuberth-Wagner, C., Schubert, R., Tüting, T., Hallek, M., et al. (2016). RIG-I activation induces the release of extracellular vesicles with antitumor activity. OncoImmunology *5*, e1219827. https://doi.org/10.1080/2162402X.2016.1219827.

42. Boelens, M.C., Wu, T.J., Nabet, B.Y., Xu, B., Qiu, Y., Yoon, T., Azzam, D.J., Twyman-Saint Victor, C., Wiemann, B.Z., Ishwaran, H., et al. (2014). Exosome transfer from stromal to breast cancer cells regulates therapy resistance pathways. Cell *159*, 499–513. https://doi.org/10.1016/j.cell.2014.09.051.

43. Gao, J., Aksoy, B.A., Dogrusoz, U., Dresdner, G., Gross, B., Sumer, S.O., Sun, Y., Jacobsen, A., Sinha, R., Larsson, E., et al. (2013). Integrative analysis of complex cancer genomics and clinical profiles using the cBioPortal. Sci. Signal. *6*, pl1. https://doi.org/10.1126/scisignal.2004088.

44. Chiappinelli, K.B., Strissel, P.L., Desrichard, A., Li, H., Henke, C., Akman, B., Hein, A., Rote, N.S., Cope, L.M., Snyder, A., et al. (2015). Inhibiting DNA Methylation Causes an Interferon Response in Cancer via dsRNA Including Endogenous Retroviruses. Cell *162*, 974–986. https://doi.org/10.1016/j.cell.2015.07.011.

45. Gide, T.N., Quek, C., Menzies, A.M., Tasker, A.T., Shang, P., Holst, J., Madore, J., Lim, S.Y., Velickovic, R., Wongchenko, M., et al. (2019). Distinct Immune Cell Populations Define Response to Anti-PD-1 Monotherapy and Anti-PD-1/Anti-CTLA-4 Combined Therapy. Cancer Cell *35*, 238–255.e6. https://doi.org/10.1016/j.ccell.2019.01.003.

46. Sauer, J.D., Sotelo-Troha, K., von Moltke, J., Monroe, K.M., Rae, C.S., Brubaker, S.W., Hyodo, M., Hayakawa, Y., Woodward, J.J., Portnoy, D.A., and Vance, R.E. (2011). The N-ethyl-N-nitrosourea-induced Goldenticket mouse mutant reveals an essential function of Sting in the in vivo interferon response to Listeria monocytogenes and cyclic dinucleotides. Infect. Immun. *79*, 688–694. https://doi.org/10.1128/iai.00999-10.

47. Caton, M.L., Smith-Raska, M.R., and Reizis, B. (2007). Notch-RBP-J signaling controls the homeostasis of CD8- dendritic cells in the spleen. J. Exp. Med. *204*, 1653–1664. https://doi.org/10.1084/jem.20062648.

48. Clausen, B.E., Burkhardt, C., Reith, W., Renkawitz, R., and Förster, I. (1999). Conditional gene targeting in macrophages and granulocytes using LysMcre mice. Transgenic Res. *8*, 265–277.

49. Seth, R.B., Sun, L., Ea, C.K., and Chen, Z.J. (2005). Identification and characterization of MAVS, a mitochondrial antiviral signaling protein that activates NF-kappaB and IRF 3. Cell *122*, 669–682. https://doi.org/10.1016/j.cell.2005.08.012.

50. Alexopoulou, L., Holt, A.C., Medzhitov, R., and Flavell, R.A. (2001). Recognition of double-stranded RNA and activation of NF-kappaB by Toll-like receptor 3. Nature *413*, 732–738. https://doi.org/10.1038/35099560.

51. Adachi, O., Kawai, T., Takeda, K., Matsumoto, M., Tsutsui, H., Sakagami, M., Nakanishi, K., and Akira, S. (1998). Targeted Disruption of the MyD88 Gene Results in Loss of IL-1- and IL-18-Mediated Function. Immunity *9*, 143–150. https://doi.org/10.1016/S1074-7613(00)80596-8.

52. Stetson, D.B., and Medzhitov, R. (2006). Recognition of Cytosolic DNA Activates an IRF3-Dependent Innate Immune Response. Immunity *24*, 93–103. https://doi.org/10.1016/j.immuni.2005.12.003.

53. Harshil Patel, P.E. (2023). Alexander Peltzer, Olga Botvinnik, Gregor Sturm, Denis Moreno, Pranathi Vemuri, silviamorins, Maxime U Garcia, Lorena Pantano. nf-core/rnaseq: nf-core/rnaseq v3.11.2 - Resurrected Radium Rhino.

54. Felix Krueger, F.J., Ewels, P., Afyounian, E., Weinstein, M., Schuster-Boeckler, B., and Hulselmans, G. (2023). TrimGalore: v0.6.10. https://doi.org/10.5281/zenodo.7598955.

55. Dobin, A., Davis, C.A., Schlesinger, F., Drenkow, J., Zaleski, C., Jha, S., Batut, P., Chaisson, M., and Gingeras, T.R. (2013). STAR: ultrafast universal RNA-seq aligner. Bioinformatics *29*, 15–21. https://doi.org/10.1093/bioinformatics/bts635.

56. Patro, R., Duggal, G., Love, M.I., Irizarry, R.A., and Kingsford, C. (2017). Salmon provides fast and bias-aware quantification of transcript expression. Nat. Methods *14*, 417–419. https://doi.org/10.1038/nmeth.4197.

57. Love, M.I., Huber, W., and Anders, S. (2014). Moderated estimation of fold change and dispersion for RNA-seq data with DESeq2. Genome Biol. *15*, 550. https://doi.org/10.1186/s13059-014-0550-8.

58. Sergushichev, A.A. (2016). An algorithm for fast preranked gene set enrichment analysis using cumulative statistic calculation. Preprint at bioRxiv. https://doi.org/10.1001/060012.

59. Hita, A., Brocart, G., Fernandez, A., Rehmsmeier, M., Alemany, A., and Schvartzman, S. (2022). MGcount: a total RNA-seq quantification tool to address multi-mapping and multi-overlapping alignments ambiguity in non-coding transcripts. BMC Bioinf. *23*, 39. https://doi.org/10.1186/s12859-021-04544-3.

60. Smit, A., Hubley, R., and Green, P.. RepeatMasker Open-4.0. http://www.repeatmasker.org.

61. Simon, S.R., and Ershler, W.B. (1985). Hormonal influences on growth of B16 murine melanoma. J. Natl. Cancer Inst. *74*, 1085–1088.

62. Reithmair, M., Buschmann, D., Märte, M., Kirchner, B., Hagl, D., Kaufmann, I., Pfob, M., Chouker, A., Steinlein, O.K., Pfaffl, M.W., and Schelling, G. (2017). Cellular and extracellular miRNAs are blood-compartment-specific diagnostic targets in sepsis. J. Cell Mol. Med. *21*, 2403–2411. https://doi.org/10.1111/jcmm.13162.

63. The Molecular Signatures Database (MSigDB). https://www.gsea-msigdb.org/gsea/msigdb/index.jsp.

64. Britten, C.M., Meyer, R.G., Frankenberg, N., Huber, C., and Wölfel, T. (2004). The use of clonal mRNA as an antigenic format for the detection of antigen-specific T lymphocytes in IFN-gamma ELISPOT assays. J. Immunol. Methods *287*, 125–136. https://doi.org/10.1016/j.jim.2004.01.026.

65. cgdsr: R-Based API for Accessing the MSKCC Cancer Genomics Data Server (CGDS). https://github.com/cBioPortal/cgdsr.

66. Snyder, A., Makarov, V., Merghoub, T., Yuan, J., Zaretsky, J.M., Desrichard, A., Walsh, L.A., Postow, M.A., Wong, P., Ho, T.S., et al. (2014). Genetic Basis for Clinical Response to CTLA-4 Blockade in Melanoma. N. Engl. J. Med. *371*, 2189–2199. https://doi.org/10.1056/NEJMoa1406498.

67. Macosko, E.Z., Basu, A., Satija, R., Nemesh, J., Shekhar, K., Goldman, M., Tirosh, I., Bialas, A.R., Kamitaki, N., Martersteck, E.M., et al. (2015). Highly Parallel Genome-wide Expression Profiling of Individual Cells Using Nanoliter Droplets. Cell *161*, 1202–1214. https://doi.org/10.1016/j.cell.2015.05.002.

68. Zhu, A., Ibrahim, J.G., and Love, M.I. (2019). Heavy-tailed prior distributions for sequence count data: removing the noise and preserving large differences. Bioinformatics *35*, 2084–2092. https://doi.org/10.1093/bioinformatics/bty895.

69. Subramanian, A., Tamayo, P., Mootha, V.K., Mukherjee, S., Ebert, B.L., Gillette, M.A., Paulovich, A., Pomeroy, S.L., Golub, T.R., Lander, E.S., and Mesirov, J.P. (2005). Gene set enrichment analysis: A knowledge-based approach for interpreting genome-wide expression profiles. Proc. Natl. Acad. Sci. USA *102*, 15545–15550. https://doi.org/10.1073/pnas.0506580102.

70. Erdbrügger, U., Rudy, C.K., Etter, M.E., Dryden, K.A., Yeager, M., Klibanov, A.L., and Lannigan, J. (2014). Imaging flow cytometry elucidates limitations of microparticle analysis by conventional flow cytometry. Cytometry A. *85*, 756–770. https://doi.org/10.1002/cyto.a.22494.

71. Headland, S.E., Jones, H.R., D'Sa, A.S.V., Perretti, M., and Norling, L.V. (2014). Cutting-edge analysis of extracellular microparticles using ImageStream(X) imaging flow cytometry. Sci. Rep. *4*, 5237. https://doi.org/10.1038/srep05237.

72. Görgens, A., Bremer, M., Ferrer-Tur, R., Murke, F., Tertel, T., Horn, P.A., Thalmann, S., Welsh, J.A., Probst, C., Guerin, C., et al. (2019). Optimisation of imaging flow cytometry for the analysis of single extracellular vesicles by using fluorescence-tagged vesicles as biological reference material. J. Extracell. Vesicles *8*, 1587567. https://doi.org/10.1080/20013078.2019.1587567.

73. Tertel, T., Bremer, M., Maire, C., Lamszus, K., Peine, S., Jawad, R., Andaloussi, S.E.L., Giebel, B., Ricklefs, F.L., and Görgens, A. (2020). High-Resolution Imaging Flow Cytometry Reveals Impact of Incubation Temperature on Labeling of Extracellular Vesicles with Antibodies. Cytometry A. *97*, 602–609. https://doi.org/10.1002/cyto.a.24034.

74. Inglis, H.C., Danesh, A., Shah, A., Lacroix, J., Spinella, P.C., and Norris, P.J. (2015). Techniques to improve detection and analysis of extracellular vesicles using flow cytometry. Cytometry A. *87*, 1052–1063. https://doi.org/10.1002/cyto.a.22649.

75. György, B., Módos, K., Pállinger, E., Pálóczi, K., Pásztói, M., Misják, P., Deli, M.A., Sipos, A., Szalai, A., Voszka, I., et al. (2011). Detection and isolation of cell-derived microparticles are compromised by protein complexes resulting from shared biophysical parameters. Blood *117*, e39–e48. https://doi.org/10.1182/blood-2010-09-307595.

Cell Reports Medicine
Article

CellPress
OPEN ACCESS

STAR★METHODS

KEY RESOURCES TABLE

REAGENT or RESOURCE	SOURCE	IDENTIFIER
Antibodies		
Rat monoclonal anti-mouse IFN-β (clone RMMB-1)	PBL Assay Science	Cat#22400-1; RRID: AB_387846
Anti-mouse Interferon-beta rabbit serum	PBL Assay Science	Cat#32400-1; RRID: AB_387872
Anti-rabbit IgG coupled with horseradish peroxidase	Abcam	Cat#ab6721, RRID: AB_955447
Anti-human IFN-γ antibody (clone 1-D1K)	Mabtech	Cat#3420-3-250
Anti-mouse IFNaR1 antibody (clone MAR1-5A3)	BioXCell	Cat#BE0241; RRID: AB_2687723
Anti-mouse CTLA-4 antibody (clone 9H10)	BioXCell	Cat#BE0131; RRID: AB_10950184
Anti-mouse PD-1 antibody (clone RMP1-14)	BioXCell	Cat#BE0146; RRID: AB_10949053
Anti-mouse CD8a antibody (clone 2.43)	BioXCell	Cat#BE0118; RRID: AB_10949065
Anti-mouse CDNK1.1 antibody (PK136)	BioXCell	Cat#BE0036; RRID: AB_1107737
Western blot antibodies, see Table S5		
Flow cytometry antibodies, see Table S6		
Biological samples		
Human PBMCs from healthy donors	This paper	N/A
Chemicals, peptides, and recombinant proteins		
rmGM-CSF	Immunotools	Cat#12343123
rhGM-CSF	Peprotech	Cat#300-03
rhIL-4	Peprotech	Cat#200-04
Alt-R S.p. Cas9 Nuclease V3	IDT	Cat#1081058
DNAzol Reagent	Thermo Fisher	Cat#10503027
In vivo-jetPEI	PolyPlus	Cat#101000040
Lipofectamine 2000 Transfection Reagent	Thermo Fisher	Cat# 11668019
Critical commercial assays		
Total exosome isolation (from cell media) reagent	Thermo Fisher	Cat#4478359
Exo-spin mini	Cell Guidance Systems	Cat#EX01-25
Total Exosome RNA and Protein Isolation Kit	Thermo Fisher	Cat#4478545
Qubit 1X dsDNA HS Assay Kit	Thermo Fisher	Cat#Q33230
miRNeasy Mini Kit	Qiagen	Cat#217084
PKH67 Green Fluorescent Cell Linker Kit	Sigma-Aldrich	Cat#PKH67GL-1KT
Deep Red CellMask Plasma Membrane Stains	Invitrogen	Cat#C10046
SYTO RNASelect Green Fluorescent cell Stain	Invitrogen	Cat#S32703
iTAg MHC-I murine SIINFEKL tetramers	MBL	Cat#TS-5001-1C
Deposited data		
Murine B16 melanoma cell EV RNA-seq	This study	European Nucleotide Archive (ENA); PRJEB59517
RNA-seq human melanoma biopsies (TCGA databank)	Gao et al.[43]	cBioPortal skcm_tcga
RNA-seq healthy human skin tissue	GTEx Project	https://gtexportal.org; UBERON:0036149
Bulk tumor RNA-seq murine B16 melanoma	Heidegger et al.[12]	ENA; PRJEB32241
RNA-seq melanoma biopsies from anti-CTLA-4-treated patients	Chiappinelli et al.[44]	N/A
RNA-seq melanoma biopsies from anti-PD-1-treated patients	Gide et al.[45]	N/A

(*Continued on next page*)

Continued

REAGENT or RESOURCE	SOURCE	IDENTIFIER
Experimental models: Cell lines		
Murine: B16.OVA	Biocytogen	Cat#311537
Murine: B16 F10	ATCC	CRL-6475
Murine: CT26	ATCC	CRL-2638
Murine: 4T1	ATCC	CRL-2539
Murine: Panc02	CLS	Cat#300501; RRID: CVCL_D627
Human: THP1-Dual™ KI-hSTING-R232	InvivoGen	Cat#thpd-r232
Human: THP1-Dual™ KO-STING Cells	InvivoGen	Cat#thpd-kostg
Human: HEK-Blue IFN-α/β Cells	InvivoGen	Cat#hkb-ifnab
Human: SK-MEL-29	Laboratory of Barbara Schmidt	Cellosaurus CVCL_6031
Experimental models: Organisms/strains		
Mouse: C57BL/6J wildtype	Janvier Labs	C57BL/6JRj
Mouse: Sting$^{-/-}$ (Tmem173$^{gt/gt}$)	Sauer et al.[46]	N/A
Mouse: Itgax-Cre^{+}Ifnar1$^{f/f}$	Caton et al.[47]	N/A
Mouse: LysM-Cre^{+}Ifnar1$^{f/f}$	Clausen et al.[48]	N/A
Mouse: Mavs$^{-/-}$	Seth et al.[49]	N/A
Mouse: Tlr3$^{-/-}$	Alexopoulou et al.[50]	N/A
Mouse: Myd88$^{-/-}$	Adachi et al.[51]	N/A
Oligonucleotides		
3pRNA sequence: sense, 5′- UCA AAC AGU CCU CGC AUG CCU AUA GUG AGU CG -3′	Poeck et al.[3]	N/A
synRNA	Eurofins	N/A
Interferon-stimulating DNA (ISD)	Stetson et al.[52]	N/A
Primers for *mActin*, forward 5′-CACACCCGCCA CCAGTTCG-3′ backward 5′-CACCATCACACCCTGGTGC-3′	This paper	N/A
Primers for *mRab27a*, forward 5′-GCATTGATTTC AGGGAAAAGAGAG-3′ backward 5′-TTCTCCACACACCGCTCCATCCGC-3′	This paper	N/A
CRISPR sgRNA target sequences, see Table S4	This paper	N/A
Alt-R CRISPR-Cas9 tracrRNA	IDT	Cat#1072533
Recombinant DNA		
pSpCas9(BB)-2A-GFP (PX458)	Addgene	Addgene Plasmid #48138
Software and algorithms		
Flowjo	TreeStar	https://www.flowjo.com
nf-core/rnaseq v3.11.2	Patel et al.[53]	https://zenodo.org/record/3503887
Trim Galore!	Krueger et al.[54]	https://github.com/FelixKrueger/TrimGalore
STAR	Dobin et al.[55]	https://github.com/alexdobin/STAR/releases
Salmon	Patro et al.[56]	https://github.com/COMBINE-lab/Salmon
DESeq2	Love et al.[57]	https://bioconductor.org/packages/release/bioc/html/DESeq2.html
fgsea R package	Sergushichev et al.[58]	https://bioconductor.org/packages/release/bioc/html/fgsea.html
MSigDB	GSEA	https://www.gsea-msigdb.org/gsea/msigdb/index.jsp.
MGcount	Hita et al.[59]	https://github.com/hitaandrea/MGcount
RepeatMasker	Smit et al.[60]	http://www.repeatmasker.org.
cgdsr R package	CGDS	https://github.com/cBioPortal/cgdsr.
GraphPad Prism	Dotmatics	https://www.graphpad.com
R package cgdsr	CGDS	https://github.com/cBioPortal/cgdsr

Cell Reports Medicine
Article

CellPress
OPEN ACCESS

RESOURCE AVAILABILITY

Lead contact

Further information and requests for resources and reagents should be directed to and will be fulfilled by the lead contact, Hendrik Poeck (hendrik.poeck@ukr.de).

Materials availability

The CRISPR-Cas9-edited murine and human melanoma cell lines generated for this study may be requested under a material transfer agreement as per institutional requirements from the lead contact.

Data and code availability

- RNA-sequencing of murine melanoma EV cargo data have been deposited to the European Nucleotide Archive (ENA) and are publicly available. The accession number is listed in the key resources table. This paper analyzes existing, publicly available data. The sources of these datasets are listed in the key resources table. Adjective data reported in this paper will be shared by the lead contact upon request.
- This paper does not report original code.
- Any additional information required to reanalyze the data reported in this paper is available from the lead contact upon request.

EXPERIMENTAL MODEL AND STUDY PARTICIPANT DETAILS

Mice

Female C57BL/6J mice were purchased from Janvier. Mice genetically deficient for *Mavs*, *Sting* (*Tmem173*$^{gt/gt}$), as well as Itgax-Cre^{+}Ifnar1$^{f/f}$ and LysM-Cre^{+}Ifnar1$^{f/f}$ transgenic mice have been described previously.[46–49] Mice were at least six weeks of age at the onset of experiments, had not been involved in previous procedures and were maintained in specific pathogen-free conditions. Wild-type and genetically deficient mice included in the same experiments were either littermates from heterozygous breeding or were co-housed for at least four weeks before the onset of experiments. Tumor growth of B16 melanoma has previously been reported to be similar in male and female mice.[61] Animal studies were approved by the local regulatory agency (Regierung von Oberbayern, Munich, Germany) and conformed to institutional and national guidelines and regulations. Mice genetically deficient for *Tlr3* or *Myd88* were only used as bone marrow donors and have been described previously.[50,51]

Cell lines

The B16 murine melanoma cell line expressing full-length chicken ovalbumin (here referred to as B16.OVA; male) was cultured in a complete DMEM medium supplemented with 400 μg/mL G418 (from Sigma-Aldrich). B16 F10 (male), CT26 (female), 4T1 (female), Panc02 (male) and NIH3T3 (male) cells were cultured in complete DMEM medium or RPMI medium, respectively. Human melanoma SK-MEL-5 (female), SK-MEL-29 (male), SK-MEL-30 (male), IGR-37 (male) and IGR-39 (male) cells were a gift from Barbara Schmidt (University of Regensburg) and were cultured in complete DMEM medium. Further, the human melanoma cell lines D04mel (sex unspecified), Ma-Mel-86b (female), or the ovarian cancer cell line Skov (female) were cultured in complete RPMI medium.

THP1-Dual KI-hSTING-R232 (Cat#thpd-r232, male) cells, THP1-Dual KO-STING (Cat#thpd-kostg, male) cells and HEK-Blue IFN-α/β (Cat#hkb-ifnab, female) Cells were purchased from InvivoGen (Toulouse, France). RPMI-1640 medium (Invitrogen) and DMEM (Invitrogen) were supplemented with 10% (v/v) FCS (EV-depleted by 100,000 G ultracentrifugation for 24 h at 4°C to minimize possible contamination with xenogenous EVs), 3 mM L-glutamine, 100 U/mL of penicillin and 100 μg/mL of streptomycin (all from Sigma-Aldrich). All cell lines were cultured in a humidified incubator with 5% CO_2 at 37°C.

METHOD DETAILS

Generation of Rab27a deficient murine melanoma cells

B16.OVA cells genetically deficient for Rab27a were engineered using the CRISPR-Cas9 system as described previously for clones deficient for RIG-I, IRF3/7, Caspase 3 or MLKL.[12] In brief, the Streptococcus pyogenes nuclease Cas9 in conjunction with various single guide (sg)RNAs was used to genetically edit B16.OVA cells. The specific target sequences of sgRNAs were designed for optimal on-target activity, and are listed in Table S4. The sgRNAs were cloned into pSpCas9(BB)-2A-GFP (pX458, a gift from Feng Zhang; Addgene plasmid #48138), which is a bicistronic expression vector containing Cas9 and a sgRNA. These constructs were transiently introduced into B16.OVA cells by lipofection using Lipofectamine 2000 in OptiMEM. After 6 h, the culture medium was removed and cells were provided with fresh medium. 24 h post transfection, GFP-expressing single-cell clones were isolated using fluorescence-activated cell sorting (FACS), and were expanded to monoclonal cell clines. Rab27a-deficiency was confirmed by immunoblotting and mRNA PCR.

CellPress
OPEN ACCESS

Cell Reports Medicine
Article

Generation of gene deficient SK-mel-29 human melanoma cells

Gene-deficient SK-mel-29 cells (RIG-I, STING, cGAS, IFNAR1) were engineered using CRISPR-Cas9 technology. Two guide (g)RNAs (crRNAs, IDT, Leuven, Belgium) were designed to target each of the above genes, sequences are listed in Table S4 gRNAs were prepared using respective crRNA (200 μM) and Alt-R CRISPR-Cas9 tracrRNA (200 μM, IDT). The mixture was incubated for 5 min at 95°C in a ThermoCycler, and was cooled down to room temperature. Cas9 endonuclease protein (Thermo Fisher) was then mixed with two respective gRNAs to form ribonucleoprotein (RNP) complexes at room temperature for at least 20 min. Melanoma cells were prepared in P3 primary cell kit buffer (Lonza, Cologne, Germany). After mixing RNP complexes and cell suspensions in a PCR tube, the mixture was transferred to Nucleocuvette Strip (Lonza), and nucleofection was performed on the Lonza 4days nucleofector (Lonza) using program CM137. Then the cells were seeded in pre-warmed medium and cultured for 5–7 days. Bulk cells were collected for DNA isolation, gene knockout efficacy was determined by targeted PCR, TIDE sequencing, and/or immunoblotting.

Reagents

OptiMEM reduced serum medium was from Invitrogen. Double-stranded *in vitro*-transcribed 3pRNA (sense, 5′- UCA AAC AGU CCU CGC AUG CCU AUA GUG AGU CG -3′) was generated as described.[3] Synthetic dsRNA lacking the 5′-triphosphate (synRNA) was purchased from Eurofins (Ebersberg, Germany). A previously described 45-base pair non-CpG double-stranded DNA oligonucleotide (interferon stimulatory DNA, ISD)[52] was used for activation of cGAS/STING signaling in tumor cells. ISD single-strand oligonucleotides were purchased from Sigma-Aldrich (Munich, Germany) and were annealed by heating to 75°C for 30 min and re-cooling to room temperature (RT).

Preparation of EVs and nucleic acid extraction

Tumor cells were harvested, washed twice with PBS and were then seeded at a fixed concentration of $5x10^5$ cells per mL media containing 10% (v/v) EV-depleted FCS (to ~90% cell density). For *in vitro* transfection of tumor cells, nucleic acids were complexed with Lipofectamine 2000 (Life Technologies, Darmstadt, Germany) in OptiMEM (Invitrogen). Tumor cells were transfected with 3pRNA, synRNA (both 3 μg/mL) or ISD (6 μg/mL), or were left untreated. After 24 h, cell culture supernatants were collected, centrifuged at 400 G for 5 min, and subsequently 2,000 G for 30 min to remove cell debris and were then filtered through a Millex GV 220 nm PVDF membrane (Merck Millipore). Each sample of cell-free culture supernatant was transferred to a fresh tube. For precipitation-based EV purification, each sample was combined with ½ volume of 'Total Exosome Isolation Reagent (from cell media)' (Thermo Fischer) and mixed well by vortexing or pipetting up and down until a homogeneous solution was formed. Typical cell media volume utilized was 1 mL. The samples were incubated at 4°C overnight and then centrifuged at 4 °C at 10,000 G for 1 h. The supernatant was aspirated and discarded, and the EV pellet was resuspended in PBS buffer and stored at −80°C. EV pellets purified from 1 mL B16.OVA cell culture supernatant each were resuspended in 5 μL PBS (EV stock solution). Preparation of EVs by size-exclusion chromatography was performed with the "Exo-spin" kit (Cell GS, Cambridge, UK). Cell debris-depleted media was combined with ½ volume of "Exo-spin" precipitation buffer and mixed well, incubated overnight at 4°C and then centrifuged at 4°C and 16,000 G for 1h. The supernatant was discarded, and the EV-containing pellet was resuspended in PBS buffer before being applied to the size-exclusion chromatography column according to the manufacturer's instructions. Separation of EV subsets through differential ultracentrifugation was performed by sequential centrifugation of cell debris-depleted media with 2,000 G for 20 min, 10,000 G for 40 min, and 100,000 G for 90 min at 4°C. After each centrifugation step, the EV pellet was washed at the same speed for the same time before resuspension in 5 μL PBS buffer. EV-RNA was extracted with the 'Total Exosome RNA and Protein Isolation Kit' (Thermo Fisher) according to the manufacturer's instructions. RNA concentration was analyzed using the Qubit 1X dsDNA HS Assay Kit (Thermo Fisher) and RNA quality was assessed using the TapeStation System (Agilent). DNA was obtained using DNAzol reagent (Thermo Fisher) according to the manufacturer's protocol. In brief, 1 mL of DNAzol was added to isolated EVs. EVs were lyzed for 30 min at RT, and DNA was subsequently precipitated from the lysate with ethanol. Following an additional ethanol wash, DNA was solubilized in water. For some experiments, EVs were purified from 1:1 co-culture of B16.OVA melanoma cells and NIH3T3 fibroblasts, or from short-term cultures of bulk melanoma tumor tissue. To this end, subcutaneous melanoma tumors of approximately 1000 mm^3 were dissected, finely minced and filtered through a 100 μm nylon strainer (BD Bioscience), before single cell suspensions were cultured in DMEM supplemented with 10% EV-depleted FCS.

Murine bone marrow-derived dendritic cell culture

Murine bone marrow-derived DCs were generated by culturing bone marrow cells in complete RPMI medium supplemented with 20 ng/mL GM-CSF (Immunotools, Friesoythe, Germany). For EV stimulation, DC cultures were supplemented with 7 μL EV stock solution per 1 mL RPMI medium (corresponding to approximately 5×10^8 particles derived from 10^6 tumor cells per condition). In case of EVs derived from size exclusion chromatography, the stock solution applied to DCs was calibrated to include EVs from 1.4 mL tumor culture supernatant per 1mL RPMI. In some experiments, tumor EVs were mixed with Lipofectamine 2000 prior to BMDC exposure. As positive control, BMDCs were treated with *in vitro* transcribed 3pRNA (1 μg/mL) or ISD (2 μg/mL) using Lipofectamine 2000. As negative control, DCs were cultured under steady-state conditions ('Unstim.'), or with EVs enriched from tumor cell cultures exposed to just the transfection reagent lipofectamine (Vehicle-EVs). IFN-I secretion was determined by ELISA after 24 h. The expression of CD86 on BMDCs was quantified by flow cytometry after 24 h. To analyze uptake patterns, DCs were exposed to tumor EV samples that were labeled with the fluorescent membrane marker PKH67 (PKH67 Green Fluorescent Cell Linker Kit, Sigma-Aldrich). For some

Cell Reports Medicine
Article

CellPress
OPEN ACCESS

experiments, the inhibitors dynasore (Sigma-Aldrich), amiloride (Sigma-Aldrich), D-Mannose (Fisher Scientific) and EDTA (Thermo Fisher) were added in the indicated concentrations. 10 μL of EV suspension were mixed with 50 μL of diluent and 0.4 μL PKH67 and incubated for 15 min at room temperature in the dark. Meanwhile Exosome Spin Columns (Invitrogen) were prepared according to the manufacturer's protocol. The labeled EVs were pipetted onto the Exosome Spin Columns and centrifuged at 750 G for 2 min. EV uptake in DCs was visualized by confocal fluorescent microscopy. 7 x 10^3 BMDCs were seeded in 18-well flat μ-slides (IBIDI) and incubated with PKH67 labeled EVs for 3 h at 37°C and 5% CO_2. Nuclei were stained with DAPI (2 μL/mL; Sigma-Aldrich) for 10 min and the cell membrane of DCs was stained with CellMask Deep Red plasma membrane stain (Invitrogen) according to the manufacturer's protocol. BMDCs were transfected with EV-extracted RNA (800 ng/mL) or DNA (140 ng/mL). For some conditions, RNA was treated with alkaline phosphatase (Apex, Epicentre) according to the manufacturer's protocol. In brief, 1 μL of Apex was added to EV-RNA (up to 1 μg) and incubated for 10 min at 37°C. The phosphatase was inactivated by heat inhibition for 5 min at 70°C. For RNA transfer experiments, EV RNA was labeled with SYTO RNASelect fluorescent cell stain (500 nM; Thermo Fisher) for 20 min at 37°C. Afterward, excessive stain was removed via Exosome Spin Columns (Invitrogen) which were prepared according to the manufacturer's protocol.

Quantification of cytokines

IFN-β concentration in murine cell culture supernatants was determined with a custom-made ELISA, as described previously.[12] In brief, Flat-bottom 96-well plates (Nunc) were coated with rat anti-mouse IFN-β antibody (PBL Assay Science Cat# 22400-1, RRID:AB_387846; 1 μg/mL) in coating buffer (eBioscience) for 16 h at 4°C. After extensive washing with PBS +0.5% Tween, the plate was blocked with PBS +10% FCS for 3 h on room temperature (RT). Samples were incubated on 4°C for 24 h, and plates were extensively washed. Anti-mouse Interferon-beta rabbit serum (PBL Assay Science Cat# 32400-1, RRID:AB_387872; 620 ng/mL) was added and incubated for 3 h at room temperature. After additional washing, polyclonal goat anti-rabbit IgG coupled with horseradish peroxidase (Abcam Cat# ab6721, RRID:AB_955447; 56 ng/mL) was added and incubated for 1 h at room temperature. After intensive washing, 100 μL of substrate solution (1xTBM Substrate, eBioscience) was added. When the reaction was complete, 100 μL of stop solution (2N H_2SO_4) was added to the substrate solution. Optical density of each well was immediately assessed, using a microplate reader set to 450 nm (Tecan). IFN-β production in human THP-1 monocytic cells was determined using the THP1-Dual KI-hSTING-R232 Cells reporter system (Invivogen). These cells are derived from the human THP1 monocyte cell line, which stably integrated a secreted inducible reporter construct to monitor type I IFN pathway activation. THP1 reporter cells were incubated for 24 h with EVs derived from control or 3pRNA-treated melanoma cells (40 μg/mL, determined via BCA assay), then type I IFN pathway activation was measured according to the manufacturer's instructions. PBMC culture supernatants were analyzed for cytokine secretion by ELISA (BD OptEIA Kits) or IFN-I release with the reporter cell line HEK-Blue IFN-α/β Cells (Invivogen) according to the manufacturers' protocol.

Western blot

Cells or EVs isolated from cell culture supernatants were solubilised in RIPA buffer (Pierce), separated by SDS-PAGE on 12% polyacrylamide gels and transferred onto a nitrocellulose blotting membrane (GE Healthcare). The membranes were blocked in 3–5% blocking reagent (GE Healthcare) in PBS-Tween (PBST) for 1 h at room temperature and incubated with respective antibodies (Abs) in 0.5–1% blocking reagent in PBST over night at 4°C. A list of antibodies used for Western blot can be found in Table S5. After 3 × 5 min washing in PBST, the peroxidase-conjugated secondary antibody was applied at 1:40,000 dilution in 1–2% blocking agent in PBST for 1.5 h at room temperature. After 3 × 5 min PBST washes, the bands were detected by Amersham ECL plus and developed on Amersham ECL developing film (GE Healthcare).

Flow cytometry

Cell suspensions were stained in PBS with 3% FCS. Fluorochrome-coupled antibodies were purchased from eBioscience or BioLegend and are listed in Table S6. For intracellular cytokine staining the Foxp3 Transcription Factor Fixation/Permeabilization Kit (eBioscience) was used. Data were acquired on a FACSCanto II (BD Biosciences) and analyzed using FlowJo software (TreeStar).

Immunization with EVs

For subcutaneous (sc) immunization, mice were injected sc in the hock of the hind leg with 6.25 μL EV stock solution (corresponding to approximately 8 x 10^9 particles per condition, based on preliminary titration experiments) derived from the indicated tumor cell cultures. The treatment was repeated at day 7. In some experiments, mice were pre-treated intraperitoneally (ip) with 400 μg anti-murine IFNaR1 antibody (clone MAR1-5A3, BioXCell, West Lebanon, NH) one day prior to the above immunization. On day 14, mice were sacrificed and draining lymph nodes and the spleen were removed. Lymphocytes of these organs were collected and *ex vivo* plated on a tissue-treated cell culture plate and cultured in the presence of 1 μg/mL OVA protein in complete RPMI medium for 72 h. IFN-γ levels of $CD8^+$ T cells were analyzed by flow cytometry and ELISA from culture supernatant.

Tumor challenge and treatment

For tumor challenge with therapeutic treatment, mice were injected subcutaneously (sc) with 10^5 B16.OVA cells or 2 x 10^6 Panc02 cells in the right flank on day 0. When tumors were readily visible, 18.75 μL EV stock solution derived from corresponding tumor cell

CellPress
OPEN ACCESS

Cell Reports Medicine
Article

cultures (corresponding to approximately 2.4 x 10^{10} particles per condition, based on preliminary titration experiments) were injected in PBS peritumorally (pt). To exclude only localized innate immune responses, in some experiments mice were treated with subcutaneous (sc) isEV applications in tumor distant sites. Generally, injections were repeated 2 times (days 6, 9 and 12). In some experiments, anti-CTLA-4 (clone 9H10) and anti-PD-1 (clone RMP1-14) or appropriate isotype controls (200 μg, all from BioXCell, West Lebanon, NH) were additionally administered intraperitoneally (ip) at the same time points. Treatment with anti-CD8a (clone 2.43, BioXCell) or anti-NK1.1 (clone PK136) depleting antibodies was initiated two days prior to tumor induction (100 μg ip) and was repeated twice weekly (50 μg ip). For tumor rechallenge experiments, mice were injected iv with 10^5 B16.OVA melanoma cells. Naive mice were challenged with melanoma cells as controls. For *in situ* 3pRNA treatment, mice were injected sc with B16.OVA (2.4 x 10^5 right flank, 0.8 x 10^5 left flank) cells on day 0. Starting when tumors were readily visible (volume approximately 100 mm^3), 25 μg 3pRNA complexed in 3.5 μL in vivo-jetPEI (Polyplus) were repeatedly injected into the right-sided tumors on day 6, 9 and 12. Generally, mice were euthanized when the maximum tumor diameter exceeded 15 mm according to standard legal procedure (responsible state office Regierung von Oberbayern). Expansion of OVA-specific CD8 T cells was determined on day 15 after tumor induction using iTAg MHC-I murine SIINFEKL tetramers (Cat#TS-5001-1C, from MBL). At predefined time points, mice were sacrificed, and tumors as well as tumor-draining (inguinal) lymph nodes were removed using forceps and surgical scissors. Tumors and lymph nodes were minced and homogenized by filtering through a 100 μm nylon strainer (BD Bioscience). The cell suspensions were washed in PBS before subsequent analysis.

Sequencing of murine EV-RNA

RNA was extracted from EV samples using the miRNeasy Mini Kit (Qiagen) and eluted in 40 μL nuclease-free water. Prior to library preparation, RNAs were gently dried in a centrifugal evaporator, resuspended in 10 μL water and analyzed using capillary electrophoresis (RNA 6000 Pico Assay, 2100 Bioanalyzer, Agilent Technologies). Sequencing libraries were constructed from 6 μL of concentrated total RNA using the NEBNext Multiplex Small RNA Library Prep Set for Illumina (New England BioLabs) as previously.[62] PCR products were subjected to size selection by high-resolution gel electrophoresis and purity of libraries was assessed by capillary electrophoresis before running 50 cycles of single-end sequencing on the HiSeq2500 (Illumina). RNA-seq data was processed using the nf-core rnaseq pipeline.[53] In brief, sequencing reads were adaptor and quality trimmed using Trim Galore!,[54] and aligned to the GRCm38 reference genome using STAR.[55] Gene expression was quantified using Salmon,[56] and differential gene expression analyses were performed using DESeq2.[57] Gene set enrichment analysis was performed using the fgsea R package[58] and the Mouse MSigDB hallmark gene set.[63] To identify and quantify RNA biotypes in more detail, aligned sequencing reads were subjected to MGcount,[59] an RNA-seq quantification tool which hierarchically assigns reads to small RNA, long RNA exons, and long RNA introns accounting for length disparities and thus quantifies coding and non-coding transcripts. In addition, RepeatMasker[60] was run to identify and quantify interspersed repeats. If not stated otherwise, conservative thresholds for significantly regulated RNAs were set at a log2 fold change $\geq |1.5|$ and an adjusted p value of ≤ 0.05.

Human PBMC EV stimulation

Preparation of human PBMCs, human melanoma cell lines, human tumor EV generation, culture conditions, antibodies, reagents, and immunostimulatory oligonucleotides have been described before.[41] In brief, PBMCs were prepared by density gradient centrifugation using Biocoll (Sigma-Aldrich, #L6113) from peripheral blood of healthy donors. Human melanoma cells lines were cultured in RPMI with penicillin (1%) and streptomycin (1%) and 10% FCS (Gibco) in 10 cm dishes and at a confluence of 70–80% (5 × 10^6 cells), and were transfected with 3pRNA or poly-A RNA (ctrl RNA) as control. Therefore, 24 μg RNA were complexed with 60 μL Lipofectamine 2000 according to the manual and cells were incubated for 3 h with the transfection complexes. Afterward, cells were washed three times to remove lipofection complexes and cells were further cultured for 18 h in media supplemented with EV-reduced FCS for production of EVs. Supernatant of cells for EV purification was centrifugated for 5 min at 400 G and twice for 15 min at 10,000 G. Vesicles were pelleted twice at 100,000 G for 90 min with intermediate resuspension in PBS (SW32Ti Rotor, Beckman Coulter). The amount of EV protein (approximately 20–100 μg from 5 × 10^6 cells, dependent whether cells were activated with RIG-I ligand or not) was quantified by Bradford Assay (Carl Roth, #K015.2) or via Nanodrop (Peqlab, Erlangen, Germany). PBMCs were incubated with 10 μg/mL EVs with incubation times between 24 h and 48 h. IFN-I release was measured by HEK-Blue IFN-α/β reporter cells (Invivogen). To label particles released from human tumor cells, melanoma cells were incubated with 5 μM carboxyfluorescein succinimidyl ester (CFSE) (eBioscience, #65-0850-84). Subsequently, CFSE-positive particles were enriched from the melanoma culture supernatant as described above, and were exposed to PBMCs. Uptake of labeled particles by monocytes, NK cells, or T- and B cells was determined by flow cytometry. For generation of human immature DCs, Ficoll-separated PBMCs were used. In brief, PBMCs were adjusted to a density of 5x10^6/mL in RPMI medium and cells were plated for 1 h at 37°C. Later, non-adherent cells were removed and plastic-adherent cells were cultured for additional 24 h in RPMI supplemented with rhGM-CSF (1000 U/mL) and rhIL-4 (500 IU/mL), before EVs were added. 18 h later, the supernatant of DCs was analyzed for secretion of IFN-I using HEK-Blue IFN-α/β reporter cells.

ELISpot

IFN-γ ELISpot assays were performed as previously described.[64] Briefly, immature DCs were generated from HLA-A2 matched PBMC donors in the presence of IL-4 (500 IU/mL) and GM-CSF (1000 IU/mL) for 24 h, and were then exposed to EVs (75 μg/mL,

Cell Reports Medicine
Article

CellPress
OPEN ACCESS

derived from D05mel human melanoma cells; EV dosage based on previously published experiments[41]) for additional 24 h. Melan A or tyrosinase sensitive autologous T cell clones were thawed and kept for 24 h in AIM-V medium supplemented with 10% human serum from healthy individuals and 250 IU/mL IL-2. ELISpot plates were coated with 10 μg/mL anti-human IFN-γ antibody (Mabtech, clone 1-D1K), and EV-loaded DCs (20,000 cells) were co-cultured with autologous T cells (10,000 cells) for 4 h. Control wells contained effector cells alone or effector cells in the presence of tumor cells (D05mel). Assay conditions were tested in triplicates. Assay development was done according to standard procedures using the biotinylated monoclonal antibody anti-hIFN-γ (Mabtech, 7-B6-1), and was analyzed using the KS ELISpot Automated Reader System. Spot numbers were determined with the use of a computer-assisted video image analysis program (KS ELISpot, Zeiss, Jena).

RNA-seq analysis of human melanoma samples

RNA-seq data and clinical data from the Cancer Genome Atlas (TCGA) were downloaded for 472 cutaneous melanoma samples from cBioPortal (study ID "skcm_tcga")[43] using the R package cgdsr.[65] Excluding patients with multiple tumors and missing or invalid overall survival data resulted in a cohort of 456 patients used for further analysis. *Tumor EV pathway* and *Common EV pathway* gene sets have been defined previously.[26,35] Of these, we excluded *Myosin Light Chain 3* (*MYL3*), since we found it not to be expressed in the 456 human melanoma samples, resulting in a *Tumor EV pathway* gene set of 24 genes. The melanoma patient cohorts under treatment with anti-CTLA-4[44,66] or anti-PD-1[45] for tumor RNA-seq analysis have been described previously. The gene expression level of each EV pathway gene was median centered and scaled by its median absolute deviation using its expression levels across all tumors within the cohort. Then, the mean of the centered and scaled EV pathway gene expression levels for one tumor sample was assigned as the mean EV pathway gene set expression value for that tumor sample. Using the median EV pathway gene set expression values of one cohort as a cut-off, tumor samples were assigned to a low or high EV pathway gene set expression subgroup for survival analysis. The significance of the association between concomitantly high transcriptional activity of *DDX58* and the *Tumor EV pathway* gene set with durable clinical response to either anti-CTLA-4 or anti-PD-1 (defined as complete response, partial response or stable disease for at least 6 months) was calculated with Fisher's exact test. Using an unbiased approach, median expression of the gene set was used as cutoff to classify patients into low and high expression subgroups. The data used for comparative RNA-seq analyses in healthy skin tissue were obtained from the Genotype-Tissue Expression (GTEx) Project.

Nanoparticle tracking analysis (NTA)

Sizing and quantification of EVs was performed with the NanoSight LM10 instrument, following the manufacturer's protocol, (NanoSight, Malvern Instruments Ltd, Malvern, UK). In brief, a 1 μL aliquot of obtained EV samples was diluted in $_{dd}H_2O$ (at least 1:1000) to achieve a uniform particle distribution, and 6 sequential measurements (1 min each) at 23°C (viscosity 0.09 cp) were performed. The instrument settings were: camera shutter 25–32 ms, 24.98–24.99 frames/s; drift velocity 5011 to 6970 nm/s; analysis: blur auto, detection threshold 5–6 multi, min track length auto and min expected size auto. At least 900 tracks were recorded per measurement.

Transmission electron microscopy

EV samples were diluted 1:50 in PBS. 5 μL of each diluted sample were applied to glow-discharged carbon grids, incubated for 60 s, blotted, briefly washed with $_{dd}H_2O$ and subsequently stained in 1% w/v uranyl acetate for 40 s. Images were recorded immediately using a CM200 at a nominal magnification of 50,000x on a Tietz4K camera. The pixel size on the specimen level was 0.21 nm.

Protein quantification with BCA assay

Protein load of EV samples was determined by bicinchoninic acid (BCA) assay using the Pierce BCA Protein Assay (Thermo Scientific) according the manufacturer's protocol. In brief, EVs were lyzed with RIPA buffer during an incubation time of 30 min on ice. After 1 min of vortexing, lysates were mixed with the kit reagents and incubated for 30 min on 37°C in the dark. The purple-colored reaction product of this assay exhibits a strong absorbance at 562 nm, which correlates linearly with protein concentrations. The absorbance was measured at or near 562 nm on a Tecan plate reader.

Quantifying gene expression by real-time PCR

Total RNA was isolated from cells lysed in TRIzol (Ambion) and was reversely transcribed using standard methods and kits according to manufacturer's protocols (RNeasy Mini Kit, Qiagen; SuperScript III Reverse Transcriptase, Invitrogen). The specific primer pair sequences are listed below. Transcript amplification was visualized with the qPCR Core kit for SYBR Green I (Eurogentec) using a LightCycler 480 II (Roche) real-Time PCR system. The relative transcript level of each gene was calculated according to the $2-\Delta\Delta Ct$ method with normalization to β-Actin. The following mRNA primer sequences were used: *mActin* fwd 5′-CACACCCGCCAC CAGTTCG-3′, *mActin* rev 5′-CACCATCACACCCTGGTGC-3′, *mRab27a* fwd 5′-GCATTGATTTCAGGGAAAAGAGAG-3′, *mRab27a* rev 5′-TTCTCCACACACCGCTCCATCCGC-3′.

Bulk murine melanoma RNA-sequencing

RNA-seq library preparation, sequencing and archiving for this dataset have been published before.[12] The data are publicly available (European Nucleotide Archive, accession #: PRJEB32241). In brief, mice were injected subcutaneously with 2.4 x 10^5 B16.OVA

melanoma cells. On day 6, 25 μg 3pRNA complexed in 3.5 μL in vivo-jetPEI (Polyplus) were injected into the tumors. On day 7, tumors were removed and total cellular RNA was extracted from bulk tumor cells. Gencode gene annotations M24 and the mouse reference genome GRCm38 were derived from the Gencode homepage (EMBL-EBI). Drop-Seq tools v1.12[67] was used for mapping raw sequencing data to the reference genome. The resulting UMI filtered count matrix was imported into R v4.0.5 and lowly expressed genes were subsequently filtered out. Prior differential expression analysis with DESeq2,[57] dispersion of the data was estimated with a parametric fit using the group as response variable for the Generalized Linear Model (GLM). Apeglm[68] shrunken log2 foldchanges were calculated afterward, and used as input for the GSEAPreranked method.[69] Geneset definition was derived from a previous publication[26] Data was variance stabilized via the rlog function as implemented in DESeq2 and leading-edge genes from the GSEA-Preranked analysis were visualized as heatmap (z-transformed rlog expression values).

Imaging flow cytometry

In vitro transcribed 3pRNA was fluorescently labeled (FAM, excitation peak at 492 nm, emission peak at 518 nm) using the Silencer siRNA Labeling Kit (Thermo Fischer). B16.OVA cells were transfected with either unlabeled or FAM-labeled 3pRNA. After 48 h, EVs were isolated from cell culture supernatants as described above. Prior to analysis, 5 μL aliquots of EV stocks were thawed and diluted to a total volume of 50 μL by adding 45 μL of Dulbecco's PBS (Gibco Invitrogen) to each sample. Samples were then mixed and the total volume was acquired on an ImageStreamX MkII instrument (ISX; Amnis/MilliporeSigma) equipped with 5 lasers (70 mW 375 nm, 100 mW 488 nm, 200mW 561 nm, 150 mW 642 nm, 70 mW 785 nm, SSC). Only the 488 nm and 785 nm lasers were enabled at maximum powers, and data was acquired with 60x magnification, a 7 μm core size and low flow rate as described previously.[70,71] FAM signals were collected in channel 2 (480–560 nm filter), and channel 6 (745–800 nm filter) was used for SSC detection. Data analysis was performed using Amnis IDEAS software (version 6.1). The image display mapping was linearly adjusted on representative fluorescent particle/sEV images for each channel and then applied to all files of the respective experiment. Based on aforementioned previously described settings, optimized masking and gating settings were applied for data analysis.[72,73] For detergent lysis controls, samples were incubated for 30 min at RT after adding the non-ionic detergent Nonidet P-40 to a final concentration of 0.5% as described previously.[74,75]

QUANTIFICATION AND STATISTICAL ANALYSIS

If not stated otherwise, all data are presented as mean ± SEM. Statistical significance of single experimental findings was assessed with the independent two-tailed Student's *t* test. For multiple statistical comparisons of a dataset the one-way ANOVA test with Bonferroni or Dunnett's post-test was used. Overall survival was analyzed using the Log rank test. Significance was set at p values <0.05, $p < 0.01$, and $p < 0.001$ and was then indicated with an asterisk (*, ** and ***). If not stated otherwise, an asterisk without brackets indicates statistical comparison to 'Ctrl-EV'-treated cells. All statistical calculations were performed using Prism (GraphPad Software).

Cell Reports Medicine, Volume *4*

Supplemental information

Targeting nucleic acid sensors in tumor cells to reprogram biogenesis and RNA cargo of extracellular vesicles for T cell-mediated cancer immunotherapy

Simon Heidegger, Florian Stritzke, Sarah Dahl, Juliane Daßler-Plenker, Laura Joachim, Dominik Buschmann, Kaiji Fan, Carolin M. Sauer, Nils Ludwig, Christof Winter, Stefan Enssle, Suqi Li, Markus Perl, André Görgens, Tobias Haas, Erik Thiele Orberg, Sascha Göttert, Catherine Wölfel, Thomas Engleitner, Isidro Cortés-Ciriano, Roland Rad, Wolfgang Herr, Bernd Giebel, Jürgen Ruland, Florian Bassermann, Christoph Coch, Gunther Hartmann, and Hendrik Poeck

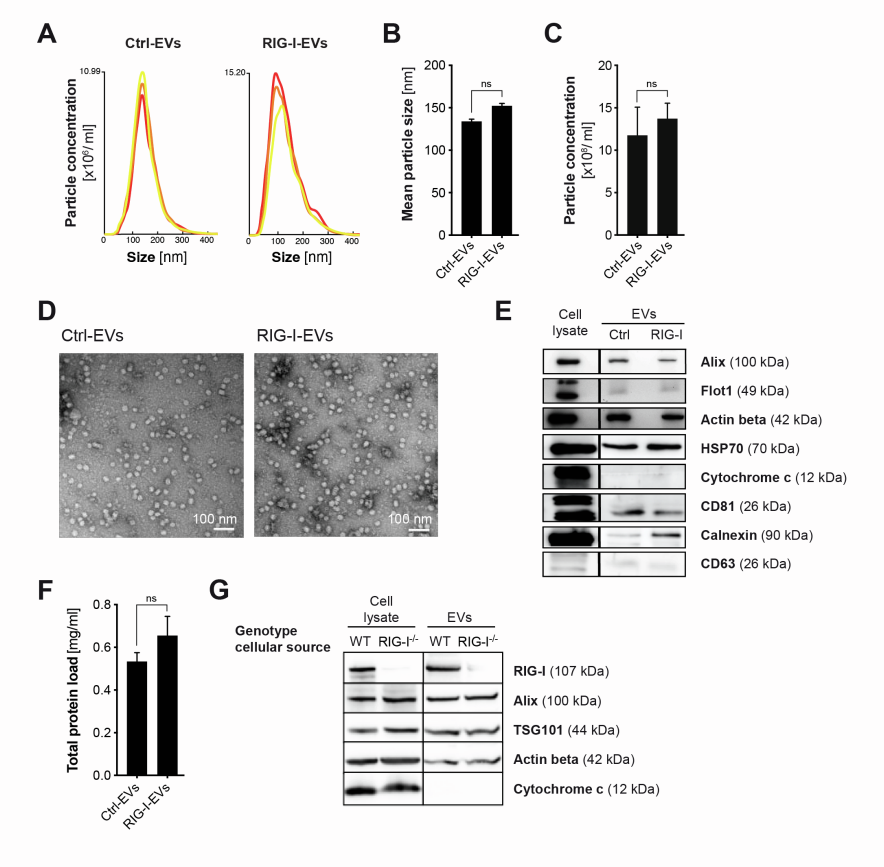

Figure S1. RIG-I signaling does not influence quantitative EV biogenesis in tumor cells. B16.OVA melanoma cells were transfected *in vitro* with 3pRNA as described for Figure 1. **(A)** Extracellular vesicles (EVs) were enriched from the supernatant of untreated (Ctrl-EVs) or 3pRNA-treated (RIG-I-EVs) B16.OVA cells by precipitation-based assays and were analyzed by nanoparticle tracking analysis (NTA). Different colors represent independent measurements (n=3). **(B)** Mean particle size (diameter in nm) as by NTA (n=3). **(C)** Particle quantity within EV samples enriched from culture supernatant of a defined number of 3pRNA-treated or untreated B16.OVA cells analyzed by NTA ($n = 3$). **(D)** Representative transmission electron microscopy of EV samples enriched from the supernatant of B16.OVA cells (magnification of 50,000x, bar size is 100 nm). **(E)** Presence of protein markers alix, flotillin1, HSP70, CD81 and CD63, as well as actin, calnexin, and cytochrome c were determined by western blot analysis of EV preparations and bulk cell lysates. **(F)** Total EV sample protein load was determined by bicinchoninic acid (BCA) assay ($n = 3$). **(G)** The presence of RIG-I protein in EV samples and bulk cell lysates from both wild-type (WT) and RIG-I-deficient (RIG-I$^{-/-}$) B16.OVA melanoma cell lines was determined by western blot. All bar graphs give mean values ± S.E.M. of at least triplicate technical replicates. Data are representative of at least two independent experiments. Related to Figure 1.

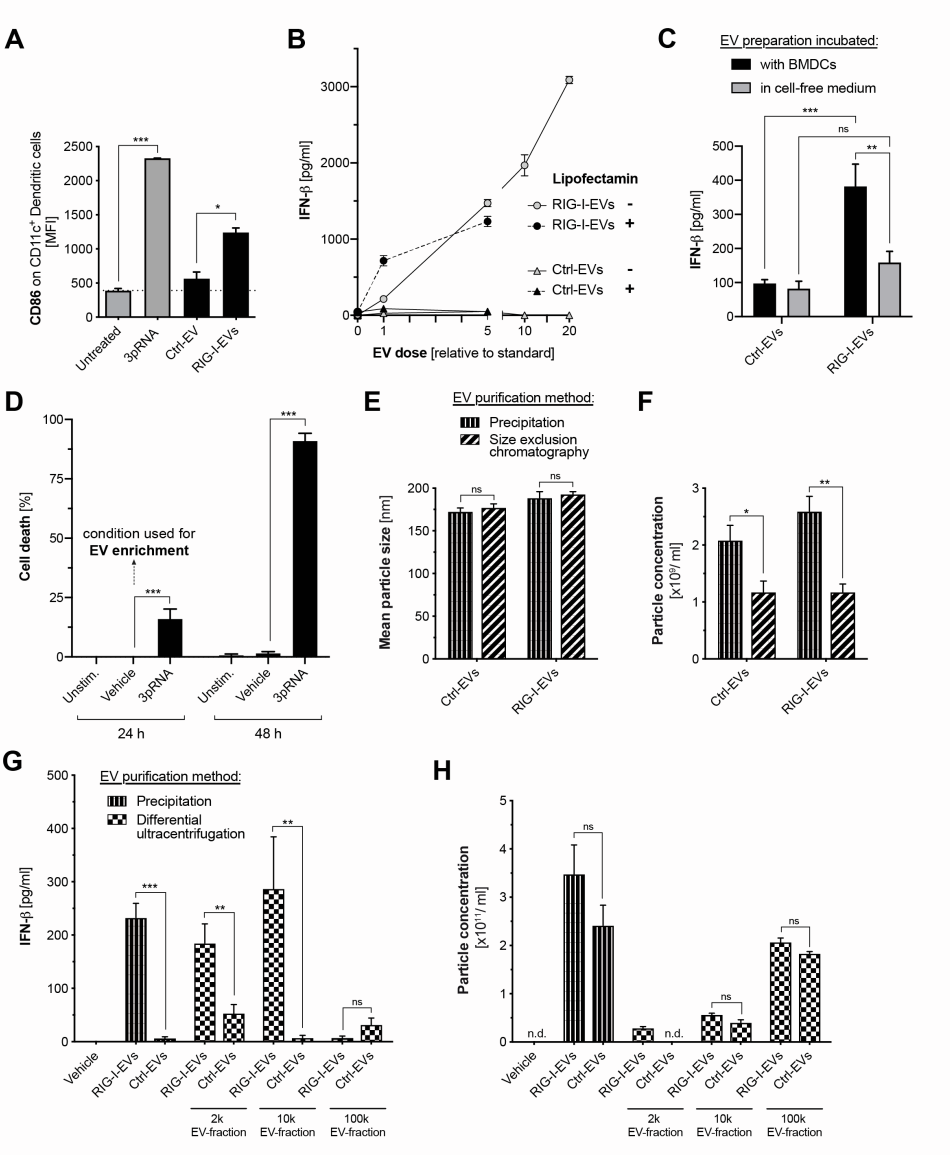

Figure S2. EV samples from RIG-I-activated tumor cell culture supernatant contain potent immunostimulatory activity independent of the enrichment technique. (A) Murine bone marrow-derived DCs were exposed to melanoma cell-derived EVs in vitro, as described for Figure 1A. CD86 expression on DCs was determined by flow cytometry. **(B)** IFN-ß induction in bone marrow-derived DCs exposed to increasing concentrations of B16 melanoma RIG-I-EV samples enriched by precipitation. For some conditions, EVs were complexed with transfection reagent lipofectamine. **(C)** Precipitation-enriched tumor EV preparations were incubated with either DCs or cell-free medium. 24 h later, IFN-ß in the culture supernatant was determined by ELISA. **(D)** B16.OVA melanoma cells were transfected with 3pRNA *in vitro* and were harvested at the indicated time points. Cell viability was determined by an LDH release assay. **(E-F)** EVs were enriched from the culture supernatant of B16 melanoma cells by precipitation or size-exclusion chromatography. **(E)** Particle size in EV

preparations (diameter in nm) as per NTA. **(F)** Quantity of particles within EV samples enriched from culture supernatant of a defined number of B16.OVA cells analyzed by NTA. **(G-H)** EVs were enriched from the culture supernatant of B16 melanoma cells by differential ultracentrifugation: 2,000 G (cell debris), 10,000 G ('large' EV), 100,000 G ('small' EV). **(G)** IFN-ß induction in BMDCs stimulated with different EV fractions. **(H)** Particle concentration in different EV fractions. All data give the mean value ± S.E.M. of at least triplicate technical replicates and are representative of two or more independent experiments. nd, not determined; ns, not significant. Related to Figure 1.

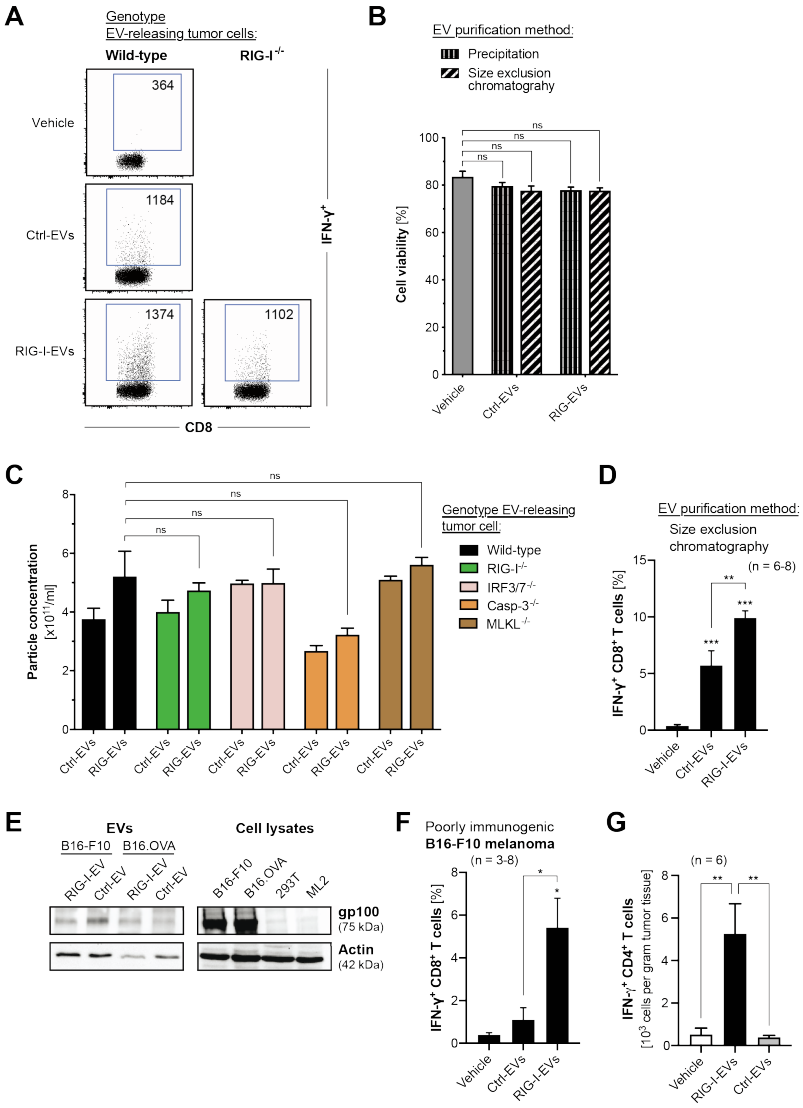

Figure S3. RIG-I activation is associated with the release of potent, non-toxic isEVs in murine models of highly and poorly immunogenic malignant melanoma. (A-B) Mice were repeatedly immunized with EVs derived from either wild-type or RIG-I-deficient (RIG-I$^{-/-}$) B16.OVA melanoma cells as described for Figure 1G. One week later, cells in the draining lymph nodes and spleen were analyzed by flow cytometry. **(A)** IFN-γ release by CD8^{+} T cells in lymph nodes after *ex vivo* OVA restimulation: Representative dot blots are gated on viable CD3^{+} CD8^{+} T cells. Numbers give the mean fluorescence intensity (MFI) of the IFN-γ signal in all gated, IFN-γ^{+} T cells. **(B)** Cell viability in the spleen was determined by Annexin V / propidium iodide staining (n = 5-9 mice per group). **(C)** EVs were enriched by precipitation-based assays from the supernatant of B16.OVA cells with different genetic deficiencies (as indicated), and were enumerated by nanoparticle tracking analysis (NTA). **(D)** Mice were repeatedly injected s.c. with B16.OVA-derived EV samples enriched by size exclusion

chromatography from either untreated (Ctrl-EVs) or 3pRNA-treated (RIG-I-EVs) tumor cell cultures. IFN-γ release by $CD8^+$ T cells from draining lymph nodes after *ex vivo* OVA restimulation was analyzed by flow cytometry. **(E-F)** EVs were enriched from the culture supernatant of poorly immunogenic B16-F10 melanoma cells by precipitation. Prior to EV preparation, some cell cultures were transfected with 3pRNA. **(E)** The protein content of EV samples was analyzed for the presence of the melanoma-associated antigen gp100 by western blot. A human embryonic kidney cell line expressing a mutant version of the SV40 large T antigen (293T) and an acute myelomonocytic leukemia cell line (ML2) were used as negative controls. **(F)** Mice were repeatedly injected sc with EV samples enriched from B16-F10 melanoma cell culture. IFN-γ release by $CD8^+$ T cells was analyzed by flow cytometry. **(G)** B16 melanoma-bearing mice were peritumorally injected with melanoma cell-derived EVs as described for Figure 2F. Abundance of activated, IFN-γ-producing $CD4^+$ T cell in the TME were determined by flow cytometry. All data give mean values ± S.E.M. All results are pooled from or are representative of at least two independent experiments. All in vitro data show at least triplicate technical replicates. The number of experimental animals per group are depicted. An asterisk without brackets indicates significant difference to the 'vehicle' control group. Related to Figure 1 and Figure 2.

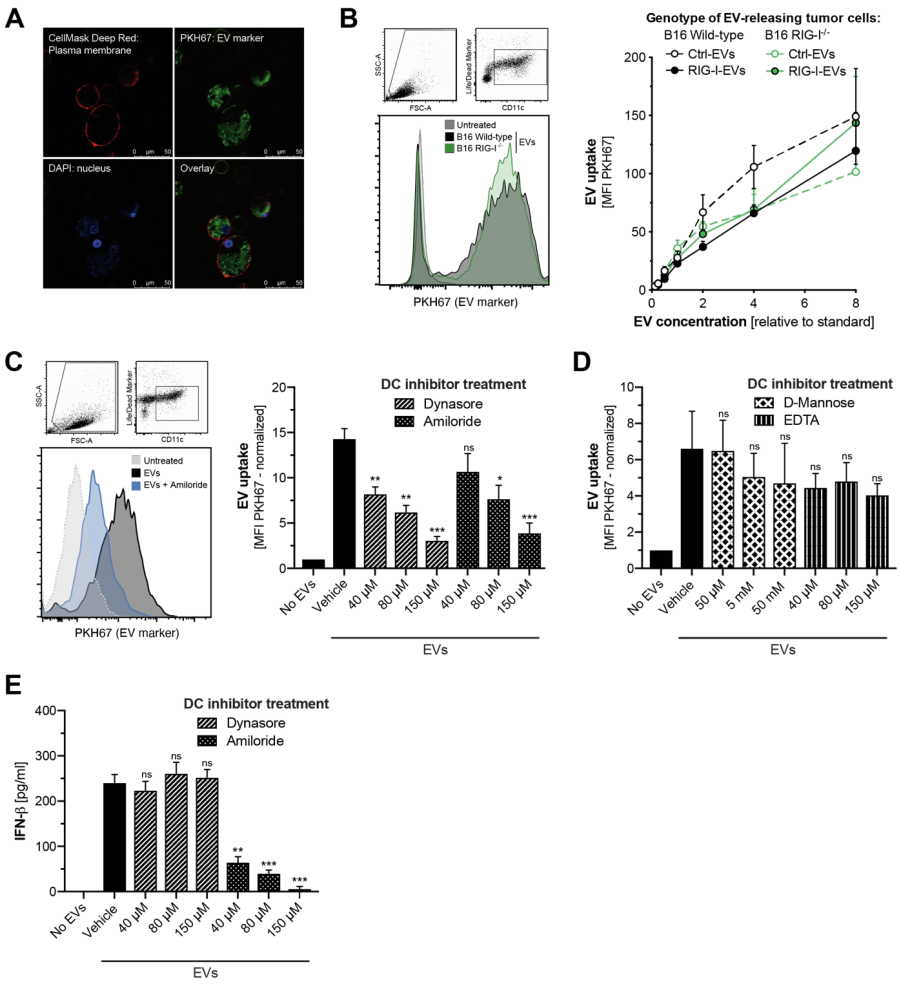

Figure S4. Tumor cell EVs are actively taken up by dendritic cells via endocytic pathways independent of RIG-I activity in the producer tumor cells. Bone marrow-derived DCs were exposed for 6 h to fluorescently-labeled tumor EV samples enriched from B16 melanoma cell cultures under steady-state or RIG-I pathway stimulation. **(A)** Uptake and intracellular distribution pattern of labeled particles in DCs imaged by fluorescent microscopy. **(B)** Semi-quantitative analysis of particle uptake by DCs using flow cytometry. Representative histograms are gated on viable $CD11c^+$ cells. The graph gives mean particle uptake of triplicate samples ± S.E.M. **(C-E)** DCs were pre-treated with the inhibitors dynasore (Clathrin- and caveolin-dependent endocytosis), amiloride (macropinocytosis), D-mannose or EDTA (both inhibitors of C-type lectin receptor interactions) before exposure to fluorescently labeled tumor EV samples. Particle uptake by DCs following inhibition with **(C)** dynasore or amiloride, and **(D)** D-mannose or EDTA. Representative histograms are gated on viable $CD11c^+$ cells. Graphs give mean labeled particle uptake of triplicate samples ± S.E.M. **(E)** IFN-I induction in DCs in response to EV exposure and inhibitor treatment. All bar graphs give mean values of triplicate technical replicates ± S.E.M. All data are representative of at least two independent experiments. An asterisk indicates significant difference to the 'vehicle' control group. Related to Figure 2 and Figure 4.

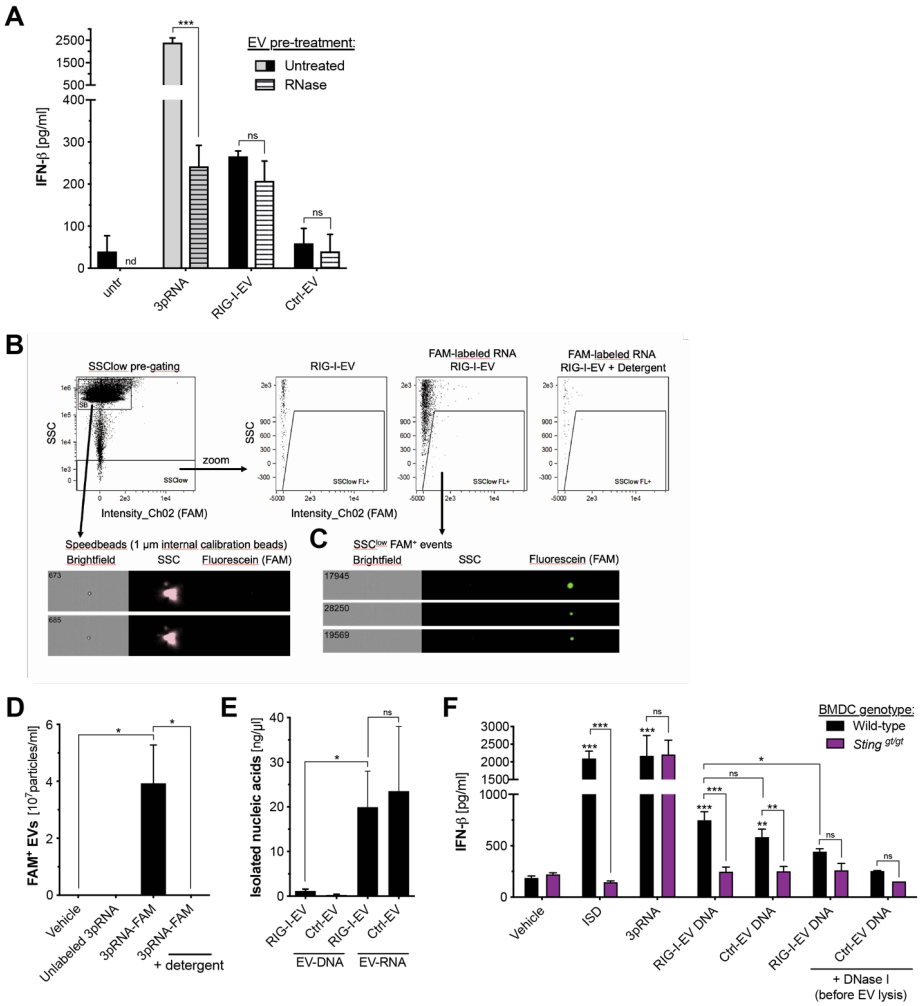

Figure S5. Immunostimulatory DNA and exogenous therapeutic RNA can be shuttled in tumor-derived EVs. (A) IFN-β release by DCs upon exposure to B16.OVA melanoma cell-derived EVs or *in vitro* transcribed 3pRNA was determined by ELISA. Some EV samples were treated with RNase before exposure to DCs *in vitro*. **(B-D)** *In vitro* transcribed 3pRNA was labeled with a fluorescent dye (FAM) and was then transfected into B16.OVA cells. 24 h later, EVs were enriched from tumor cell culture supernatant and were analyzed for FAM signal using imaging flow cytometry. Transfection of unlabeled 3pRNA and subsequently produced B16.OVA-derived EVs were used as a negative control. Some samples were additionally treated with a detergent to rupture membranous EVs for control purposes. **(B)** EV gating strategy including 1 µm speed-beads, which are used for instrument calibration. Representative dot plots are gated on side scatter $(SSC)^{low}$ EVs and give the concentration of FAM^+ EVs per sample **(C)** Single particle example images of EVs derived from B16.OVA cells that had been transfected with either 3pRNA-FAM or unlabeled 3pRNA are shown. **(D)** Absolute amount of fluorescence signal (FAM) positive events per EV formulation. **(E-F)** DNA and RNA were extracted from B16 melanoma cell-derived RIG-I- and Ctrl-EV samples. **(E)** Quantification of nucleic acids extracted from melanoma-derived EV samples. **(F)** DNA concentrations from different samples were analyzed and adjusted. DCs were transfected with EV-extracted DNA and IFN-β release was determined by ELISA. For some conditions, EV samples were

treated with DNase I prior to lysis and DNA extraction. All data are representative of at least two independent experiments. All bar graphs give the mean value ± S.E.M. of at least triplicate technical replicates. An asterisk without brackets indicates comparison to the ‘vehicle’ control group. Related to Figure 5.

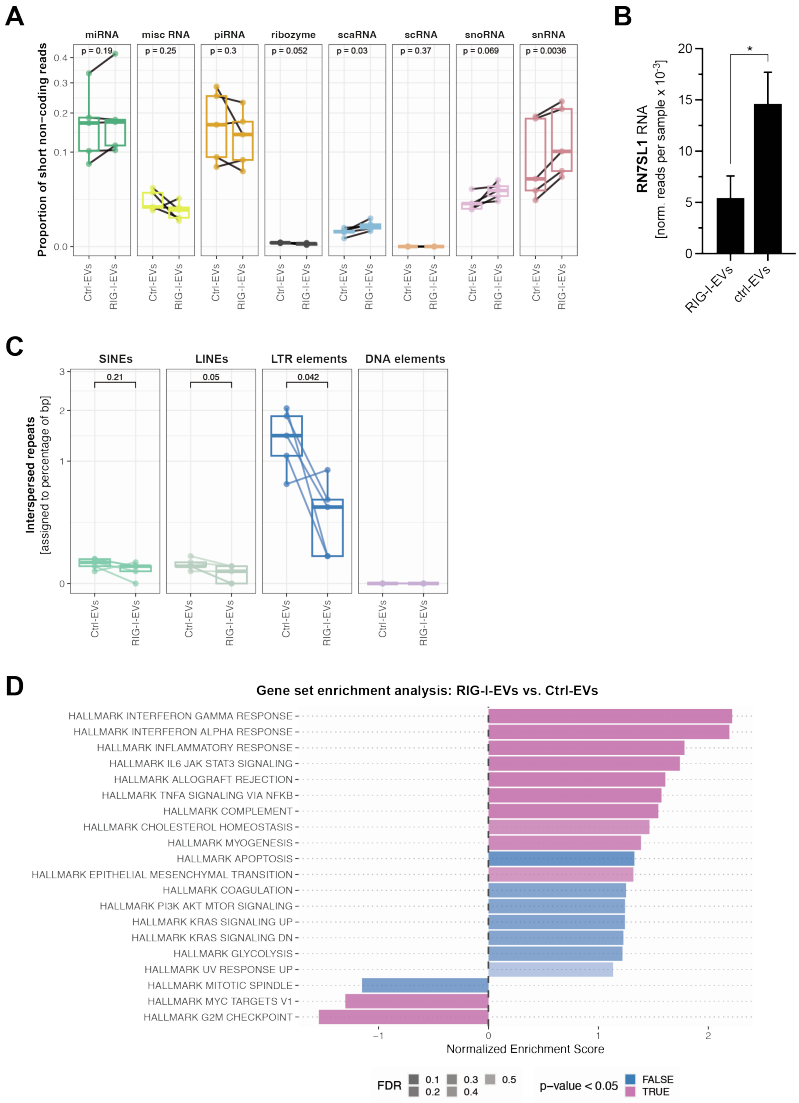

Figure S6. Tumor cell-intrinsic RIG-I pathway activity modulates the snRNA and snoRNA content of tumor-derived EVs. RNA was extracted from B16.OVA cell-derived RIG-I- and Ctrl-EV samples ($n = 3$ biological replicates per group), and the small RNA content of EV samples was analyzed by next generation sequencing as described for Figure 5. **(A)** Comparison of relative abundance of different short non-coding RNA subtypes in the cargo of RIG-I- and Ctrl-EVs. **(B)** Relative abundance of RN7SL1 reads in the RNA content of RIG-I- and Ctrl-EVs. **(C)** Comparison of abundance of repetitive elements within the RNA cargo of RIG-I- and Ctrl-EVs. **(D)** Gene set enrichment analysis (GSEA) on all differentially expressed genes in RIG-I- versus Ctrl-EVs. Related to Figure 5.

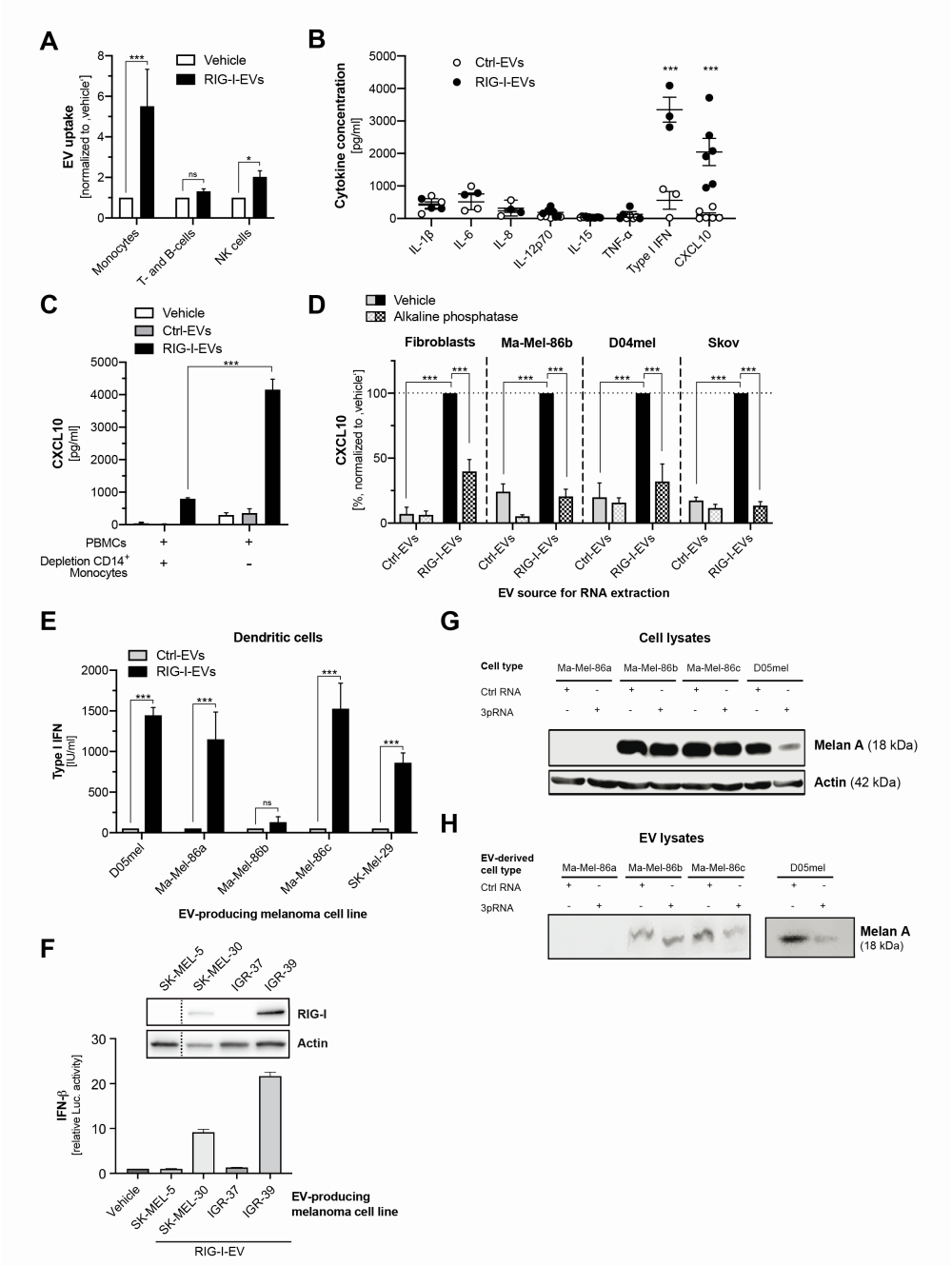

Figure S7. RIG-I-induced isEVs from different human cancer cell lines activate IFN-I signaling mainly in monocytes and dendritic cells. Freshly isolated human PBMCs were stimulated *ex vivo* with melanoma cell (D04mel)-derived, CFSE-labeled EV samples as described for Figure 6A-C. **(A)** Uptake of CFSE-labeled particles by different PBMC subsets. **(B)** Production of different cytokines by PBMCs in response to EV

exposure was determined by ELISA or the HEK-Blue IFN-α/β reporter cell line. **(C)** EV-induced release of CXCL10 in bulk and monocyte-depleted PBMCs. **(D)** PBMCs were stimulated with EV-RNA extracted from EV preparations derived from two different melanoma cells lines (D04mel, Ma-Mel-86b), human primary fibroblasts or an ovarian cancer cell line (Skov). For some RNA conditions, 5'-triphosphate moieties were degraded using thermosensitive alkaline phosphatase (FastAP). 24 h later, CXCL10 was measured in the supernatant. **(E)** Immature human DCs were exposed to EV samples derived from different cancer cell lines, and IFN-I production was measured in the cell free supernatant. **(F)** RIG-I protein abundance in different human melanoma cell lines determined by western blot of cell lysates. IFN-I induction in human monocytic THP-1 cells exposed to different RIG-I-EVs derived from respective human melanoma cell cultures. **(G)** Different human melanoma cell lines were transfected with a RIG-I ligand (3pRNA) or inert control RNA. Expression of Melan A in bulk cell lysates was detected by western blot. Actin was used as loading control. **(H)** EVs were enriched from culture supernatant of the indicated cell lines. Presence of Melan A melanoma antigen in EV sample lysates was detected by western blot. All data are representative of at least two biologically independent experiments. All bar graphs give the mean value ± S.E.M. of at least triplicate technical replicates. Related to Figure 6.

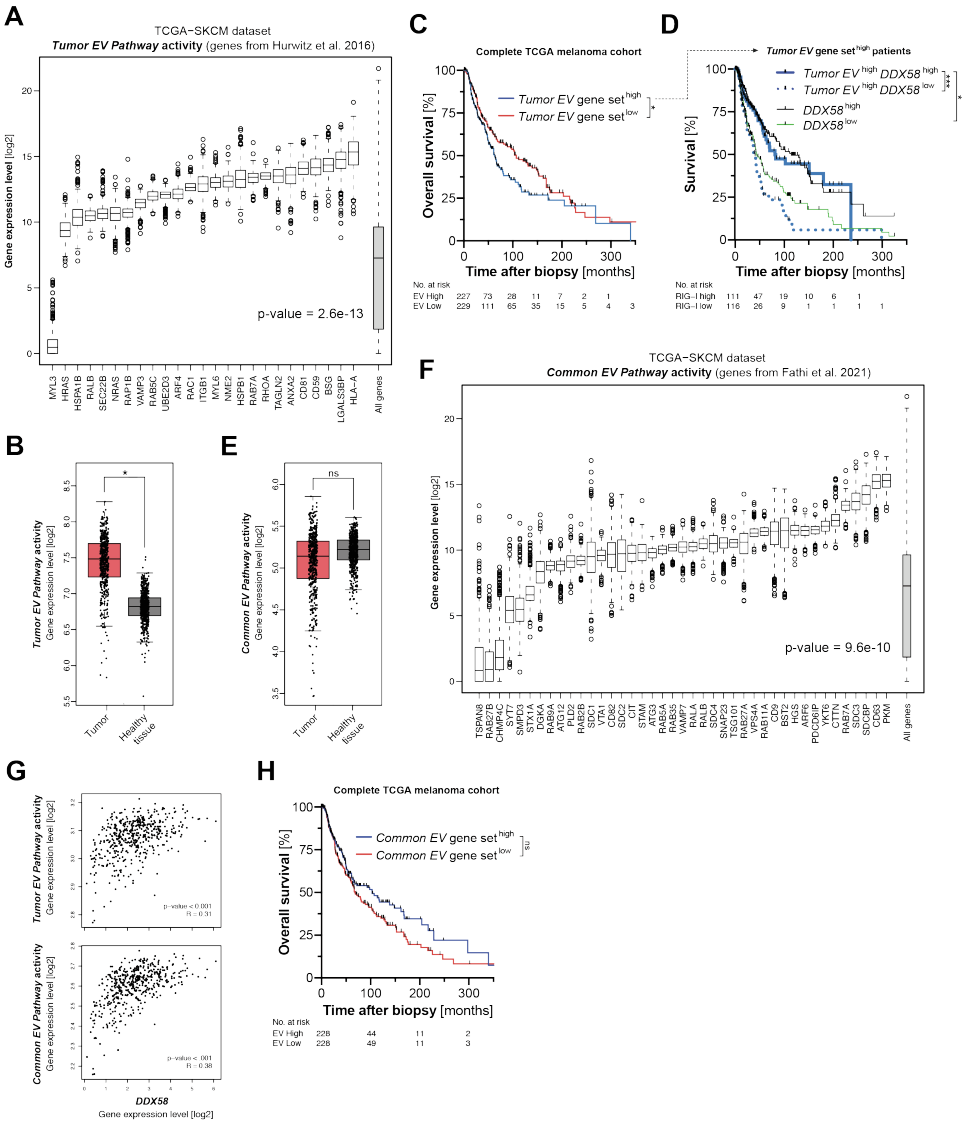

Figure S8. Transcriptional activity of a predefined set of Tumor EV pathway genes and *DDX58* are associated with beneficial response to checkpoint inhibitor treatment in melanoma patients. Expression of 25 pre-defined genes associated with tumor EV production (*Tumor EV pathway*) in tumor samples of 456 TCGA melanoma patients in relation to **(A)** the expression of all genes, and **(B)** compared to healthy tissue**.** The p-value shows statistical difference (Mann–Whitney U test) between the median gene expression of the genes in the *Tumor EV pathway* vs. all genes in human melanoma samples. **(C)** Overall survival in 456 TCGA melanoma patients by expression of the *Tumor EV pathway* gene set in tumor samples. **(D)** Overall survival in 227 selected TCGA melanoma patients with high *Tumor EV pathway* transcriptional activity stratified by co-expression of *DDX58* (encoding RIG-I) in tumor samples. **(E-F)** Expression of 41 pre-defined genes broadly associated with EV production (*Common EV pathway*) in tumor samples of 456 TCGA melanoma patients **(E)** compared to

healthy tissue, and **(F)** in relation to the expression of all genes in the tumor. The p-value shows statistical difference (Mann–Whitney U test) between the median gene expression of the genes in the *Common EV pathway* vs. all genes in human melanoma samples. **(G)** Correlation of expression levels of RIG-I-encoding *DDX58* and the two EV pathway gene sets in tumor samples of 456 TCGA melanoma patients. **(H)** Overall survival in 456 TCGA melanoma patients by expression of the *Common EV pathway* gene set in tumor samples. Related to Figure 6.

A **TCGA melanoma analysis, RIG-I and Tumor EV pathway activity** (adapted from Hurwitz et al. 2016)

Univariable Cox regression:

Overall survival (OS)

Variable	Value	n	Events	HR	p
DDX58	low	456	218	1.95 (1.49–2.56)	< 0.001
Tumor EV pathway	high	456	218	1.36 (1.04–1.77)	0.03

Disease-free survival (DFS)

Variable	Value	n	Events	HR	p
DDX58	low	398	256	1.36 (1.06–1.74)	0.01
Tumor EV pathway	high	398	256	1.21 (0.94–1.55)	0.14

Multivariable Cox regression:

Overall survival (OS)

Variable	Value	n	Events	HR	p
DDX58	low	456	218	1.98 (1.51–2.6)	< 0.001
Tumor EV pathway	high	456	218	1.4 (1.07–1.84)	0.01

Disease-free survival (DFS)

Variable	Value	n	Events	HR	p
DDX58	low	398	256	1.37 (1.07–1.75)	0.01
Tumor EV pathway	high	398	256	1.22 (0.95–1.57)	0.12

B **TCGA melanoma analysis, RIG-I and Common EV pathway activity** (adapted from Fathi et al. 2021)

Univariable Cox regression:

Overall survival (OS)

Variable	Value	n	Events	HR	p
DDX58	low	456	218	1.95 (1.49–2.56)	< 0.001
EXOGENES_MEAN	high	456	218	0.78 (0.59–1.02)	0.07

Disease-free survival (DFS)

Variable	Value	n	Events	HR	p
DDX58	low	398	256	1.36 (1.06–1.74)	0.01
EXOGENES_MEAN	high	398	256	0.89 (0.69–1.14)	0.4

Multivariable Cox regression:

Overall survival (OS)

Variable	Value	n	Events	HR	p
DDX58	low	456	218	1.9 (1.44–2.51)	< 0.001
EXOGENES_MEAN	high	456	218	0.89 (0.67–1.17)	0.4

Disease-free survival (DFS)

Variable	Value	n	Events	HR	p
DDX58	low	398	256	1.34 (1.04–1.73)	0.02
EXOGENES_MEAN	high	398	256	0.94 (0.73–1.21)	0.6

Table S3. Low RIG-I-encoding *DDX58* expression and high *Tumor EV pathway* transcriptional activity in melanoma biopsies are independent risk factors for death. Uni- and multi-variable Cox regression analysis for overall (OS) and disease-free survival (DFS) in patients with malignant melanoma from the TCGA databank based on transcriptional activity of the **(A)** *Tumor EV pathway* or **(B)** *Common EV pathway gene set*. Definitions can be found in the main text. HR, hazard ratio with 95 % confidence interval. EXOGENE_MEAN, mean EV pathway gene expression. Related to Figure 6.

mRab27a #1	5′-TGGTTAAGCTACGAAACCTA-3′
mRab27a #2	5′-AACCCAGATATAGTGCTGTG-3′
hDDX58 (RIG-I) #1	5′-AAAAGTGTGGCAGCCTCCAT-3′
hDDX58 (RIG-I) #2	5′-CTAGGGCATCCAAAAAGCCA-3′
hTMEM173 (STING) #1	5′-TGAAAAAGGGAATTTCAACG-3′
hTMEM173 (STING) #2	5′-GCTGGGACTGCTGTTAAACG-3′
hCGAS #1	5′-AAAGCCAGTTTTGAATGCGC-3′
hCGAS #2	5′-AATATCTGTGGATATAACCC-3′
hIFNAR1 #1	5′-ATGTCGACCTCTACTTTTTG-3′
hIFNAR1 #2	5′-AACAGGAGCGATGAGTCTGT-3′

Table S4. Target sequences of sgRNAs used for CRISPR/Cas9-mediated engineering of murine and human cell lines. Related to STAR Methods.

Target	Isotype	Clone	Distributor	Identifier
Alix	Mouse IgG1	3A9	Cell Signaling	Cat#2171; RRID: AB_2299455
Calnexin	Rabbit IgG	Polyclonal	Abcam	Cat#ab22595; RRID: AB_2069006
CD63	Mouse IgG1	MX-49.129.5	Santa Cruz	Cat#sc-5275; RRID: AB_627877
CD81	Rabbit IgG	Polyclonal	Sigma-Aldrich	Cat#SAB3500454; RRID: AB_10640751
Cytochrome c	Rabbit IgG	D18C7	Cell Signaling	Cat#11940; RRID: AB_2637071
Flotilin 1	Rabbit IgG	Polyclonal	Abcam	Cat#ab41927; RRID: AB_941621
HSP70	Mouse IgG1	5A5	Abcam	Cat#ab2787; RRID: AB_303300
gp100	Rabbit IgG	EPR4864	Abcam	Cat#ab137062
Ovalbumin	Mouse IgG	OVA-14	Sigma-Aldrich	Cat#A6075; RRID: AB_258279
Rab27	Rabbit IgG	Polyclonal	Biorbyt	Cat#orb381996
RIG-I	Rabbit IgG	D14G6	Cell Signaling	Cat#3743; RRID: AB_2269233
TSG101	Mouse IgG1	4A10	GeneTex	Cat#GTX70255; RRID: AB_373239
Tubulin	Rabbit IgG	11H10	Cell Signaling	Cat#2125; RRID: AB_2619646
β-Actin	Mouse IgG1	13E5	New England Biolabs	Cat#4970; RRID: AB_2223172
Rat IgG	Goat IgG	Polyclonal	Cell Signaling	Cat#7077; RRID: AB_10694715
Rabbit IgG	Goat IgG	Polyclonal	New England Biolabs	Cat#7074; RRID: AB_2099233
Mouse IgG	Horse IgG	Polyclonal	New England Biolabs	Cat#7076; RRID: AB_330924

Table S5. Antibodies used for western blot analysis of murine proteins. The polyclonal antibodies are linked to horseradish peroxidase (HRP) and were used as secondary antibodies. Related to STAR Methods.

11. Acknowledgement

The first and foremost thanks go to my family, partner, and friends, who have supported me throughout this study by sharing mental and material resources. Finding an open ear when things were challenging was invaluable. Significantly, the support from Eva Stritzke, Jochen Nagel, and Amelie Freitag laid the foundation I could build on.

I thank Hendrik Poeck and Simon Heidegger for their outstanding supervision throughout this project, including their thoughtful guidance, feedback, and in-depth discussions. They have elicited my fascination with the immune system and the vision to leverage its clinical potential. It has stuck with me since.

I am thankful for the framework TUM's dissertation program, “Translationale Medizin,” provided for my first work of research. The scholarship from “Else Kröner-Fresenius-Stiftung” supported me financially so I could take the time and focus on this endeavor.

Personal interactions have inextricably shaped my experience and the outcome of this project. I thank Sarah Dahl, Tatjana Nedelko, Laura Joachim, Sascha Göttert, Stefan Enßle, Yunus Barth, Erik Thiele-Orberg as well as all the other lab collegues and cooperation partners for their kind collaboration. I am looking forward to the next opportunity to work together.